ATLAS COLLABORATION

Search for MSSM neutral Higgs bosons decaying to a $\mu^+\mu^-$ pair in the mass range up to 130 GeV

Simonetta Gentile[1]
Halina Bilokon[2], **Vitaliano Chiarella**[2], **Giovanni Nicoletti**[2]
(1) Dipartimento di Fisica, Università La Sapienza, Sez. I.N.F.N., Roma,
(2) Laboratori Nazionali di Frascati, I.N.F.N., Frascati, Roma.

ATL-PHYS-PUB-2007-001
11 January 2007

Abstract

Results are presented on the discovery potential for MSSM neutral Higgs bosons in the $m_{\mathrm{h}} - max$ scenario. The region of large tanβ, between 15 and 50, and mass between $\approx$ 95 and 130 GeV is considered in the framework of the ATLAS experiment at the Large Hadron Collider (LHC), for a centre-of-mass energy $\sqrt{s} = 14$ TeV.

The h/A bosons, supposed to be very close in mass in this parameter region, are studied in the channel h/A $\rightarrow \mu^+\mu^-$, accompanied by two b-jets. For completeness, a possible contribution of the H boson is studied in the same tanβ, m_{A} region. In this context use can be made of the method described in Ref. [1] to control the most copious background, $\mathrm{b\bar{b}Z} \rightarrow \mu^+\mu^-$ accompanied by two b-jets. The region studied is not fully covered by the present data either from LEP or from Tevatron.

These results override the ones from the preliminary study [2].

1 Introduction

The Minimal Supersymmetric Standard Model (MSSM) is the most investigated extension of the Standard Model (SM).

The theory requires two Higgs doublets giving origin to five Higgs bosons: two CP-even neutral scalars, h and H (h is the lighter of the two), one CP-odd neutral scalar, A, and one pair of charged Higgs bosons, $H^{\pm}$ [3–5]. The discovery of any one of these particles is crucial to prove the model. This is a key point in the physics program of future accelerators and in particularly of LHC.

After the conclusion of the LEP program in the year 2000, the experimental limit on the mass of the Standard Model Higgs boson H [6] was established, and for neutral [7] and charged [8] MSSM Higgs bosons mass limits were obtained for most of the representative sets of the model parameters.

The motivation of this study is to explore the potential of the ATLAS detector for the discovery of neutral MSSM Higgs bosons in the parameter region not excluded by the LEP data. In particular, the search for the lightest of the neutral Higgs bosons, which is predicted to have a mass smaller than 140 GeV, including radiative corrections ([7] and references therein), thus close to the mass of the Z boson, $m_{\rm Z}$, constitutes a challenging test for the detector performance and the analysis method when disentangling the signal from the background.

In the first part of this note we analyze the MSSM framework, the present experimental situation, the discovery potential of MSSM Higgs bosons at LHC, and the production mechanism in hadron collisions. We also describe the Monte Carlo generator and the software tools used. In the second part we discuss the detector performances relevant for this search, the analysis strategy and the results of the scan over the MSSM ($\tan\beta$, $m_{\rm A}$) plane.

In the conclusion results on the discovery (or exclusion) potential are presented.

2 Minimal Supersymmetric Standard Model

In this paragraph the fundamental points of the model, useful for the following discussion, are summarized, referring to elsewhere for a complete review [4, 9].

The mass of the five Higgs bosons required by the MSSM, the two CP-even (h,H), the CP-odd A and the two charged $H^{\pm}$, at tree level can be expressed in terms of two independent input parameters, the ratio of the vacuum expectation values of the two Higgs fields, $\tan\beta$, and the pseudoscalar Higgs-boson mass, $m_{\rm A}$. A simple relation holds between these particle masses :

$$m^2_{H,h} = \frac{1}{2}[m^2_A + m^2_Z \pm \sqrt{(m^2_A + m^2_Z)^2 - 4m^2_A m^2_Z \cos^2 2\beta}] \qquad (1)$$

$$m^2_{H^{\pm}} = m^2_{\rm W} + m^2_{\rm A}$$

(Recent precise measurements of W and Z masses, $m_{\rm W}$ and $m_{\rm Z}$, are available [10]).

In comparison with the SM, the MSSM requires more free parameters. However, the assumption that the scalar fermions masses, the gaugino masses and the trilinear Higgs-fermion couplings must unify at the Grand Unification scale (GUT) reduces the number of free parameters. In one of the possible constrained models the parameters chosen are:

- $M_{\rm SUSY}$, a common mass for all sfermions (scalar fermions) at the electroweak scale.

- M_2, a common $SU(2)_L$ gaugino mass at the electroweak scale.
- μ, the strength of the supersymmetric Higgs mixing.
- tanβ, the ratio of the vacuum expectation values of the two Higgs fields .
- A = A_t= A_b a common trilinear Higgs-squarks coupling at the electroweak scale. It is assumed to be the same for up-type squarks and for down-type squarks.
- m_A, the mass of the CP-odd Higgs boson.
- $m_{\tilde{g}}$, the gluino mass.

Three of these parameters define the stop and sbottom mixing parameters $X_t = A_t - \mu \cot\beta$ and $X_b = A_b - \mu \cot\beta$.

For the Higgs boson search, two extremes of the stop mixing are considered: the maximal mixing $X_t = 2\ M_{SUSY}$, and the minimal mixing, when X_t is zero. Usually a set of benchmarks are applied and also in this case there are only two free parameters: tanβ and m_A. In this search three CP-conserving benchmark scenarios are considered (Tab.1).

Parameter	$m_h - max$	*no-mixing*	*large-*μ
M_{SUSY}[GeV]	1000	1000	400
μ [GeV]	-200	-200	1000
M_2[GeV]	200	200	400
X_t=A - $\mu \cot\beta$	$2M_{SUSY}$	0	- 300
$m_{\tilde{g}}$[GeV]	$0.8M_{SUSY}$	$0.8M_{SUSY}$	200
m_A[GeV]	0.1-1000	0.1-1000	0.1-400
tanβ	0.4-50	0.4-50	0.7-50

Table 1: CP-conserving benchmark scenarios.

The characteristics of the three scenarios are as follows.

- $m_h - max$

  As the name indicates, it allows in the model the maximum value of m_h [7]. For fixed values of m_t and M_{SUSY}, it gives the most conservative range of excluded tanβ values. A negative search of the h boson implies an exclusion of the model.

- *no-mixing*

  It assumes no-mixing between the scalar partners of the left-handed and the right-handed top quarks. The highest value of m_h can be 114 GeV.

- *large-*μ

  It is designed such that the h boson doesn't decay into pairs of b quarks due to large corrections from SUSY loop processes. The dominant decay modes are to $c\bar{c}$, gg, W^+W^-, $\tau^+\tau^-$. The highest value of m_h can be 108 GeV.

The difference between $m_{\rm h}-max$ and *no-mixing* scenario is mainly due to the fact that to the same point of the parameter space ($m_{\rm A}$, tanβ) corresponds a different mass of the h boson, thus a different sensitivity of the channel under consideration.

This work is focused on the first scenario as the most promising for the search of the h boson due to the relatively high value predicted for $m_{\rm h}$. In the following we refer to it often shortly as MSSM.

3 Experimental Status

In the past decade the huge amount of high quality data collected at LEP gave a most important contribution to the assessment of the Standard Model and its supersymmetric extension. High precision tests of the Standard Model were performed, and a combined mass limit $m_{\rm H}>$ 114.4 GeV was set for the SM Higgs boson [6]. The validity of the Minimal Supersymmetric Standard Model was also investigated. In particular the MSSM was studied in representative scans of the parameters within the constrained framework outlined in Sec. 2. For the mass of the charged Higgs bosons the combined limit obtained was $m_{\rm H_{\pm}}>$ 78.6 GeV [8]. The search for neutral CP-even and CP-odd Higgs bosons was performed at LEP energies considering the main production processes:

$$\rm e^+e^- \rightarrow hZ \qquad\qquad e^+e^- \rightarrow hA$$

with the tree-level cross sections related to the Standard Model Higgs-strahlung cross section, $\sigma^{\rm SM}_{\rm HZ}$, as [11]:

$$\sigma_{\rm hZ} = \sin^2(\beta-\alpha)\sigma^{\rm SM}_{\rm HZ} \qquad\qquad \sigma_{\rm hA} = \cos^2(\beta-\alpha)\tilde{\lambda}\sigma^{\rm SM}_{\rm HZ}$$

where α is the mixing angle which diagonalizes the CP-even Higgs boson mass matrix and $\tilde{\lambda}$ is a kinematic factor depending on the Higgs boson masses, $m_{\rm h}$ and $m_{\rm A}$, and the center-of-mass energy $\sqrt{s}$.

For most of the MSSM parameter space considered at LEP energies, the neutral Higgs bosons are predicted to decay dominantly into $\rm b\bar{b}$ and $\tau^+\tau^-$. However, in certain parameter regions, other decays, like $\rm h \rightarrow AA$ and $\rm A \rightarrow c\bar{c}$, become important.

No indication of signal was found in the combined data at center-of-mass energies up to 209 GeV [7] and lower limits on the Higgs boson masses were set as a function of tanβ for several scenarios ($m_{\rm h}$-*max* scenario in Fig. 1). The mass limits obtained (at 95% C.L. and with the top mass $m_{\rm t}$=174.3 GeV) are approximately:

$$m_{\rm h}, m_{\rm A} \geq 93 \text{ GeV}$$

In the $m_{\rm h}$-*max* scenario, designed to extend the search to the maximal theoretical bound of $m_{\rm h}$ for any value of tanβ, the LEP data do not exclude the parameter space defined by tanβ larger than 10 and $m_{\rm A} \sim 93$ GeV (Fig. 1).

A natural continuation of the LEP physics is the investigation of the possible existence of the CP-even Higgs boson h in this region of $m_{\rm A}$ and tanβ. The ATLAS [12] and CMS [13] experiments starting in the nearest future at the Large Hadron Collider (LHC), at CERN, will constitute a fantastic laboratory for such search.

The exploration of the parameter space, with a view to either discovering a supersymmetric Higgs boson or excluding the model considered, constitutes the motivation of the analysis described in this paper.

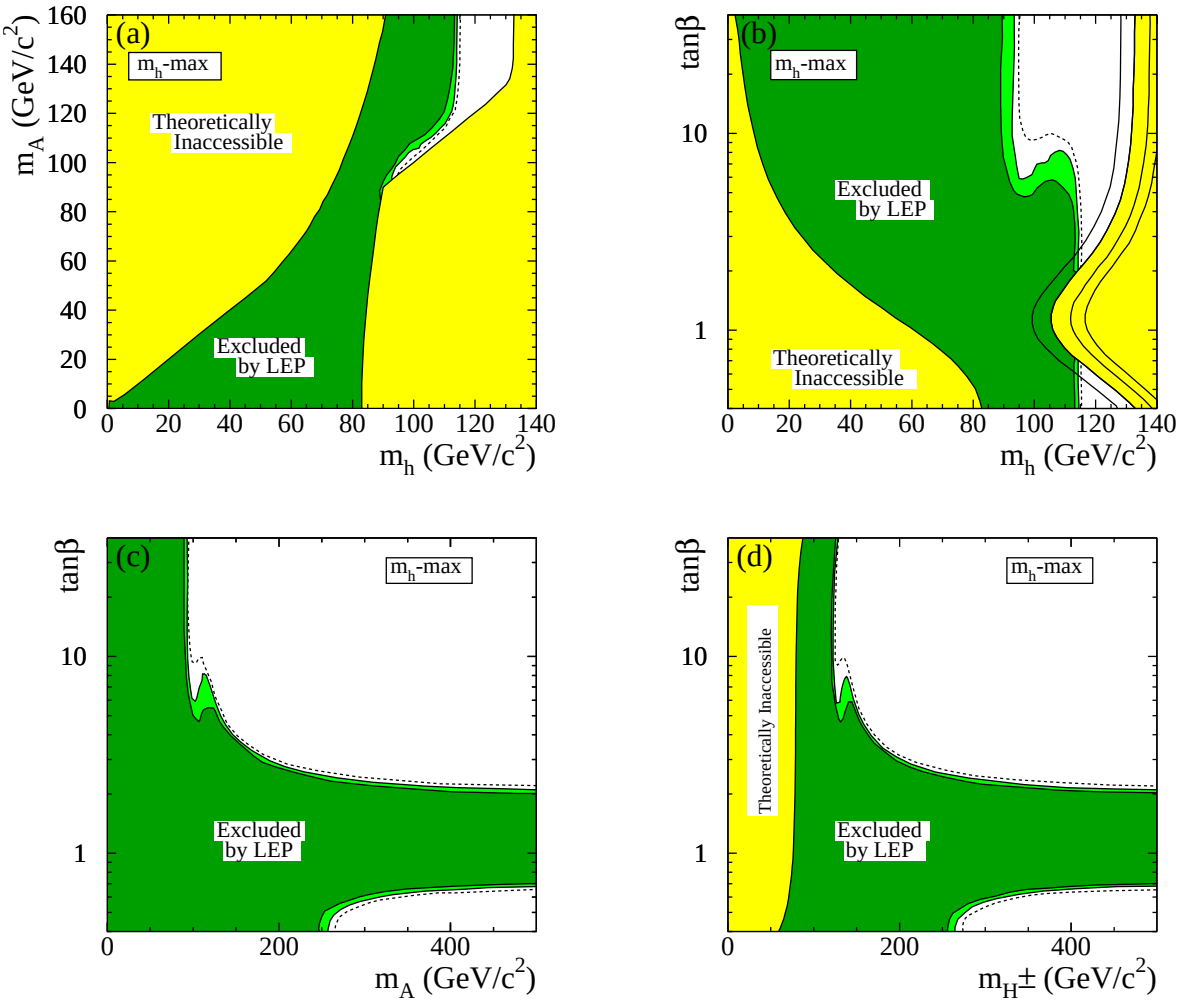

Figure 1: The combined LEP results for the search for the MSSM neutral Higgs bosons (from Ref. [7]). The figure shows the theoretically inaccessible regions (yellow) and the regions experimentally excluded by LEP searches, at 95% C.L. (light-green) and 99.7% C.L. (dark-green), for the $m_{\rm h}$-*max* scenario with the top mass $m_{\rm t}$= 174.3 GeV, in four projections of the MSSM parameters ($m_{\rm h}$, $m_{\rm A}$), ($m_{\rm h}$, tanβ), ($m_{\rm A}$, tanβ), ($m_{\rm H^{\pm}}$, tanβ). The dashed lines indicate the boundaries of the regions which are expected to be excluded, at 95% C.L., on the basis of Monte Carlo simulations with no signal. In the ($m_{\rm h}$, tanβ) projection, the upper boundary of the parameter space is indicated for four values of the top mass; from left to right: $m_{\rm t}$= 169.3, 174.3,179.3 and 183.0 GeV.

The extraction of the h boson signal from the competing enormous background of Z decays, in the region of $m_{\rm h}$ close to $m_{\rm Z}$ constitutes a challenging search, where all performances of the experimental setup have to be exploited.

4 Minimal Supersymmetric Standard Model Higgs search at hadron colliders

The prospect for the detection of MSSM Higgs bosons at LHC has been evaluated [12,14,15] for benchmark sets preventing Higgs boson decays to SUSY particles. The evaluation was made in terms of discovery potential conveniently quantified [14, 16]. The interest was focused on the discovery potential of decay modes common to MSSM and SM Higgs bosons [12].

The conclusion of these studies is that the complete region of parameter space $m_{\rm A} = 50$ – 500 GeV and $\tan\beta = 1$ – 50 is open to Higgs boson discovery by the ATLAS experiment, already with an integrated luminosity of $\int \mathcal{L}\,{\rm d}t = 30$ fb^{-1}. Over a large region of this parameter space, more than one Higgs boson and more than one decay mode could be observed – the detection of a signal in more than one decay channel would constitute an undoubted proof of discovery. An exhaustive list of all these decay modes can be found in Ref. [12].

A few points should be underlined starting with Fig. 2 from Ref. [14] which shows the discovery potential contour for two values of $\int \mathcal{L}\,{\rm d}t$, 30 fb^{-1} (left) and 300 fb^{-1} (right) in the MSSM CP-conserving scenario.

At low luminosity the $\rm h \to \tau^+\tau^-$ decay mode represents the main contribution to the discovery potential and covers most of the parameter space not yet explored.
The contribution of $\rm b\bar{b}h \to \mu^+\mu^-$ appears to be crucial in the region of moderate $\tan\beta$ and mass close to $m_{\rm Z}$. The channel $\rm b\bar{b}h \to \mu^+\mu^-$ requires an excellent performance in μ detection and b-tagging. It is well suited to the ATLAS experiment thanks to a design highly demanding on the muon spectrometer and the inner detector.

At high luminosity channels such as: $\rm h \to \gamma\gamma$, $\rm h \to ZZ \to 4\ell$ and $\rm h \to b\bar{b}$ in associated production with $\rm t\bar{t}$ give a significant contribution.
The channel $\rm h \to \gamma\gamma$ requires an excellent $M_{\gamma\gamma}$ mass resolution and jet/γ separation. The expected MSSM rates for $\rm h \to \gamma\gamma$ are generally suppressed with respect to the SM case. However, they could also be slightly enhanced in a limited region of the parameter space.
The search for the h boson in the decay mode $\rm h \to b\bar{b}$ is performed analogously to the SM case. Only the $\rm t\bar{t}h$ production followed by the $\rm h \to b\bar{b}$ decay can be observed clearly above the background. This channel, as in the SM case, requires an excellent b-tagging performance, since the extraction of the signal requires the identification of four b-jets. In the MSSM case, the rates can be enhanced by 10-20% compared to the SM case.

Considering all MSSM Higgs bosons, the region in the $m_{\rm A}$, $\tan\beta$ plane which corresponds to $m_{\rm h} \approx 100$ GeV and $\tan\beta > 10$ is only accessible with a neutral h boson decaying to $\mu^+\mu^-$ and $\tau^+\tau^-$ and with a charged $\rm H^{\pm}$ boson decaying to $\tau\nu$.

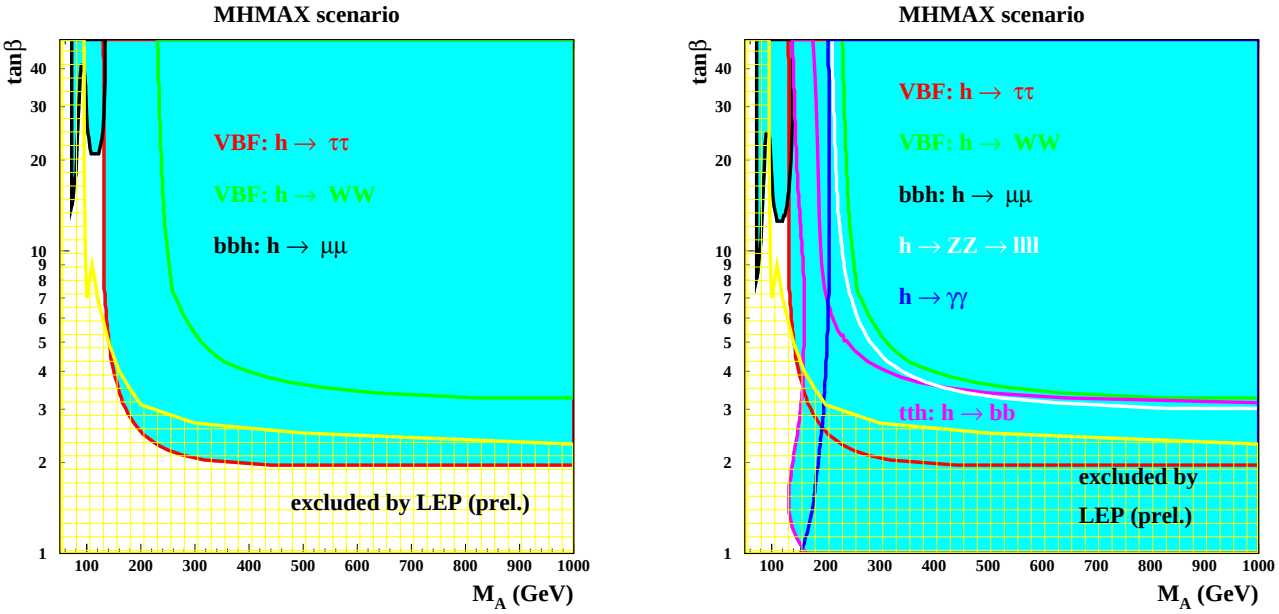

Figure 2: Discovery potential for the light CP-even Higgs boson in the $m_{\rm h}$-*max* CP-conserving scenario after collecting 30 fb^{-1} (left) and 300 fb^{-1} (right). The cross hatched area is excluded by LEP at 95 % C.L.. From Ref. [14].

5 Production in hadronic interaction

5.1 Signal processes: the lightest Supersymmetric Higgs boson

The neutral h boson and the other Higgs bosons are important elements of the MSSM model. Their couplings at tree level to fermions and massive gauge bosons are easily obtained from the SM Higgs boson couplings (shown in Tab. 2 [15]) via correction factors summarized in Tab. 3 [15]. These correction factors depend on the parameters α and β which were introduced in Sec. 2 and are related by the following expression:

$$\cos 2\alpha = -\cos 2\beta \, \frac{m_A^2 - m_Z^2}{m_H^2 - m_h^2} \tag{2}$$

SM	Fermions	W^+W^-	$ZZ \to b\bar{b}\mu^+\mu^-$
H	$\frac{igm_f}{2m_W}$	$igm_W g^{\mu\nu}$	$\frac{igm_Z}{2\cos\theta_W} g^{\mu\nu}$

Table 2: Standard Model Higgs boson couplings at tree level to fermions and massive gauge bosons.

At high tanβ the MSSM correction factors to the SM Higgs bosons couplings to fermions and massive gauge bosons (see Tab. 3) are larger for down-type quarks (b) and leptons (τ and

MSSM	$d\bar{d}$, $s\bar{s}$,$b\bar{b}$ e^+e^-, $\mu^+\mu^-$, $\tau^+\tau^-$	$u\bar{u}$, $c\bar{c}$, $t\bar{t}$	W^+W^-, ZZ
h	$-\sin\alpha/\cos\beta$	$\cos\alpha/\sin\beta$	$\sin(\beta-\alpha)$
H	$\cos\alpha/\cos\beta$	$\sin\alpha/\sin\beta$	$\cos(\beta-\alpha)$
A	$-i\gamma_5\tan\beta$	$-i\gamma_5\cot\beta$	0

Table 3: MSSM correction factors to the SM Higgs boson couplings to fermions and massive gauge bosons at tree level.

μ) than for up type-quarks. This fact implies that the MSSM coupling to down-type quarks and leptons are strongly enhanced in this region.

Since the MSSM and SM couplings differ only by a correction factor, the most natural choice is to explore the decay channels common to both, as mentioned in Sec. 4. The decay channels $h \to b\bar{b}$ and $h \to gg$ are extensively studied [12]. Other decay channels deserving consideration are $h \to \tau^+\tau^-$ and $h \to \mu^+\mu^-$.

The Higgs boson couplings, both in SM and in MSSM, are proportional to the fermion mass (Tab. 2), consequently the heavy mass $\tau^+\tau^-$state is favored in comparison to the $\mu^+\mu^-$ one, and its production rate is higher by a factor $(\frac{m_\tau}{m_\mu})^2$. This apparent advantage of the $\tau^+\tau^-$ channel is counterbalanced by the difficulty of identifying the hadronic decay of a τ-jet in hadronic events, by a smaller acceptance of the detector and by a worse mass resolution due to the presence of neutrinos in the final state.

Instead, with a final state containing muons, like in $h \to \mu^+\mu^-$, one exploits the excellent combined performance of the muon spectrometer and inner detector, that compensates the smaller branching ratio with respect to the decay mode $h \to \tau^+\tau^-$.

To reduce the competing background it is convenient to perform the search for the $h \to \mu^+\mu^-$ decay mode in a channel with two b-jets in the final state. The associated $b\bar{b}h$ production proceeds by the Yukawa bh coupling, which is enhanced at high tanβ. The corresponding larger cross section makes the $b\bar{b}h$ production the dominant process in the production of h bosons in the high tanβ region. The Feynman diagrams contributing to the process $gg \to b\bar{b}h \to b\bar{b}\mu^+\mu^-$and $q\bar{q} \to b\bar{b}h \to b\bar{b}\mu^+\mu^-$ are shown in Fig. 3 and Fig. 4.

Before concluding this section it should be reminded [15] that the CP-odd supersymmetric boson A in this region of high tanβ and m_h around 100 GeV has a mass slightly higher than the CP-even h and a competitive branching ratio (Tab. 3) in the corresponding decay channel $A \to \mu^+\mu^-$. The cross-section, the mass and width difference, which are functions of the parameters tanβ and m_A , are close in some points of the parameters space (Sec. 6). Thus in these points the CP-odd and CP-even bosons are indistinguishable from the experimental point of view. Therefore, it is more correct to think in terms of h/A search.

In the following sections the A boson contribution to the signal is taken into account. One refers to the boson searched as h/A boson (however its mass is noted m_h or m_A, accordingly).
.

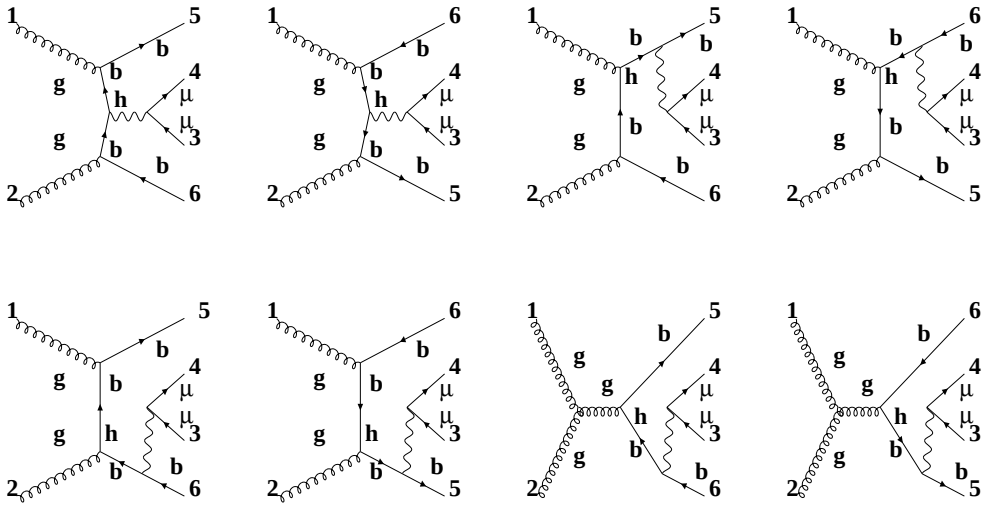

Figure 3: Diagrams contributing at "tree level" to the process $gg \to b\bar{b}h \to b\bar{b}\mu^+\mu^-$.

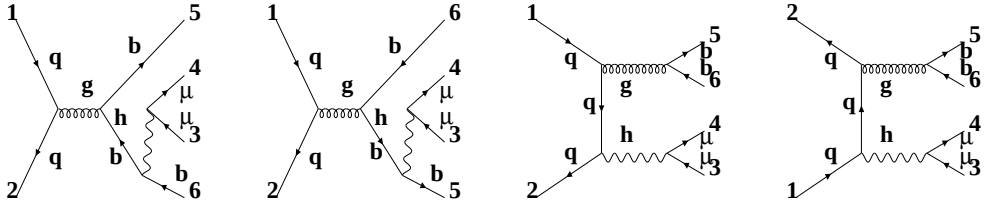

Figure 4: Diagrams contributing at "tree level" to the process $q\bar{q} \to b\bar{b}h \to b\bar{b}\mu^+\mu^-$.

5.2 Background processes

Some other processes have the same final state, a μ-pair and two b-jets. These reactions constitute the background of the h/A search and have higher production cross-sections than the signal. Thus, one has to pay a lot of effort in controlling and understanding them.

The main background originates from the Z/γ^* production with two b-jets and a subsequent decay into a μ-pair. The cross section of this process is a few orders of magnitude larger than for the signal. For example, the effective production cross section of a Z boson accompanied by two b-jets and decaying to a $\mu^+\mu^-$ pair, $\sigma_{b\bar{b}Z} \cdot \mathrm{Br}_{Z\to\mu^+\mu^-}$, is ≈ 22.8 pb[1)] and is larger than the h cross section, $\sigma_{hb\bar{b}} \cdot \mathrm{Br}_{h\to\mu^+\mu^-} \approx 0.24$ pb (at $\tan\beta = 45$ and $m_h = 110$ GeV).
In Figs. 5 – 6 diagrams corresponding to $b\bar{b}Z \to b\bar{b}\mu^+\mu^-$productions are shown. Comparing Figs. 3 – 4 with Figs. 5 – 6, it is clear that they differ only in the kind of boson produced, h (or A) in the signal and Z/γ^* in the background. The distinction between the signal and the background when m_h is approaching m_Z is an extremely hard task due to the similar topology of the decays.

A possible contribution of Z accompanied by (mistagged) light flavors was neglected.

[1)] Evaluated from AcerMC(2.3) [17] and PYTHIA 6.226 (with $m_Z > 60$ GeV) (Sec. 6).

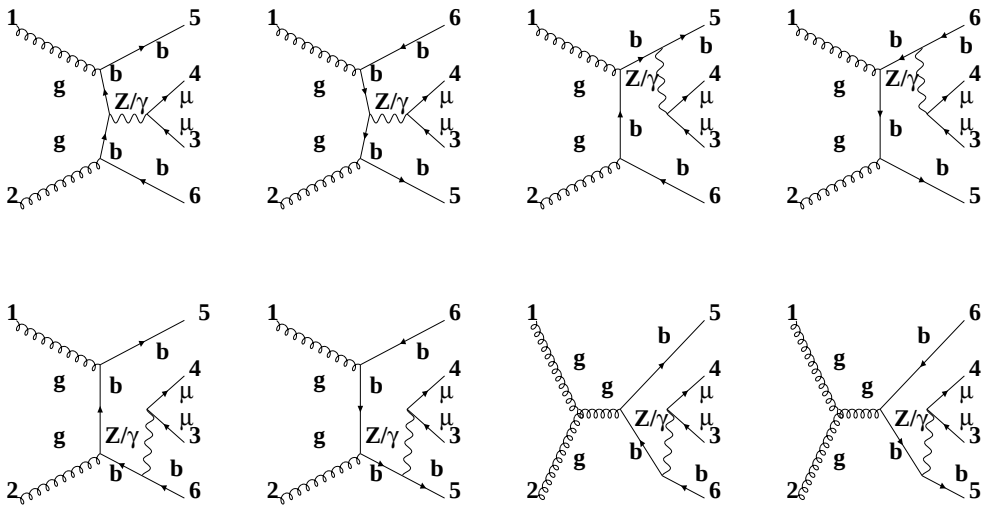

Figure 5: Subset of the diagrams contributing at "tree level" to the process $gg \to Z/\gamma^* b\bar{b} \to \mu^+\mu^- b\bar{b}$.

Another background that contributes to the same final state is the ZZ associated production, when one Z decays into $b\bar{b}$ and the second one decays into $\mu^+\mu^-$. The cross section of this process is negligible with respect to the main background, $\sigma_{ZZ} \cdot Br_{Z\to\mu^+\mu^-} \cdot Br_{Z\to b\bar{b}} \approx 0.13$ pb [2)]. Nevertheless it is of the same order of magnitude as the signal. The contribution of this background can be easily suppressed using the kinematic characteristics of these events, see following sections.

Also contributing to the same final state is the associated production of two t quarks $t\bar{t}$ (Fig. 7), followed by a top-quark decay into a b-quark and a W boson and a subsequent W decay in $\mu\nu$. This process has a cross section which is $\sigma_{t\bar{t}} \cdot Br_{t\to bW} \cdot Br_{W\to\mu\nu} \cdot Br_{t\to bW} \cdot Br_{W\to\mu\nu} \approx 5.71$ pb [3)] The presence of two neutrinos implies missing transverse energy in the event, as it will be discussed in the following sections, and this characteristic is used to strongly reduce this background.

Naively, it can be thought to discriminate the signal from the background on the basis of the different b-jets characteristics. In fact, the two background b-jets are usually more energetics than those accompanying the signal; consequently the probability of their identification is higher. However the requirements needed for the identification of two b-jets will suppress the signal more than the background.

6 Monte Carlo Samples

The efficiency of the selection criteria, the detector acceptance and the purity of the data sample are estimated using Monte Carlo events for the signal and the background generated using the PYTHIA program (v.6.226) [18]. The MSSM neutral Higgs bosons h, A and H are generated in associated production with two b-quarks.

The background events are considered to originate from the following channels:

[2)] Evaluated from PYTHIA 6.226 (Sec.6).
[3)] Evaluated from PYTHIA 6.226 (Sec.6).

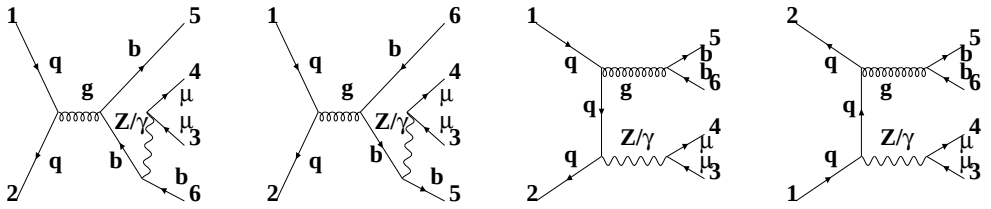

Figure 6: Diagrams contributing at "tree level" to the process $q\bar{q} \rightarrow Zb\bar{b} \rightarrow \mu^+\mu^- b\bar{b}$.

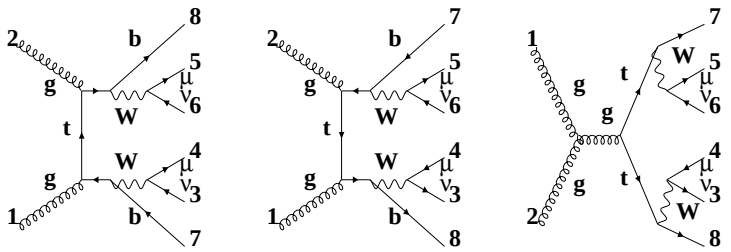

Figure 7: Diagrams contributing at "tree level" to the process $t\bar{t} \rightarrow b\bar{b}\mu^+\mu^-\nu\bar{\nu}$; the diagram including quarks fusion is obtained from third diagram replacing the two gluons with incoming quarks (corresponding to a contribution to the total cross section of about 10 %.

- $b\bar{b}Z \rightarrow b\bar{b}\mu^+\mu^-$. The sample of Z produced in association with two b-jets and decaying to a muon pair has been used in this study. The event generator used is AcerMC(2.3) [17] for the $b\bar{b}Z \rightarrow b\bar{b}\mu^+\mu^-$ process. The hadronization process is described with the PYTHIA (v.6.226) Monte Carlo [4)]. A generator level cut-off is applied to the $\mu^+\mu^-$ invariant mass, $M^{\rm inv}_{\mu\mu} > 60$ GeV [5)].

- $t\bar{t} \rightarrow b\bar{b}\mu^+\mu^-\nu\bar{\nu}$ generated with PYTHIA (v.6.226).

- $ZZ \rightarrow b\bar{b}\mu^+\mu^-$ generated with PYTHIA (v.6.226). This background has been considered, but due to its low cross section its importance is relatively low.

Monte Carlo events are generated for a center-of-mass energy $\sqrt{s}$= 14 TeV through the ATHENA interface (v.9.0.4). The ATLAS detector response [12] is simulated using the GEANT program [19], [20] which takes into account the effects of energy loss, multiple scattering and showering in the detector through the ATHENA interface (v.10.0.1).

A number of events corresponding to an integrated luminosity $\int \mathcal{L}\,dt \approx 300$ fb^{-1} has been simulated for each channel, with the exception of $b\bar{b}Z \rightarrow \mu^+\mu^-$. In this latter case, for practical reasons, a number of events corresponding to half the mentioned luminosity has been generated. We note that $\int \mathcal{L}\,dt \approx 300$ fb^{-1} corresponds to ten times the integrated luminosity expected after three years of data taking.

[4)] Using PHOTOS package for *inner bremsstrahlung* generation.

[5)] A low energy cut is fixed on *inner bremsstrahlung* photons at $P_{\rm T} > 5$ GeV.

A sample of $b\bar{b}Z \to e^+e^-$ events, $\approx$ 600000 events ($\sigma \approx 22.8$ pb), corresponding to an integrated luminosity $\int \mathcal{L}\, dt \approx 30\ fb^{-1}$, has also been simulated. This sample has been used for background studies [1].

For the h/A signal the parameters chosen [21] are reported in Tab. 4. The two parameters tanβ and m_A are varied to scan the MSSM plane. In this study, the values of m_h and m_H are derived from PYTHIA as a function of m_A. The results are presented as a function of m_A, the input parameter.

Parameter		value	PYTHIA parameter [18]
common gaugino mass	$M_2 \equiv m_{1/2}$ [GeV]	200	RMSS(2)
gluino mass	$m_{\tilde{g}}$ [GeV]	800	RMSS(3)
strength of supersymmetric Higgs	μ [GeV]	- 200	RMSS(4)
ratio of Higgs fields	tanβ	15-50	RMSS(5)
common scalar mass	m_0 [GeV]	1000	RMSS(8)
squark left 3 gen	$M_{\tilde{q}_L}$ [GeV]	1000	RMSS(10)
sbottom mass	$M_{\tilde{b}_R}$ [GeV]	1000	RMSS(11)
stop mass	$M_{\tilde{t}_R}$ [GeV]	1000	RMSS(12)
stop-trilinear coupling	A	2440	RMSS(16)
mass of CP-odd boson	m_A [GeV]	95-135	RMSS(19)

Table 4: Parameters for A, h and H generation in PYTHIA (v.6.226) [18].

The signal, $b\bar{b}h \to b\bar{b}\mu^+\mu^-$, has been simulated in 104 points of the parameter space (tanβ, m_A), corresponding to eight steps in tanβ, chosen equally spaced between 15 and 50 and thirteen steps of 2.5 GeV in m_h between 95 GeV and 125 GeV (the largest value allowed by PYTHIA(v.6.226)). These are also the points where the decay $b\bar{b}A \to b\bar{b}\mu^+\mu^-$ has been simulated.

As discussed in Sec. 5, the cross section, mass and width of h and A bosons, shown for tanβ = 45 in Fig. 8, are close, thus suggesting a unique h/A search.

The H cross section in the mass range considered is one order of magnitude lower than the h/A cross section. The mass m_H is shown in Fig. 8 as a function of the mass m_A at tanβ = 45.

The values of the mass, cross section and width of the A/h and H neutral bosons are reported and plotted in Appendix A for all the points analyzed of the (tanβ, m_A) plane.
For the following discussion a reference point has been chosen at tanβ = 45, m_A=110.31 GeV (m_h= 110 GeV, m_H= 127.46 GeV)

process (background)	$\sigma_{b\bar{b}\mu^+\mu^-}$ [pb]	$N^{exp_{300}}$	N^{MC}	w
$bbZ \to bb\mu^+\mu^-$	22.789	6836700	3314000	2.06
$t\bar{t} \to bb\mu^+\mu^-\nu\bar{\nu}$	5.71	1713420	1806437	0.95
$ZZ \to b\bar{b}\mu^+\mu^-$	0.1273	33819	97244	0.35

Table 5: Background cross section times branching ratios, $\sigma_{b\bar{b}\mu^+\mu^-}$, number of expected events for $\int \mathcal{L}\, dt \approx$ 300 fb^{-1}, $N^{exp_{300}}$, number of Monte Carlo generated events, N^{MC}, and their weight in the analysis, w, for the three processes considered.

The cross section times branching ratios, together with the number of expected events for $\int \mathcal{L}\,dt \approx 300$ fb^{-1}, the number of Monte Carlo generated events and their weight, is reported in Tab. 5 for three background processes. The corresponding quantities for the signal processes are reported in Appendix D as obtained varying tanβ and $m_{\rm A}$.

7 Preliminaries

The detector acceptance considered in the following analysis is $|\eta| \leq 2.5$. No simulation of the trigger is implemented; however the transverse momentum, $P_{\rm T}$, is required to be above the experimental threshold.

Two points are crucial for our analysis:

- The muon reconstruction efficiency in the analysis acceptance and the $\mu^+\mu^-$ invariant mass resolution.
- The b-jet identification.

These items deserve to be studied in some detail before they are used in the h/A analysis.

7.1 Muon resolution studies on Z$\rightarrow\mu^+\mu^-$ events

For this purpose only events with two reconstructed muons of opposite charge found within the $|\eta| \leq 2.5$ acceptance were considered. The μ reconstruction performances of the apparatus were studied with a sample of Z$\rightarrow\mu^+\mu^-$events [22]. The distributions of the transverse momentum, $P_{\rm T\mu}$, pseudorapidity, η_μ, and polar angle, ϕ_μ, of reconstructed muons (full color) reproduce with good efficiency the generated data (hatched color), Fig. 9.

A discriminating variable used in the analysis for the A/h search, Sec. 8.1, is the dimuon invariant mass. This variable was studied in a sample of Z decaying to $\mu^+\mu^-$.

A Gaussian fit to the distribution of reconstructed dimuon invariant mass in Z$\rightarrow\mu^+\mu^-$ events, Fig. 10 (top), yields the following values for the fit parameters $< M^{\rm inv}_{\mu\mu} >$ and $\sigma(M^{\rm inv}_{\mu\mu})$:

$$< M^{\rm inv}_{\mu\mu} >= 90.47 \pm 0.05 \text{ GeV} \qquad \sigma(M^{\rm inv}_{\mu\mu}) = 3.02 \pm 0.06 \text{ GeV} \tag{3}$$

The fit mean is smaller than the nominal $m_{\rm Z}$ [10]. The Z natural width contributes to $\sigma(M^{\rm inv}_{\mu\mu})$ for approximately 1.9 GeV thus implying a measurement accuracy $\sigma_{\rm res} = 2.3$ GeV. This is just the value obtained unfolding the reconstructed distribution with the distribution of the Z generated mass, $M^{\rm Z}_{\rm gen}$. When the difference between reconstructed and generated mass $M^{\rm inv}_{\mu\mu} - M^{\rm Z}_{\rm gen}$ is plotted, Fig. 10 (right), the Gaussian fit of the distribution gives the following results for the fit parameters $< M^{\rm inv}_{\mu\mu} - M^{\rm Z}_{\rm gen} >$ and $\sigma_{\rm res}$:

$$< M^{\rm inv}_{\mu\mu} - M^{\rm Z}_{\rm gen} >= -0.82 \ \pm \ 0.03 \text{ GeV} \qquad \sigma_{\rm res} = 2.35 \ \pm \ 0.03 \text{ GeV} \tag{4}$$

From this study at the Z pole we conclude that in this region the reconstructed invariant mass distribution shows a mean value shifted by 820 MeV with respect to the nominal value, towards the low mass region, and a resolution of ~ 2.6 %. These results will be used later in Sec. 8.1.

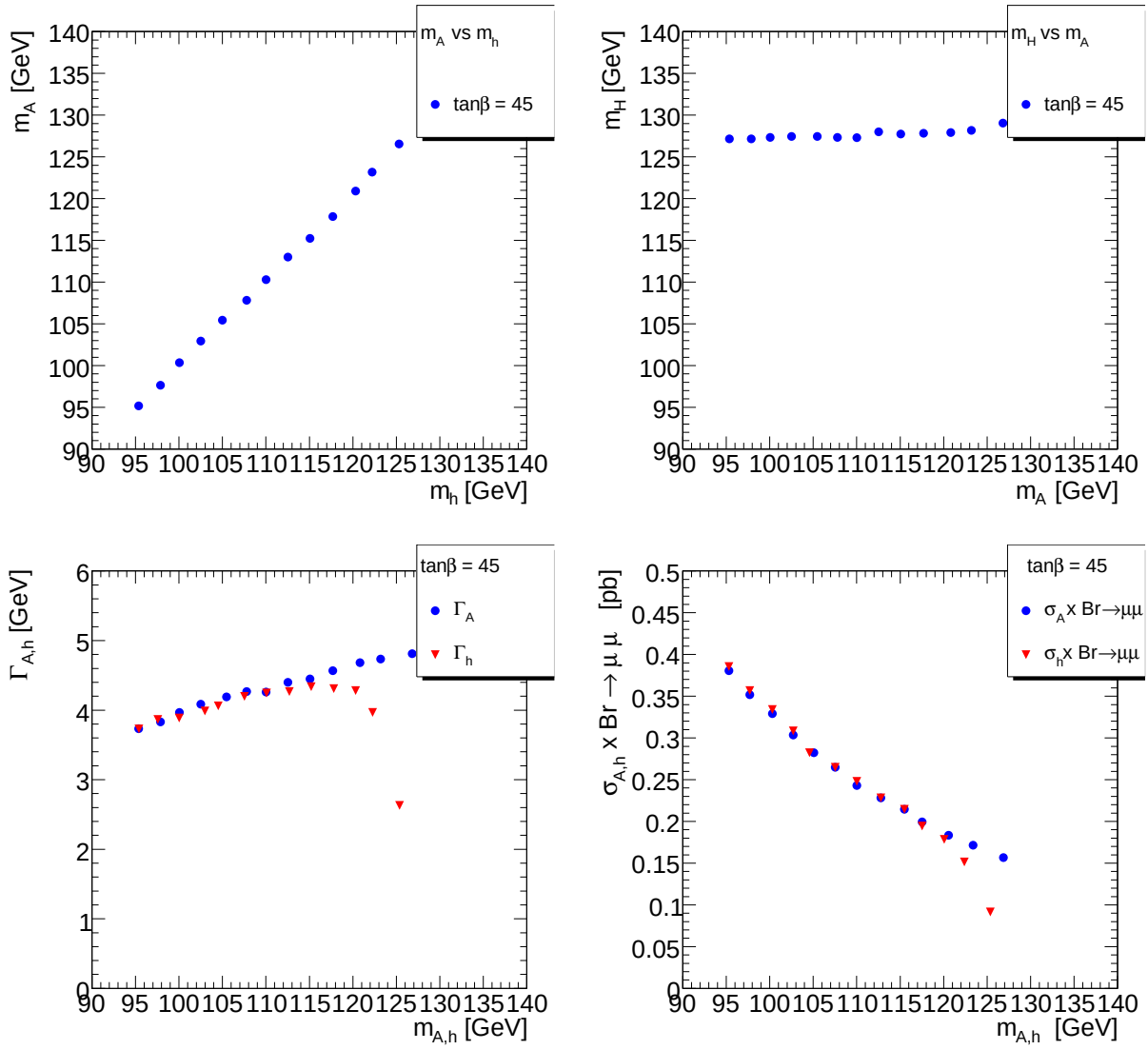

Figure 8:
(top left) m_{A}, the mass of the neutral A boson, as a function of m_{h}, the mass of the neutral h boson. (top right) m_{H}, the mass of the neutral H boson, as a function of m_{A}, the mass of the neutral A boson. (bottom left) $\Gamma_{\mathrm{A,h}}$, the width of the neutral A (black $\bullet$), h (red $\triangledown$) boson, as a function of its mass, $m_{\mathrm{A,h}}$. (bottom right) $\sigma_{\mathrm{A,h}}\cdot\mathrm{Br} \to \mu\mu$, the production cross section, $\sigma_{\mathrm{A,h}}$, times the muon pair branching ratio, $\mathrm{Br} \to \mu\mu = \mathrm{Br}_{\mathrm{A,h}\to\mu^+\mu^-}$, for the neutral A (black $\bullet$), h (red $\triangle$) boson, as a function of its mass, $m_{\mathrm{A,h}}$. All values are plotted at $\tan\beta = 45$ [17, 18].

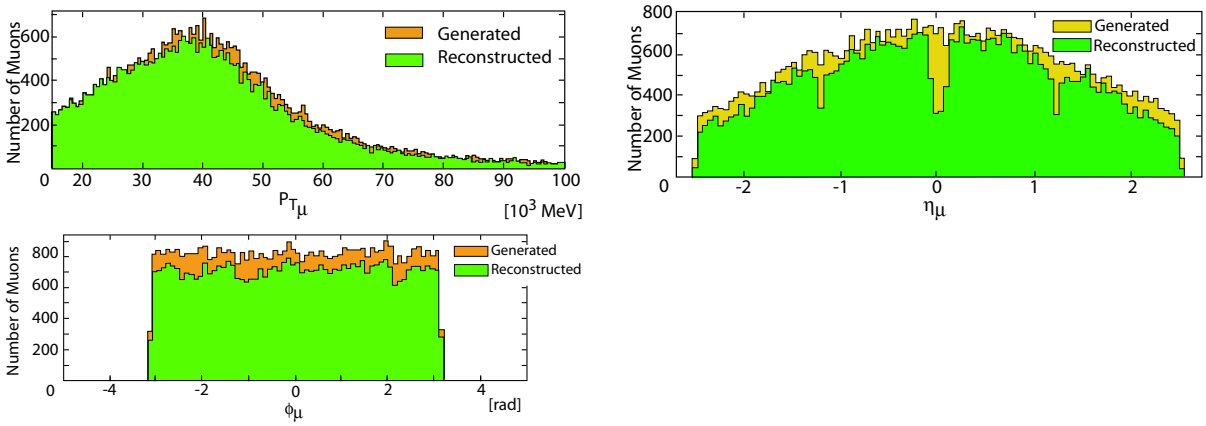

Figure 9: Distributions of the transverse momentum $P_{\mathrm{T}\mu}$, pseudorapidy η_μ and polar angle ϕ_μ for muons from Z$\rightarrow \mu^+\mu^-$ Monte Carlo events, generated (brown) and both reconstructed (green) within the $|\eta| \leq 2.5$ acceptance.

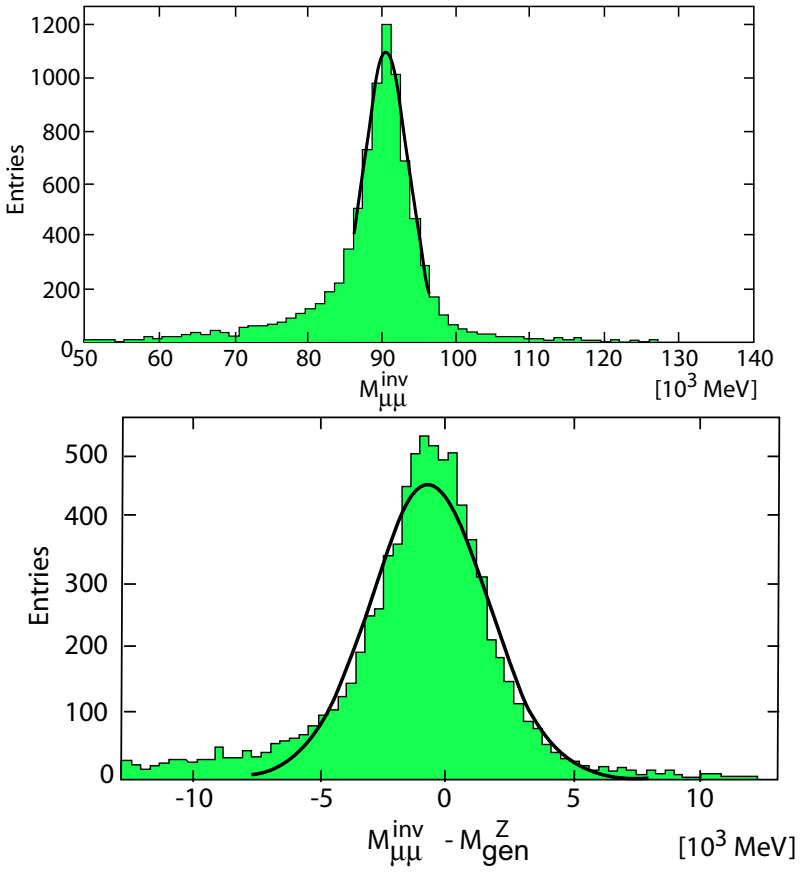

Figure 10: (top) Distribution of the invariant mass $M^{\mathrm{inv}}_{\mu\mu}$ reconstructed in Z$\rightarrow \mu^+\mu^-$ events. (bottom) Distribution of the difference between reconstructed and generated mass $M^{\mathrm{inv}}_{\mu\mu} - M^{\mathrm{Z}}_{\mathrm{gen}}$ for the same sample of events.

7.2 b-tagging studies

Two inclusive b-tagging algorithms used by the ATLAS collaboration, named 3D and SV2 [23], were studied in a subsample of $b\bar{b}h \to b\bar{b}\mu^+\mu^-$ events.

The first algorithm, 3D, is based on the computation of track weights from the transverse and longitudinal impact parameter significances for each jet track, as defined by the cone algorithm. The latter considers all particles inside a cone of opening angle: $\Delta R = \sqrt{\Delta\eta^2 + \Delta\phi^2}$ and requires at least one track reconstructed in the tracker. Two values of the opening angle were studied, $\Delta R = 0.7$ and $\Delta R = 0.4$. The track weight is given by the ratio of the likelihood functions for a track to originate from a b-jet or a u-jet which depend on the track significances.

In turn the jet weight, w_{jet}, is defined as the sum of the logarithms of the tracks weights. By applying different cuts on this variable, a rejection factor R_j is obtained for light jets (u, d, s quark and gluon) for a given b-jet selection efficiency ϵ_b.

The performance of the 3D b-tagging method can be improved by using additional information on secondary vertex in the jet, as it is done in the SV2 algorithm. This algorithm discriminates events by adding to the 3D information other variables, which are not too strongly correlated with the impact parameters (as *e.g.* fraction of the jet energy in the secondary vertex, invariant mass of all particles in the secondary vertex, number of two track secondary vertex).

In Tab. 6, the results on a study of a $b\bar{b}h \to b\bar{b}\mu^+\mu^-$ sample are reported. Similar results are obtained from a $b\bar{b}Z \to b\bar{b}\mu^+\mu^-$ sample.

For both samples, a selection cut, $P_{Tjet} > 15$ GeV, is applied, since below this value the efficiency of b-identification drops. The study is limited to the inner detector acceptance $|\eta| \leq 2.5$.

Algorithm	ΔR	ϵ_b	R_j	w_{cut}	ΔR	ϵ_b	R_j	w_{cut}
SV2	0.7	49%	71	1	0.4	50%	58	1
3D	0.7	55%	27	1	0.4	54%	26	1
SV2	0.7	46%	219	2	0.4	46%	200	2
3D	0.7	49%	52	2	0.4	49%	50	2

Table 6: b-tag performance. The table shows, for the two algorithms used, the jet opening angle ΔR, the efficiency on b-jet identification ϵ_b, the rejection of light quarks jets (udsc) R_j and the separation value between light and b jets w_{cut}.

As results of this study, it is possible to conclude that:

- The SV2 algorithm, which uses more information on b decays products, is more promising.
- No relevant improvement is obtained by shrinking the jet cone opening angle, ΔR, from 0.7 to 0.4. Therefore the ATHENA (v. 10.0.1) default value, ΔR=0.7, will be used in the following analysis.
- The cut value $w_{cut} = 1$ is a good compromise which provides a good b-jet identification by keeping the rejection of light jets at acceptable level.

8 Search for $b\bar{b}A \to b\bar{b}\mu^+\mu^-$, $b\bar{b}h \to b\bar{b}\mu^+\mu^-$

The signature of the h/A channel is a pair of well isolated high energy muons with opposite charge and two hadronic jets containing b quarks. The invariant mass of the reconstructed muons is supposed to originate from a h or A boson and must be compatible, within the mass resolution, with the corresponding mass, $m_{\rm h}$ or $m_{\rm A}$.

The main background sources, as discussed in Sec. 6, are the Z production followed by the decay to $\mu^+\mu^-$, with kinematical characteristics similar to the signal ones, and $t\bar{t} \to b\bar{b}\mu^+\mu^-\nu\bar{\nu}$ decays. The Z-pair production followed by the decay to $\mu^+\mu^-$ of one Z and the decay to $b\bar{b}$ of the other is less copious.

The event selection is divided in three steps: *preselection*, *tt selection*, *final selection*.

The *preselection*, cuts 1-2-3 in Tab. 7, requires in the event at least two well identified opposite charge muons with $P_{\rm T\mu} \geq 10$ GeV, in the pseudo-rapidity range $|\eta_\mu| \leq 2.5$ (cut 1). The presence of a jet pair, with $P_{\rm Tjet} \geq 10$ GeV and $|\eta_{\rm jet}| \leq 2.5$ is as well demanded, without any b-identification requirement (cut 2).
A further requirement (cut 3) is that at least one of these jets is identified as originating from a b-quark with $P_{\rm Tjet} > 15$ GeV, that is the energy lower limit for a reliable b-jet identification [23](Sec. 7.2). These cuts are designed to select events fulfilling the minimum conditions to be analyzed later. The events excluded are in any case not suitable to undergo any further analysis.

The *tt selection* is designed to suppress this background, characterized by a large missing transverse energy due to the presence of neutrinos, $E_{\rm T}^{\rm miss}$, requiring an upper bound less than 45 GeV (cut 4). Other cuts (cut 5-6) are applied on the first and second most large muon transverse momentum, $P_{\rm T\mu 1}$ and $P_{\rm T\mu 2}$, and (cut 7-8) on the first and second most large jet transverse momentum, $P_{\rm Tjet1}$ and $P_{\rm Tjet2}$. At least one of these jets was previously identified as originating from a b-quark (cut 3).

The *final selection* criteria are designed mainly to disentangle the signal events from the irreducible Z background. The main requirement is that the $\mu^+\mu^-$ invariant mass has to lie inside a window around h/A mass, determined by the natural width of the bosons and by the experimental resolution of the $\mu^+\mu^-$ invariant mass, Sec. 7.

The muons originating from b decays in bbbb events, with a cross section of ≈ 500 pb [24], can mimic the signal events. To avoid this possible contamination a low hadronic activity near both muons is required. The isolation criteria demands that the sum of the charged track momenta in a cone ($\Delta {\rm R} < 0.2$) around the muon direction be less than 5 GeV. These selection cuts are summarized in Tab. 7.

A key point of the selection is the determination of the mass window used (cut 9). Its value is determined as a function of $\Gamma_{\rm h}$ ($\Gamma_{\rm A}$), the total width of the h (A) Higgs boson, and the experimental mass resolution $\sigma_{\rm m} = 2.6\%$ (Sec. 7.1). The mass window is centered in $m_{\rm h}$ ($m_{\rm A}$), the h (A) mass:

$$m_{\rm h,A} - {\rm k} \pm {\rm f} \cdot \left(\left(\frac{\Gamma_{\rm h,A}}{2.36} \right)^2 + \sigma_{\rm m}^2 \right)^{\frac{1}{2}}, \qquad (5)$$

where k= -820 MeV is the shift factor (Sec. 7.1) correcting for the bias in the muon reconstruction and f is the standard deviation factor corresponding to a chosen probability. In our analysis f = 2, which corresponds to including 97.7% of the signal. The event is selected if its invariant mass is inside the window either for A or h mass. The same procedure is applied to

Cut Number	Variable
1	$N_\mu \geq 2$, $P_{\mathrm{T}\mu} \geq 10$ GeV, $\lvert\eta_\mu\rvert < 2.5$
2	$N_{\mathrm{jet}} \geq 2$, $P_{\mathrm{Tjet}} \geq 10$ GeV, $\lvert\eta_{\mathrm{jet}}\rvert < 2.5$
3	$N_{\mathrm{bjet}} \geq 1, P_{\mathrm{Tjet}} \geq 15$ GeV, $\mathrm{w_{btag}} > 1$
4	$E_{\mathrm{T}}^{\mathrm{miss}} < 45$ GeV
5	25 GeV $< P_{\mathrm{T}\mu 1} <$ 95 GeV
6	20 GeV $< P_{\mathrm{T}\mu 2} <$ 60 GeV
7	$P_{\mathrm{Tjet2}} < 40$ GeV
8	$P_{\mathrm{Tjet1}} < 70$ GeV
9	$\lvert M_{\mu\mu}^{\mathrm{inv}} - m_{\mathrm{A}}\rvert$ or $\lvert M_{\mu\mu}^{\mathrm{inv}} - m_{\mathrm{h}}\rvert < 2\sigma$
10	$\Sigma\lvert P_{\mathrm{Ttracks}}\rvert <$ 5 GeV in cone ΔR $<$ 0.2

Table 7: Selection criteria for h/A $\rightarrow \mu^+\mu^-$ with two b-quarks final state.

the H search (Sec. 11).

Appendix B, shows, for the tanβ values considered, the h/A/H masses, $m_{\mathrm{h,A,H}}$ - k = $\mathrm{m}_{\mathrm{h,A,H}}^{\mathrm{corr}}$, corrected for the shift factor k and the selection window, $\xi_{\mathrm{h,A,H}} = ((\frac{\Gamma_{\mathrm{h,A}}}{2.36})^2 + \sigma_{\mathrm{m}}^2)^{\frac{1}{2}}$.

The distribution of the variables used in this selection are reported step by step, before applying the cut concerned, in Appendix C, for all signals and backgrounds studied. The most significant distributions, calculated at a reference point in the plane (m_{A}, tanβ), will be discussed in Sec. 8.1.

8.1 Reference Point

In this section the analysis procedure is discussed for the reference point $m_{\mathrm{A}} = 110.31$ GeV, tan$\beta = 45$ ($m_{\mathrm{h}} = 110.00$ GeV, $m_{\mathrm{H}} = 127.46$ GeV).

For the three bosons considered the production cross section times the $\mu^+\mu^-$ decay branching ratio, $\sigma_{\mathrm{b\bar{b}}\mu^+\mu^-}$, the expected number of signal events at $\int \mathcal{L}\,\mathrm{d}t \approx 300$ fb^{-1}, $\mathrm{N}^{\mathrm{exp}_{300}}$, the number of Monte Carlo generated events N^{MC} and their weight w are reported In Tab. 8.
The weight of the signal events is close to one as it is for all (m_{A}, tanβ) points listed in Appendix D. The background weights (Tab. 5) are also close to one.

The H search, due to the very low cross section, will be described in Sec. 11.

process (signal)	$\sigma_{\mathrm{b\bar{b}}\mu^+\mu^-}$ [pb]	$\mathrm{N}^{\mathrm{exp}_{300}}$	N^{MC}	w
$\mathrm{b\bar{b}h} \rightarrow \mathrm{b\bar{b}}\mu^+\mu^-$	0.245	73500	76517	0.96
$\mathrm{bbA} \rightarrow \mathrm{bb}\mu^+\mu^-$	0.2433	72900	74965	0.97
$\mathrm{bbH} \rightarrow \mathrm{bb}\mu^+\mu^-$	0.001619	486	600	0.88

Table 8: h, A, H production at the reference point tan$\beta = 45$, $m_{\mathrm{A}} = 110.31$ GeV($m_{\mathrm{h}} = 110.00$ GeV, $m_{\mathrm{H}} = 127.46$ GeV): process, cross section times $\mu^+\mu^-$ decay branching ratio, $\sigma_{\mathrm{b\bar{b}}\mu^+\mu^-}$, number of events expected for $\int \mathcal{L}\,\mathrm{d}t \approx 300$ fb^{-1}, $\mathrm{N}^{\mathrm{exp}_{300}}$, number of Monte Carlo generated events, N^{MC}, their weight w.

The distributions of the number of muons N_μ and of the muon transverse momentum $P_{\mathrm{T}\mu}$ in the processes $\mathrm{b\bar{b}h} \rightarrow \mathrm{b\bar{b}}\mu^+\mu^-$ and $\mathrm{b\bar{b}Z} \rightarrow \mathrm{b\bar{b}}\mu^+\mu^-$are displayed in Fig. 11 for the generated (hatched) and reconstructed (full color) events without any cut applied. These distributions

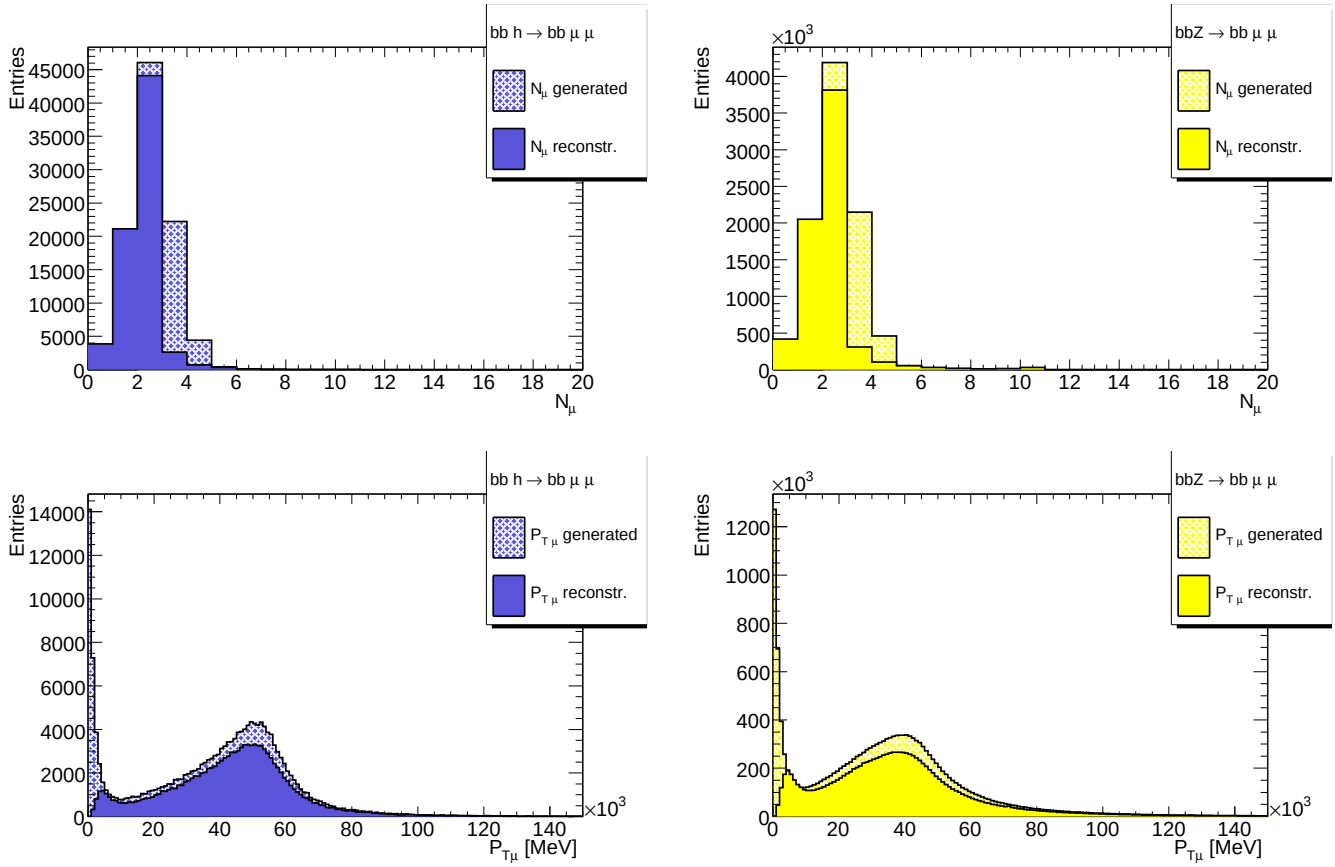

Figure 11: **Without cut.** Distributions of the number of muons N_μ (top) and of the transverse momentum $P_{\mathrm{T}\mu}$ (bottom) for generated (hatched) and reconstructed (full color) events are plotted without cuts applied: a) $\mathrm{b\bar{b}h} \to \mathrm{b\bar{b}}\mu^+\mu^-$ events at the reference point ($\tan\beta = 45$, $m_{\mathrm{h}} = 110.00$ GeV)(left, dark blue); b) $\mathrm{b\bar{b}Z} \to \mathrm{b\bar{b}}\mu^+\mu^-$ events (right, yellow). All distributions are normalized at $\int \mathcal{L}\,\mathrm{d}t = 300$ fb^{-1}.

as well as the distributions of the other variables used in the analysis (see above) are shown in Appendix C for each signal and background channel considered. In all cases the reconstructed distributions without cuts (full colour) compare to the generated distributions (hatched colour) as expected.

The *preselection* requirement on muon pair (cut 1, Tab. 7) reduces approximately to same fraction signal ($\sim 62\%$) and background (Z$\sim 59\%$, $\mathrm{t\bar{t}} \sim 67\%$). The requirement on jet pair (cut 2) leaves almost untouched $\mathrm{t\bar{t}}$ ($\sim 63\%$) reducing Z to $\sim 54\%$, because of the more energetic P_{Tjet} spectra of the top decay (Appendix C). Unfortunately this cut reduces the signal sample significantly to $\sim 30\%$ for the same reason, see Tab. 9.

The mean jet transverse momentum $< P_{\mathrm{Tjet}} >$ is ~ 2.6 GeV for the MSSM h boson, and ~ 3.6 GeV for Z decays, see Fig. 12 and Appendix C. Then, as stated in Sec. 5.2, the requirement that two b-jets be identified will not enhance the signal over this specific background. This requirement will suppress more the signal than the Z background, since the two b-jets of this background events are usually more energetic than those accompanying the signal. According to the study in Sec. 7.2, the b-tag requirement is applied by requiring one jet in the event.

After the three preselection cuts (1-2-3) the signal sample of h or A is reduced to $\sim 10\%$. The backgrounds are reduced to $\sim 17\%$ for the Z, $\sim 53\%$ for $\mathrm{t\bar{t}}$, and $\sim 28\%$ for ZZ.

The *tt selection* is designed to exploit features of t decays. The $\mathrm{t\bar{t}}$ sample is characterized by a transverse missing energy $E_{\mathrm{T}}^{\mathrm{miss}}$, which, due to neutrinos, is larger than in the h/A sample,

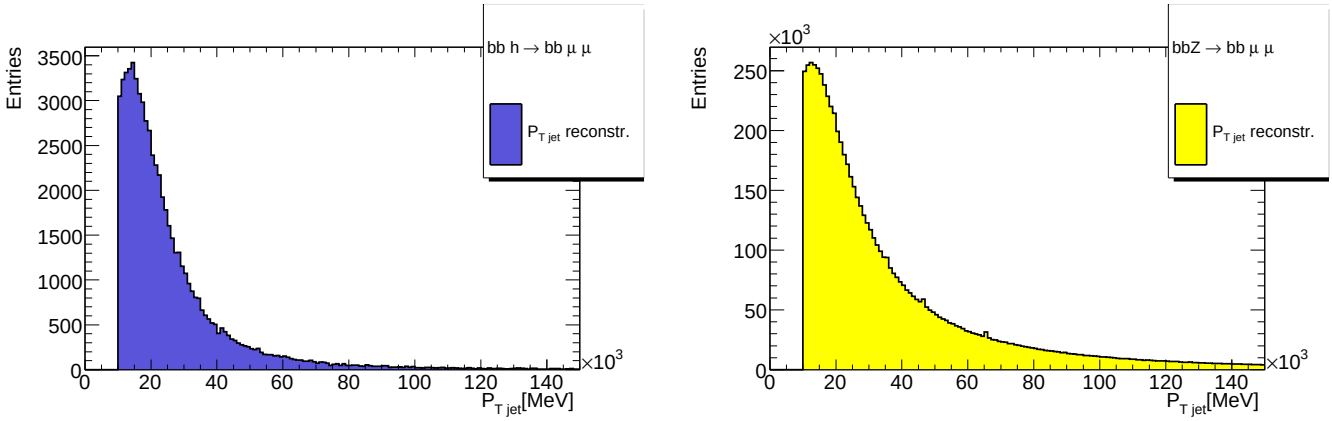

Figure 12: **After 1-2 cuts.** Distributions of the reconstructed jet transverse momentum P_{Tjet} are plotted after cuts 1 and 2 (Tab. 7) for :
a) $b\bar{b}h \to b\bar{b}\mu^+\mu^-$ events at the reference point ($\tan\beta = 45$, $m_{\mathrm{h}} = 110.00$ GeV), (left, dark blue); b) $b\bar{b}Z \to b\bar{b}\mu^+\mu^-$ events (right, yellow). All distributions are normalized at $\int \mathcal{L}\,dt = 300$ fb^{-1}.

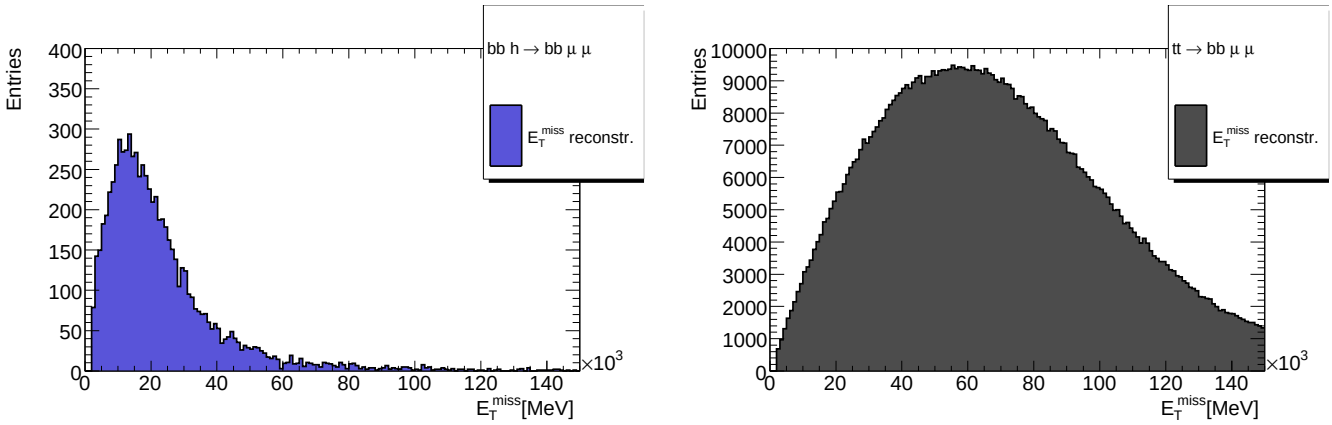

Figure 13: **After 1-2-3 cuts.** Distributions of the reconstructed transverse missing energy $E_{\mathrm{T}}^{\mathrm{miss}}$ are plotted after cuts 1, 2 and 3 (Tab. 7) for :
a) $b\bar{b}h \to b\bar{b}\mu^+\mu^-$ events at the reference point ($\tan\beta = 45$, $m_{\mathrm{h}} = 110.00$ GeV), (left, dark blue); b) $t\bar{t} \to b\bar{b}\mu^+\mu^-\nu\bar{\nu}$ events (right, gray). All distributions are normalized at $\int \mathcal{L}\,dt = 300$ fb^{-1}.

as shown in Fig. 13. The $E_{\mathrm{T}}^{\mathrm{miss}}$ cut (cut 4, Tab. 7) is extremely effective reducing $t\bar{t}$ to $\sim$ 14 % of the original sample while keeping the signal at $\sim$ 9 % almost unchanged and the Z background at $\sim$ 14 %. The two cuts (5-6), related to $P_{\mathrm{T}\mu}$ distributions, reduce the $t\bar{t}$ original sample to $\sim$ 8 %, but are little effective on the Z sample (to $\sim$ 10%) and the signal samples of h and A (to $\sim$ 8 %). A further reduction of the $t\bar{t}$ background to 1.4 % is obtained by applying cuts (7-8) on P_{Tjet}. At this stage, the Z sample is reduced to $\sim$ 5.8 % while the h signal as well as the A signal is reduced to 6.0 %, see Fig. 14.

To apply the *final selection* (cut 9, Tab. 7) against the Z background, the selection window and center value have to be determined. At the reference point ($m_{\mathrm{A}} = 110.31$ GeV, $\Gamma_{\mathrm{A}} = 4.28$ GeV and $m_{\mathrm{h}} = 110.00$ GeV , $\Gamma_{\mathrm{h}} = 4.20$ GeV), Eq. 5 implies to look for the A signal in a window, ξ_{A}, of 3.394 GeV around a corrected mass value, $m_{\mathrm{A}}^{\mathrm{corr}}$, of 109.490 GeV, and for the h signal in a window, ξ_{h}, of 3.369 GeV around $m_{\mathrm{h}}^{\mathrm{corr}} = 109.180$ GeV (see Appendix B for the others values of $\tan\beta$, m_{A} and m_{h}). As for the probability requirement f = 2, the windows ξ_{h} and ξ_{A} are increased by a factor 2 to obtain the effective selection window used in Tab. 11.

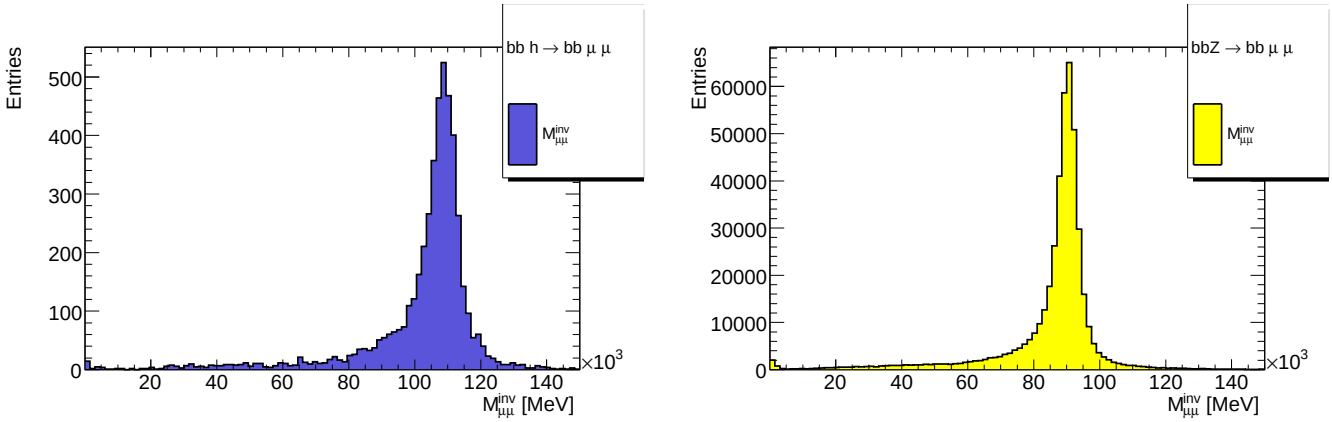

Figure 14: **After 1-8 cuts.** Distributions of the reconstructed $\mu^+\mu^-$ invariant mass $M^{\rm inv}_{\mu\mu}$ are plotted after cuts 1 – 8 (Tab. 7) for:
a) $b\bar{b}h \to b\bar{b}\mu^+\mu^-$ events at the reference point ($\tan\beta = 45$, $m_{\rm h} = 110.00$ GeV) (left, dark blue); b) $b\bar{b}Z \to b\bar{b}\mu^+\mu^-$ events (right, yellow). All distributions are normalized at $\int \mathcal{L}\,dt = 300$ fb^{-1}.

This cut reduces drastically the background samples, the Z to less than 0.13%, the $t\bar{t}$ to 0.17 % and the ZZ to a negligible 0.24 %. The event signal surviving in both A and h channels is $\sim$ 4.2 %.

The last reduction (cut 10) on muon isolation does not change significantly the previous results. Indeed this cut is expected to be effective in the data against the heavy flavour QCD background, and cannot be tested properly in Monte Carlo.

Process	$N^{exp_{300}}$	N^{MC}	N_{1cut}	N_{2cut}	N_{3cut}
$b\bar{b}h \to b\bar{b}\mu^+\mu^-$	73500	76517	47099	22969	7907
$b\bar{b}A \to b\bar{b}\mu^+\mu^-$	72900	74965	46247	22693	7919
$b\bar{b}H \to b\bar{b}\mu^+\mu^-$	486	600	394	222	95
$b\bar{b}Z \to b\bar{b}\mu^+\mu^-$	6836700	3314000	1945387	1178864	579751
$t\bar{t} \to b\bar{b}\mu^+\mu^-\nu\bar{\nu}$	1713420	1806437	1217706	1137780	953928
$ZZ \to b\bar{b}\mu^+\mu^-$	33819	97244	46487	38600	27744

Table 9: *Preselection.* Signal/Background process, number of events expected at $\int \mathcal{L}\,dt \approx 300$ fb^{-1}, $N^{exp_{300}}$, number of Monte Carlo events generated, N^{MC}, and after three preselection steps, N_{1cut}, N_{2cut} and N_{3cut} (Tab. 7). The signal is evaluated at the reference point ($\tan\beta$=45 , $m_{\rm A} = 110.31$ GeV, $m_{\rm h} = 110.00$ GeV). Cuts 1 to 3 are described in Tab. 7

8.2 Reference point conclusions

The signal events selected as A or h bosons and the (weighted) background events are plotted in Fig. 15. The A and h signal (light blue) is clearly visible on top of the remaining background events (Z $t\bar{t}$ and ZZ added up, dark brown).

The significance $\frac{S}{\sqrt{B}}$ at $\int \mathcal{L}\,dt \approx 300$ fb^{-1} is $\sim$ 56, scaling down to $\sim$ 18 at $\int \mathcal{L}\,dt \approx 30$ fb^{-1} and $\sim$ 10 at $\int \mathcal{L}\,dt \approx 10$ fb^{-1}. We can conclude that if $m_{\rm h} = 110.00$ GeV and consequently $m_{\rm A} = 110.31$ GeV there is a high probability for these bosons to be discovered at the beginning of data taking.

Process	N_{3cut}	N_{4cut}	N_{5cut}	N_{6cut}	N_{7cut}	N_{8cut}
$b\bar{b}h \to b\bar{b}\mu^+\mu^-$	7907	7099	6234	5575	5085	4636
$b\bar{b}A \to b\bar{b}\mu^+\mu^-$	7919	7096	6183	5575	5118	4595
$b\bar{b}H \to b\bar{b}\mu^+\mu^-$	95	78	66	54	50	44
$b\bar{b}Z \to b\bar{b}\mu^+\mu^-$	579751	478106	397030	334609	226414	193334
$t\bar{t} \to b\bar{b}\mu^+\mu^-\nu\bar{\nu}$	953928	256662	190672	143746	41954	25567
$ZZ \to b\bar{b}\mu^+\mu^-$	27744	24516	19102	15957	10926	8574

Table 10: *tt selection.* Signal/Background process, number of Monte Carlo generated events after the preselection cut 3 and cuts 4 to 8. The signal is evaluated at the reference point (tanβ=45 , m_A = 110.31 GeV, m_h = 110.00 GeV). Cuts 3 to 8 are described in Tab. 7.

Process	N_{8cut}	N_{9cut}	N_{10cut}
$b\bar{b}h \to b\bar{b}\mu^+\mu^-$	4636	3212	3165
$b\bar{b}A \to b\bar{b}\mu^+\mu^-$	4595	3151	3110
$b\bar{b}H \to b\bar{b}\mu^+\mu^-$	44		
$b\bar{b}Z \to b\bar{b}\mu^+\mu^-$	193334	4496	4206
$t\bar{t} \to b\bar{b}\mu^+\mu^-\nu\bar{\nu}$	25567	3148	2969
$ZZ \to b\bar{b}\mu^+\mu^-$	8574	260	234

Table 11: *Final selection.* Signal/Background process, number of Monte Carlo generated events, after cut 8 and successive cuts 9 and 10. The signal is evaluated at the reference point (tanβ = 45, m_A = 110.31 GeV, m_h = 110.00 GeV). Cuts 8 to 10 are described in Tab. 7 (see text for cut 9 window).

9 Search for $b\bar{b}A \to b\bar{b}\mu^+\mu^-$, $b\bar{b}h \to b\bar{b}\mu^+\mu^-$ in the MSSM plane

A search for neutral Higgs bosons h/A has been performed in the (tanβ, m_A) plane, in $m_h - max$ scenario, inside the limits described in Sec. 6, tanβ between 15 and 50, in steps of 5, m_h between 95 GeV and 125 GeV, in steps of 2.5 GeV.

The analysis described in Sec. 8 has been repeated for all 104 simulated points and the results are summarized in Appendix D, where for each point are reported the number of events expected at $\int \mathcal{L}\, dt \approx 300$ fb^{-1}, N_h^{exp300} (N_A^{exp300}) and Monte Carlo generated, N_h^{MC} (N_A^{MC}), for the h (A) boson.

For each point the aimed statistics has been reached giving weight factors, w_A and w_h, close to unity [6]. The final numbers of events (cut 1-10, Tab. 7) N_A^{sel} and N_h^{sel}, for the h and A signal, and N_{bbZ}^{sel}, N_{tt}^{sel} and N_{ZZ}^{sel} for the background ($b\bar{b}Z$, $t\bar{t}$, ZZ) are reported as well[7].

The use of an asymmetric selection window, centered at $m_{h,A}^{corr}$ has been tested for masses below 100 GeV, with a view to exclude the Z events, however without obtaining a significantly improved result ($\sim 10\%$) A symmetric window as described in Sec. 8 was thus applied to all masses, Appendix B.

The above information will permit to draw the results to be discussed in Sec. 10.

[6] First table of each tanβ, title: Event sample

[7] Second table of each tanβ value, title: Selection and Significance for h/A sample.

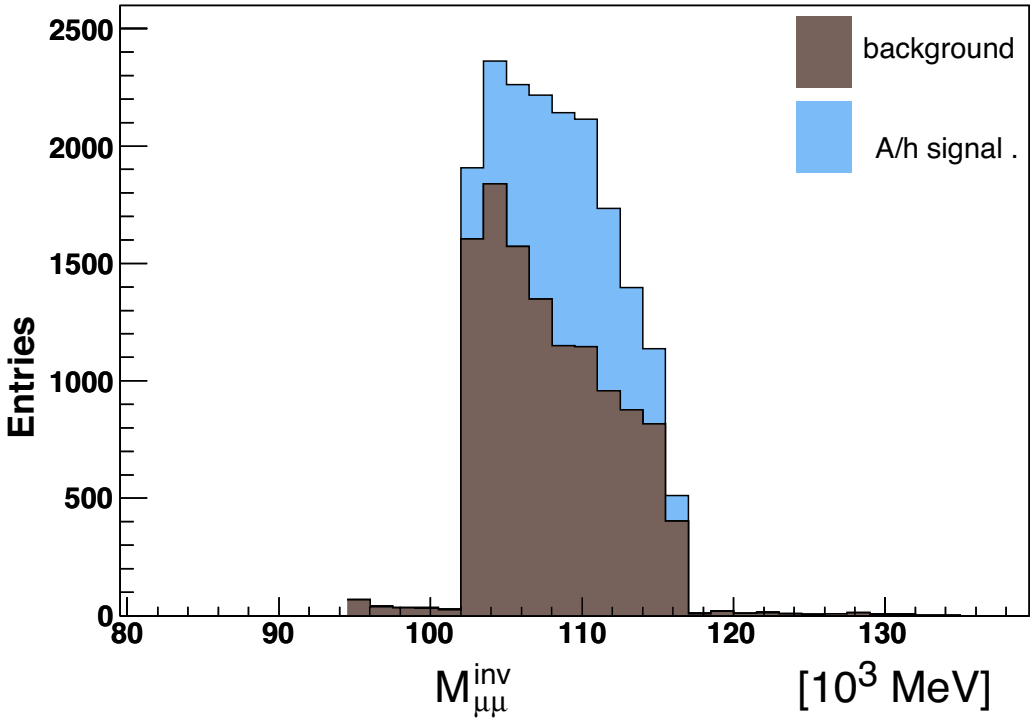

Figure 15: Distributions of the reconstructed $\mu^+\mu^-$ invariant mass, $M^{\rm inv}_{\mu\mu}$, for signal and backgrounds events, after all selection cuts (Tab. 7) at the reference point ($\tan\beta$ = 45, $m_{\rm A}$ = 110.31 GeV, $m_{\rm h}$ = 110.00 GeV); background events may contribute with more than one entry. The two distributions are normalized at $\int \mathcal{L}\,{\rm d}t$= 300 fb^{-1}. The h/A signal (light blue) emerge over the background (Z, t$\bar{\rm t}$ and ZZ) (dark brown).

10 Results on the search for $\rm b\bar{b}A \to b\bar{b}\mu^+\mu^-$, $\rm b\bar{b}h \to b\bar{b}\mu^+\mu^-$ in the MSSM plane

The significance of a search is given using $\frac{S}{\sqrt{B}}$ as a statistical estimator, where S indicates the number of signal events (h/A or h/A/H), and B the number of background events. Discovery means that the signal is larger than 5 times the background statistical error ($\frac{S}{\sqrt{B}} \geq 5$). The probability of a background fluctuation of this size is less than $\approx 2.87 \cdot 10^{-7}$. A search resulting in $\frac{S}{\sqrt{B}} \geq 3$ is interpreted as an indication of new physics. We conclude to its exclusion (within the sensitivity of the experiment) if $\frac{S}{\sqrt{B}} < 1.5$.

In Appendix D in addition to the information described in Sec. 9, the search significance is also reported, for different data taking scenarios, $S^{300}_{\rm h,\,A}$ for $\int \mathcal{L}\,{\rm d}t \approx 300$ fb^{-1}, $S^{30}_{\rm h,\,A}$ for $\int \mathcal{L}\,{\rm d}t \approx 30$ fb^{-1}, and $S^{10}_{\rm h,\,A}$ for $\int \mathcal{L}\,{\rm d}t \approx 10$ fb^{-1}. The values for the two lower luminosities were derived from the first one, which corresponds to the highest statistics.

The search significance for the h/A neutral boson is also shown, in the three luminosity scenarios, as a function of $m_{\rm A}$ up to highest allowed value of $m_{\rm h}$, in Fig. 16 for all scanned values of $\tan\beta$.

One should note that large h/A masses are penalized by a small cross section, thus implying a lower significance, while the masses near to $m_{\rm Z}$ suffer from the difficulty in disentangling the neutral Higgs boson signal from the Z background.

The best mass range for an early discovery of h is between 100 and 120 GeV at any given $\tan\beta$. If $\tan\beta > 30$ a large range of masses is accessible to discovery even after the first year

of data taking. More integrated luminosity, between $\approx$ 30 and 50 fb^{-1}, is needed for tanβ between 30 and 20. The discovery at tanβ = 15 demands a luminosity of $\approx$ 150 fb^{-1}, making the exploration of this region possible only after a few years of data taking.

These considerations are summarized in Fig. 17, where the minimum integrated luminosity $\int \mathcal{L}\,dt$, demanded for a 5 σ discovery of the h/A neutral Higgs boson, is plotted as a function of m_A up to highest allowed value of m_h, at given tanβ values. With a $\int \mathcal{L}\,dt \approx 10$ fb^{-1}, corresponding to one year of data taking, most of the masses are accessible if tan$\beta > 30$. More integrated luminosity is needed for tanβ = 20 and tanβ = 15. Low masses need as well more luminosity in order to extract the evidence of a signal from the most copious Z background.

Discovery contours in the (tanβ, m_A) plane are shown, in Fig. 18, in different $\int \mathcal{L}\,dt$ scenarios. for a significance of 5 (discovery, on the left) and of 3 (on the right) . The latter can interpreted as the contour region for an early indication of a signal or, in case of negative search, for its exclusion.

11 Search for $b\bar{b}H \to b\bar{b}\mu^+\mu^-$ in the MSSM plane

To increase the discovery potential for a neutral Higgs boson discovery in the region up 139 GeV a search for the neutral Higgs boson H has been performed in the (tanβ, m_A) plane inside the limits used for the h/A search (Sec. 9). This search requested a separated analysis due to the higher mass region involved. The procedure is the same followed for the h/A search (Sec. 8) with the value of the selection window, ξ_H, centered at the H mass, corrected for the experimental shift, m_H^{corr} (Appendix B). Due to the extremely low cross section of the H in this mass region, for a few masses with a cross section times $\mu^+\mu^-$ branching ratio $\sigma_H \cdot Br_{\mu^+\mu^-}$ smaller than 0.01 pb, common values of m_H^{corr} and ξ_H were chosen, corresponding to the mean values in that mass region. This procedure doesn't affect any result due the narrow spread of values for the mass m_H and the natural width Γ_H, implying that the window value is essentially dominated by the experimental resolution. The results are summarized in Appendix E, where are also given the values m_H^{corr} and ξ_H used in the selection for the window center and width.

From Appendix E it is clear that the discovery of the boson H demands a high integrated luminosity, $\int \mathcal{L}\,dt \approx 300$ fb^{-1}, and it would be possible at masses corresponding to m_h = 122.50 GeV and 125 GeV for values of tan$\beta \geq 30$. At tanβ = 25, only the mass m_H = 134.42 GeV (corresponding to m_h = 125 GeV) is accessible. Lower values of tanβ are excluded even at high masses.

In conclusion, a discovery of H boson is possible only in a few points of the parameter space, for a value of m_A around the maximum value of m_h , at the ultimate luminosity expected at the LHC.

12 Combined search for $b\bar{b}A \to b\bar{b}\mu^+\mu^-$, $b\bar{b}h \to b\bar{b}\mu^+\mu^-$, $b\bar{b}H \to b\bar{b}\mu^+\mu^-$ in the MSSM plane

The results of Sec. 11 on the H boson search were combined with the results from the h/A search (Sec. 9). To this purpose, the H analysis was repeated with a window not overlapping with the h/A window, thus avoiding the double counting of background events. This work was performed only for high m_h values, where the cross section times the $\mu^+\mu^-$ branching ratio (Sec. 11) has values $\geq$ 0.01 pb. In Appendix F, the numbers of selected background events (not included in the h/A background) are listed. It is straightforward to obtain the significance

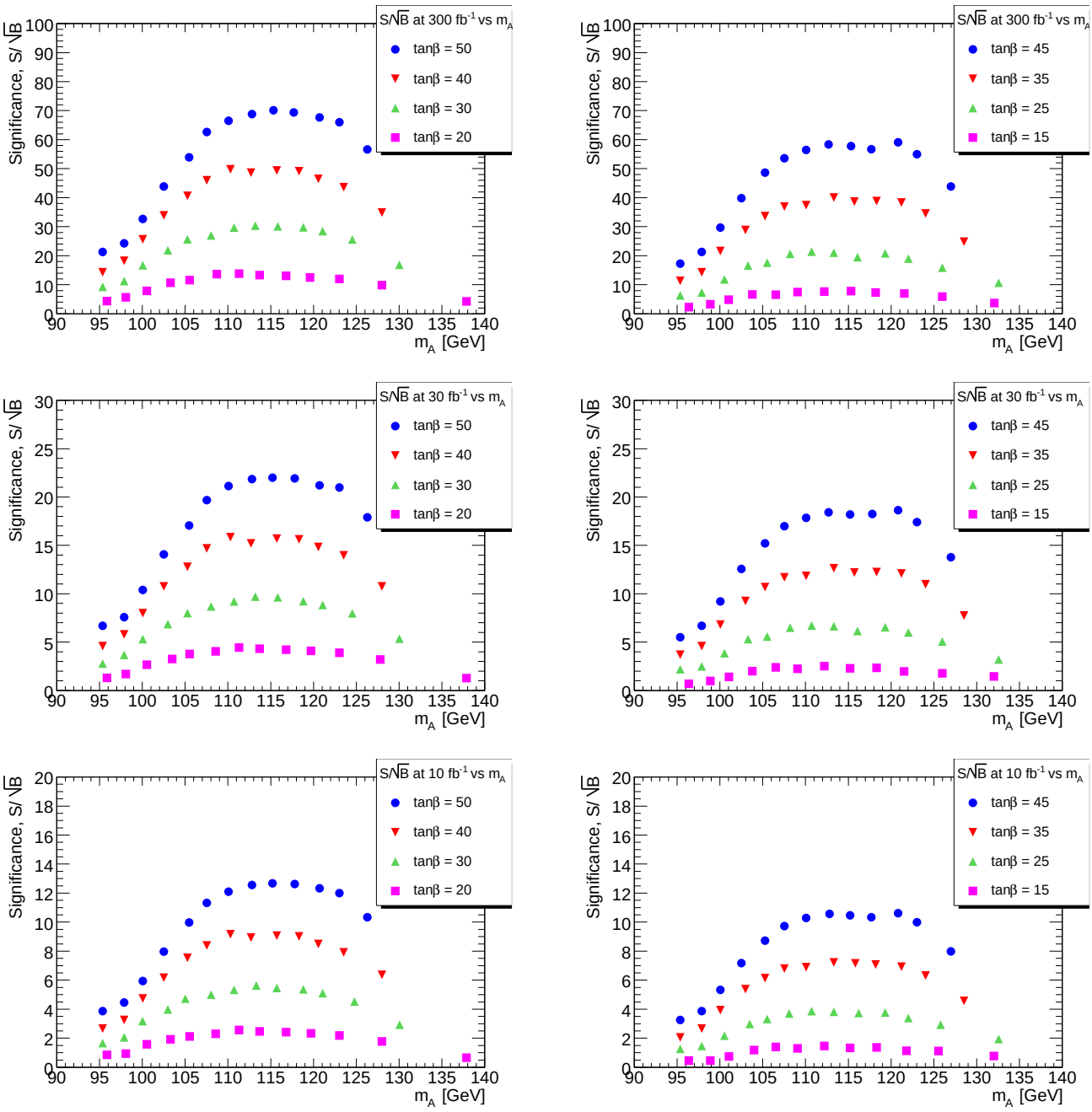

Figure 16: Search significance $\frac{S}{\sqrt{B}}$ for a h/A neutral Higgs boson, as a function of m_{A} up to the largest allowed value of m_{h} in three different data taking scenarios, $\int \mathcal{L}\,\mathrm{d}t$ = 300 , 30 and 10 fb^{-1} (S is the number of h/A signal events, B is the number of background events). On the left the results for tanβ = 50, 40, 30, 20, and on the right the results for tanβ = 45, 35, 25, 15. The data are listed in Appendix D.

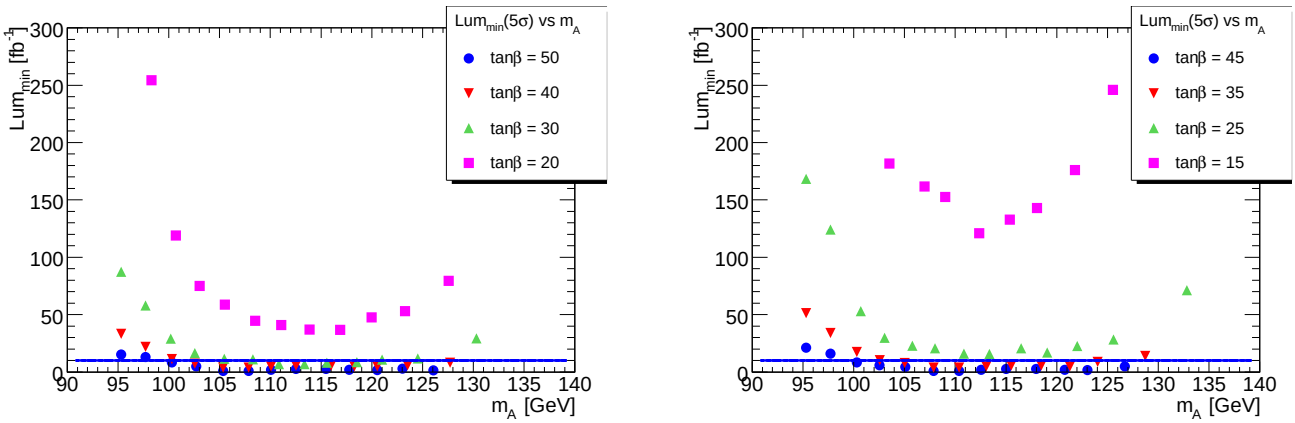

Figure 17: Minimum integrated luminosity $\int \mathcal{L}\,dt$ demanded for a 5 σ discovery of the h/A neutral Higgs boson as a function of $m_{\rm A}$ up to largest allowed value of $m_{\rm h}$. On the left the results for tanβ = 50, 40, 30, 20, and on the right the results for tanβ = 45, 35, 25, 15. The blue horizontal line is $\int \mathcal{L}\,dt$ = 10 fb^{-1}. The data are listed in Appendix D.

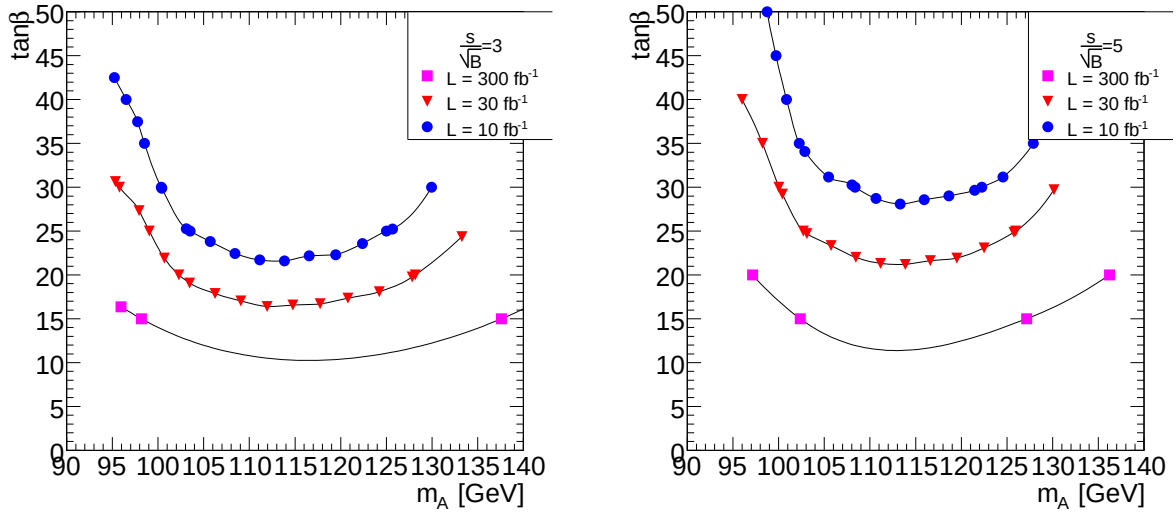

Figure 18:
Discovery potential for a neutral Higgs boson h/A of mass $m_{\rm A}$ decaying to $\mu^+\mu^-$, accompanied by two b-jets, in the $m_{\rm h} - max$ scenario (Sec. 2), as a function of $m_{\rm A}$: contours are drawn for a search significance $\frac{S}{\sqrt{B}}$ = 5 (left) and $\frac{S}{\sqrt{B}}$ = 3 (right), with an integrated luminosity of $\int \mathcal{L}\,dt$ = 300 (top), 30 (center) and 10 (bottom) fb^{-1}.

of this search by adding the h, A (Appendix D) to the H selected events (Appendix E). The backgrounds events in Appendix D and Appendix F are the total background sample. In Appendix F are also listed for different luminosities, $\int \mathcal{L}\,dt \approx 300$, 30 and 10 fb^{-1}, the values of the total significance $S^{300}_{\mathrm{h,\,A,\,H}}$, $S^{30}_{\mathrm{h,\,A,\,H}}$ and $S^{10}_{\mathrm{h,\,A,\,H}}$. As a comparison, $S^{300}_{\mathrm{h,\,A,\,H}}$, the value of the significance at 300 fb^{-1} for the search of the alone h/A , is also reported.

For reader's convenience the situation is summarized in Tab. 12, where the significance of the exclusive search for the h/A boson ($S^{300}_{\mathrm{h,\,A}}$, $S^{30}_{\mathrm{h,\,A}}$, $S^{10}_{\mathrm{h,\,A}}$) and the corresponding significance including the H search ($S^{300}_{\mathrm{h,\,A,\,H}}$, $S^{30}_{\mathrm{h,\,A,\,H}}$ and $S^{10}_{\mathrm{h,\,A,\,H}}$) are shown.

The additional H search contributes to a neutral Higgs boson discovery for tan$\beta > 15$ at the ultimate luminosity. Otherwise the contribution of this search is negligible, for a value of m_{A} around the maximum value of m_{h} , as expected from the low cross section, and the large number of background events (being m_{H} close to m_{Z}).

tanβ	$\mathbf{m}_{\mathrm{h}}^{\mathrm{nom}}$ [10^3MeV]	m_{H} [MeV]	$S^{300}_{\mathrm{h,\,A}}$	$S^{30}_{\mathrm{h,\,A}}$	$S^{10}_{\mathrm{h,\,A}}$	$S^{300}_{\mathrm{h,\,A,\,H}}$	$S^{30}_{\mathrm{h,\,A,\,H}}$	$S^{10}_{\mathrm{h,\,A,\,H}}$
15	**122.50**	136180	3.86	1.22	0.70	5.09	1.64	0.93
15	**125.00**	152610	1.51	0.48	0.28	2.27	0.73	0.19
20	**122.50**	131870	9.76	3.08	1.78	11.69	3.77	2.14
20	**125.00**	139490	4.63	1.47	0.85	7.25	2.34	0.76
25	**122.50**	130020	15.98	5.05	2.92	17.51	5.65	3.2
25	**125.00**	134420	10.27	3.25	1.88	15.20	4.9	2.78
30	**122.50**	129090	25.13	7.95	4.59	27.01	8.71	4.94
30	**125.00**	131890	16.13	5.10	2.95	22.88	7.36	4.18
35	**122.50**	128560	34.71	10.97	6.34	35.29	11.38	6.45
35	**125.00**	130470	24.18	7.65	4.41	32.66	10.54	5.09
40	**122.50**	128260	43.68	13.81	7.98	43.95	14.18	8.03
40	**125.00**	129610	34.02	10.76	6.21	43.56	14.05	7.96
45	**120.00**	127790	59.03	18.67	10.78	54.16	17.47	9.90
45	**122.50**	128090	54.70	17.30	9.99	54.61	17.62	9.98
45	**125.00**	129090	43.54	13.77	7.95	53.90	17.38	9.85
50	**120.00**	127780	67.10	21.22	12.25	60.72	19.59	11.10
50	**122.50**	128020	65.55	20.73	11.97	65.27	21.10	11.93
50	**125.00**	128760	56.16	17.76	10.25	66.70	21.52	12.19

Table 12: Significance of A/h and A/h/H searches. The significance values for the two searches, $S^{300}_{\mathrm{h,\,A}}$, $S^{30}_{\mathrm{h,\,A}}$, $S^{10}_{\mathrm{h,\,A}}$and $S^{300}_{\mathrm{h,\,A,\,H}}$, $S^{30}_{\mathrm{h,\,A,\,H}}$, $S^{10}_{\mathrm{h,\,A,\,H}}$, at $\int \mathcal{L}\,dt = 300$, 30, 10 fb^{-1}, respectively, are given for a set of tanβ values and two values of the mass of the lightest neutral Higgs boson, $m_{\mathrm{h}}^{\mathrm{nom}}$. The mass m_{H} of the corresponding H Higgs boson is also noted.

13 Conclusions

The possibility of the discovery of the MSSM h/A bosons in the region of high tanβ (larger than 15) and mass close to 100 GeV has been investigated by exploiting the decay of the neutral h/A boson into two muons, h$\rightarrow \mu^+\mu^-$ and A$\rightarrow \mu^+\mu^-$, accompanied by two b-jets. This region is also accessible by charged MSSM Higgs boson H$^{\pm}$ decays.

To this purpose Monte Carlo events have been generated for a center-of-mass energy $\sqrt{s}$= 14 TeV through the ATHENA interface (v.9.0.4), while the ATLAS detector response has been

simulated using the GEANT program through the ATHENA interface (v.10.0.1).

The results described in this note show a well defined possibility for the discovery of a neutral Higgs boson in a region traditionally difficult due to the presence of the Z resonance. This is obtained owing to the high resolution performance of the ATLAS detector, namely of the muon spectrometer and the inner detector, together with the high b-tagging capability. For completeness the search of $H \rightarrow \mu^+\mu^-$ has been explored in the same mass region.

The discovery of a neutral MSSM boson looks possible in a mass range of 100 to 120 GeV at $\tan\beta > 15$, with an integrated luminosity $\int \mathcal{L}\, dt = 10$ fb^{-1}, which corresponds to one year of data taking.

A fully experimental method to subtract the main contributing background of Z boson decays $Z \rightarrow \mu^+\mu^-$ has been suggested by us [1], to perform the analysis of this channel on real data. This method mainly relies on experimental data, with limited Monte Carlo corrections. This procedure is based on the use of a control sample of Z boson decay to electrons, $Z \rightarrow e^+e^-$. The lepton universality guarantees the same numbers of events produced in Z bosons decaying to electrons and to muons. This simple method does not depend on complex theoretical calculations nor on their implementation in Monte Carlo.

A Appendix: Mass, width, product of cross section times $\mu^+\mu^-$ branching ratio for A, h and H Higgs bosons

tan β = 15

$\mathbf{m_h^{nom}}$ [GeV]	m_A [GeV]	Γ_A [GeV]	$\sigma_A \cdot Br_{\mu^+\mu^-}$ [pb]	m_h [GeV]	Γ_h [GeV]	$\sigma_h \cdot Br_{\mu^+\mu^-}$ [pb]	m_H [GeV]	Γ_H [GeV]	$\sigma_H \cdot Br_{\mu^+\mu^-}$ [pb]
95.00	96.07	0.42222	0.041310	95.00	0.40596	0.042280	127.75	0.01464	0.0003718
97.50	98.68	0.43219	0.038080	97.50	0.41326	0.038850	127.85	0.01745	0.0004579
100.00	101.31	0.44221	0.035180	100.01	0.41974	0.035750	127.98	0.02112	0.0005707
102.50	103.96	0.45228	0.032490	102.50	0.42505	0.032810	128.13	0.02600	0.0007197
105.00	106.65	0.46246	0.030030	105.00	0.42869	0.030110	128.31	0.03267	0.0009226
107.50	109.38	0.47277	0.027800	107.50	0.42982	0.027470	128.55	0.04196	0.0012020
110.00	112.20	0.48338	0.025690	110.01	0.42702	0.024910	128.85	0.05550	0.0016030
112.50	115.12	0.49434	0.023690	112.51	0.41785	0.022210	129.27	0.07575	0.0021970
115.00	118.22	0.50594	0.021780	115.00	0.39794	0.019390	129.87	0.10739	0.0030940
117.50	121.66	0.51878	0.019910	117.51	0.35925	0.016050	130.80	0.15904	0.0044850
120.00	125.82	0.53424	0.017870	120.01	0.28862	0.011820	132.46	0.24528	0.0066280
122.50	132.05	0.55730	0.015280	122.50	0.17327	0.006494	136.18	0.38392	0.0092990
125.00	151.00	0.62675	0.009847	125.01	0.04102	0.001350	152.61	0.58642	0.0088310

Table 13: The nominal mass value of neutral boson h , m_h^{nom} and the mass, width and product of cross section and $\mu^+\mu^-$branching ratio for the neutral boson A, h and H. The values are obtained with PYTHIA(v.6.226).

tan β = 20

$\mathbf{m_h^{nom}}$ [GeV]	m_A [GeV]	Γ_A [GeV]	$\sigma_A \cdot Br_{\mu^+\mu^-}$ [pb]	m_h [GeV]	Γ_h [GeV]	$\sigma_h \cdot Br_{\mu^+\mu^-}$ [pb]	m_H [GeV]	Γ_H [GeV]	$\sigma_H \cdot Br_{\mu^+\mu^-}$ [pb]
95.00	95.65	0.74776	0.07438	95.00	0.72815	0.07587	127.40	0.01455	0.0003738
97.50	98.21	0.76517	0.06880	97.51	0.74297	0.06995	127.46	0.01737	0.0004627
100.00	100.78	0.78259	0.06353	100.01	0.75691	0.06447	127.52	0.02108	0.0005791
102.50	103.36	0.80002	0.05893	102.50	0.76961	0.05948	127.61	0.02602	0.0007334
105.00	105.97	0.81760	0.05452	105.01	0.78057	0.05476	127.71	0.03285	0.0009472
107.50	108.60	0.83527	0.05058	107.51	0.78878	0.05038	127.84	0.04250	0.0012470
110.00	111.27	0.85315	0.04687	110.01	0.79267	0.04624	128.01	0.05668	0.0016880
112.50	113.99	0.87132	0.04346	112.50	0.78929	0.04207	128.23	0.07842	0.0023510
115.00	116.82	0.89017	0.04019	115.00	0.77282	0.03763	128.56	0.11393	0.0034290
117.50	119.83	0.91017	0.03712	117.51	0.73116	0.03271	129.06	0.17577	0.0052560
120.00	123.20	0.93249	0.03397	120.00	0.63869	0.02620	129.94	0.29076	0.0085150
122.50	127.63	0.96173	0.03031	122.50	0.44415	0.01674	131.87	0.51479	0.0142800
125.00	137.75	1.02812	0.02369	125.00	0.13158	0.00450	139.49	0.89428	0.0197200

Table 14: The nominal mass value of neutral boson h , m_h^{nom} and the mass, width and product of cross section and branching ratio for the neutral boson A, h and H. The values are obtained with PYTHIA(v.6.226).

tan β = 25

$\mathbf{m_h^{nom}}$ [GeV]	m_A [GeV]	Γ_A [GeV]	$\sigma_A \cdot Br_{\mu^+\mu^-}$ [pb]	m_h [GeV]	Γ_h [GeV]	$\sigma_h \cdot Br_{\mu^+\mu^-}$ [pb]	m_H [GeV]	Γ_H [GeV]	$\sigma_H \cdot Br_{\mu^+\mu^-}$ [pb]
95.00	95.46	1.16637	0.11720	95.01	1.14251	0.11910	127.27	0.01442	0.0003715
97.50	97.99	1.19325	0.10830	97.50	1.16695	0.10990	127.30	0.01722	0.0004601
100.00	100.54	1.22027	0.10010	100.01	1.19062	0.10160	127.35	0.02091	0.0005772
102.50	103.09	1.24720	0.09278	102.51	1.21292	0.09387	127.40	0.02586	0.0007335
105.00	105.65	1.27415	0.08605	105.00	1.23338	0.08669	127.46	0.03267	0.0009490
107.50	108.23	1.30124	0.07980	107.50	1.25106	0.08012	127.55	0.04237	0.0012540
110.00	110.84	1.32857	0.07421	110.01	1.26427	0.07382	127.65	0.05677	0.0017110
112.50	113.48	1.35614	0.06898	112.51	1.26976	0.06770	127.79	0.07913	0.0024060
115.00	116.18	1.38426	0.06404	115.00	1.26110	0.06150	128.00	0.11618	0.0035610
117.50	119.00	1.41355	0.05932	117.51	1.22373	0.05469	128.31	0.18312	0.0056060
120.00	122.04	1.44504	0.05477	120.01	1.12241	0.04609	128.85	0.31620	0.0095950
122.50	125.71	1.48294	0.04986	122.51	0.86579	0.03263	130.02	0.61104	0.0179500
125.00	132.60	1.55377	0.04187	125.00	0.31548	0.01090	134.42	1.23273	0.0317200

Table 15: The nominal mass value of neutral boson h , m_h^{nom} and the mass, width and product of cross section and $\mu^+\mu^-$branching ratio for the neutral boson A, h and H. The values are obtained with PYTHIA(v.6.226).

tan β = 30

$\mathbf{m_h^{nom}}$ [GeV]	m_A [GeV]	Γ_A [GeV]	$\sigma_A \cdot Br_{\mu^+\mu^-}$ [pb]	m_h [GeV]	Γ_h [GeV]	$\sigma_h \cdot Br_{\mu^+\mu^-}$ [pb]	m_H [GeV]	Γ_H [GeV]	$\sigma_H \cdot Br_{\mu^+\mu^-}$ [pb]
95.00	95.35	1.67790	0.16940	95.00	1.64886	0.17200	127.23	0.01424	0.0003661
97.50	97.88	1.71661	0.15630	97.51	1.68531	0.15880	127.25	0.01703	0.0004547
100.00	100.40	1.75507	0.14480	100.00	1.72062	0.14690	127.28	0.02066	0.0005704
102.50	102.94	1.79370	0.13430	102.51	1.75480	0.13580	127.32	0.02557	0.0007260
105.00	105.48	1.83222	0.12460	105.00	1.78700	0.12570	127.36	0.03234	0.0009417
107.50	108.04	1.87093	0.11560	107.51	1.81646	0.11650	127.42	0.04202	0.0012480
110.00	110.61	1.90969	0.10770	110.01	1.84126	0.10750	127.49	0.05638	0.0017050
112.50	113.20	1.94865	0.10010	112.50	1.85819	0.09923	127.59	0.07879	0.0024130
115.00	115.84	1.98825	0.09317	115.01	1.86052	0.09093	127.73	0.11644	0.0035960
117.50	118.55	2.02880	0.08661	117.50	1.83255	0.08209	127.94	0.18534	0.0057440
120.00	121.41	2.07149	0.08030	120.00	1.73326	0.07127	128.30	0.32768	0.0101100
122.50	124.70	2.12045	0.07374	122.51	1.43670	0.05426	129.09	0.67361	0.0204100
125.00	130.00	2.19903	0.06453	125.01	0.63146	0.02187	131.89	1.55805	0.0434200

Table 16: The nominal mass value of neutral boson h , m_h^{nom} and the mass, width and product of cross section and $\mu^+\mu^-$branching ratio for the neutral boson A, h and H. The values are obtained with PYTHIA(v.6.226).

tan β = 35

$\mathbf{m_h^{nom}}$ [GeV]	m_A [GeV]	Γ_A [GeV]	$\sigma_A \cdot Br_{\mu^+\mu^-}$ [pb]	m_h [GeV]	Γ_h [GeV]	$\sigma_h \cdot Br_{\mu^+\mu^-}$ [pb]	m_H [GeV]	Γ_H [GeV]	$\sigma_H \cdot Br_{\mu^+\mu^-}$ [pb]
95.00	95.29	2.28256	0.23120	95.01	2.24742	0.23410	127.24	0.01406	0.0003602
97.50	97.80	2.33485	0.21320	97.50	2.29767	0.21630	127.26	0.01679	0.0004467
100.00	100.32	2.38720	0.19750	100.00	2.34709	0.20000	127.28	0.02038	0.0005618
102.50	102.85	2.43957	0.18320	102.51	2.39525	0.18520	127.31	0.02523	0.0007154
105.00	105.38	2.49180	0.17000	105.01	2.44139	0.17150	127.34	0.03191	0.0009286
107.50	107.92	2.54409	0.15790	107.51	2.48470	0.15900	127.38	0.04146	0.0012330
110.00	110.47	2.59644	0.14690	110.01	2.52338	0.14730	127.43	0.05567	0.0016850
112.50	113.04	2.64906	0.13690	112.51	2.55421	0.13620	127.50	0.07799	0.0023930
115.00	115.63	2.70196	0.12740	115.00	2.57021	0.12550	127.60	0.11539	0.0035770
117.50	118.28	2.75594	0.11870	117.50	2.55537	0.11440	127.75	0.18471	0.0057590
120.00	121.04	2.81203	0.11030	120.00	2.46526	0.10130	128.01	0.33139	0.0103400
122.50	124.09	2.87384	0.10200	122.50	2.15281	0.08138	128.56	0.70616	0.0217600
125.00	128.50	2.96291	0.09116	125.01	1.11258	0.03863	130.47	1.83617	0.0535600

Table 17: The nominal mass value of neutral boson h , m_h^{nom} and the mass, width and product of cross section and $\mu^+\mu^-$branching ratio for the neutral boson A, h and H. The values are obtained with PYTHIA(v.6.226).

tan β = 40

$\mathbf{m_h^{nom}}$ [GeV]	m_A [GeV]	Γ_A [GeV]	$\sigma_A \cdot Br_{\mu^+\mu^-}$ [pb]	m_h [GeV]	Γ_h [GeV]	$\sigma_h \cdot Br_{\mu^+\mu^-}$ [pb]	m_H [GeV]	Γ_H [GeV]	$\sigma_H \cdot Br_{\mu^+\mu^-}$ [pb]
95.00	95.24	2.97995	0.3017	95.00	2.93779	0.30570	127.28	0.01384	0.0003525
97.50	97.75	3.04824	0.2788	97.50	3.00431	0.28240	127.30	0.01653	0.0004375
100.00	100.27	3.11662	0.2578	100.01	3.07000	0.26120	127.31	0.02007	0.0005500
102.50	102.79	3.18477	0.2396	102.51	3.13420	0.24210	127.33	0.02483	0.0007011
105.00	105.31	3.25272	0.2225	105.01	3.19637	0.22430	127.36	0.03140	0.0009096
107.50	107.84	3.32075	0.2066	107.51	3.25575	0.20820	127.39	0.04079	0.0012090
110.00	110.38	3.38887	0.1922	110.01	3.31057	0.19320	127.43	0.05478	0.0016580
112.50	112.93	3.45707	0.1791	112.51	3.35749	0.17880	127.48	0.07674	0.0023580
115.00	115.50	3.52564	0.1668	115.01	3.38972	0.16540	127.55	0.11373	0.0035340
117.50	118.11	3.59509	0.1556	117.50	3.39106	0.15190	127.67	0.18248	0.0057020
120.00	120.80	3.66650	0.1448	120.00	3.31605	0.13650	127.86	0.32951	0.0103100
122.50	123.70	3.74328	0.1344	122.50	3.00518	0.11370	128.26	0.71780	0.0223200
125.00	127.55	3.84491	0.1219	125.00	1.78456	0.06213	129.61	2.04085	0.0611500

Table 18: The nominal mass value of neutral boson h , m_h^{nom} and the mass, width and product of cross section and $\mu^+\mu^-$branching ratio for the neutral boson A, h and H. The values are obtained with PYTHIA(v.6.226).

tan β = 45

$\mathbf{m_h^{nom}}$ [GeV]	m_A [GeV]	Γ_A [GeV]	$\sigma_A \cdot Br_{\mu^+\mu^-}$ [pb]	m_h [GeV]	Γ_h [GeV]	$\sigma_h \cdot Br_{\mu^+\mu^-}$ [pb]	m_H [GeV]	Γ_H [GeV]	$\sigma_H \cdot Br_{\mu^+\mu^-}$ [pb]
95.00	95.21	3.77047	0.3802	95.00	3.72038	0.38680	127.35	0.01362	0.0003437
97.50	97.72	3.85691	0.3522	97.50	3.80532	0.35700	127.36	0.01626	0.0004273
100.00	100.23	3.94311	0.3269	100.00	3.88914	0.33020	127.37	0.01973	0.0005372
102.50	102.74	4.02902	0.3029	102.50	3.97142	0.30680	127.39	0.02438	0.0006848
105.00	105.25	4.11469	0.2811	104.99	4.05164	0.28410	127.41	0.03079	0.0008895
107.50	107.78	4.20079	0.2613	107.50	4.12947	0.26380	127.43	0.04001	0.0011820
110.00	110.31	4.28667	0.2433	110.00	4.20254	0.24500	127.46	0.05370	0.0016190
112.50	112.85	4.37266	0.2271	112.50	4.26788	0.22720	127.50	0.07520	0.0023050
115.00	115.40	4.45877	0.2118	115.00	4.31867	0.21060	127.56	0.11134	0.0034520
117.50	117.99	4.54601	0.1972	117.50	4.33916	0.19400	127.65	0.17887	0.0055970
120.00	120.63	4.63472	0.1839	120.00	4.28403	0.17580	127.79	0.32347	0.0101500
122.50	123.43	4.72857	0.1711	122.49	3.98930	0.15070	128.09	0.71282	0.0222600
125.00	126.93	4.84555	0.1564	125.00	2.64794	0.09217	129.09	2.17208	0.0661800

Table 19: The nominal mass value of neutral boson h , m_h^{nom} and the mass, width and product of cross section and $\mu^+\mu^-$branching ratio for the neutral boson A, h and H. The values are obtained with PYTHIA(v.6.226).

tan β = 50

$\mathbf{m_h^{nom}}$ [GeV]	m_A [GeV]	Γ_A [GeV]	$\sigma_A \cdot Br_{\mu^+\mu^-}$ [pb]	m_h [GeV]	Γ_h [GeV]	$\sigma_h \cdot Br_{\mu^+\mu^-}$ [pb]	m_H [GeV]	Γ_H [GeV]	$\sigma_H \cdot Br_{\mu^+\mu^-}$ [pb]
95.00	95.19	4.65406	0.4701	95.00	4.59511	0.4771	127.43	0.01338	0.0003347
97.50	97.70	4.76077	0.4349	97.51	4.70064	0.4403	127.44	0.01597	0.0004165
100.00	100.21	4.86720	0.4030	100.01	4.80500	0.4071	127.45	0.01937	0.0005240
102.50	102.72	4.97326	0.3737	102.51	4.90777	0.3774	127.46	0.02394	0.0006684
105.00	105.23	5.07902	0.3468	105.01	5.00844	0.3509	127.48	0.03023	0.0008680
107.50	107.75	5.18491	0.3229	107.51	5.10647	0.3261	127.50	0.03923	0.0011550
110.00	110.27	5.29052	0.3006	110.01	5.19981	0.3025	127.52	0.05259	0.0015800
112.50	112.80	5.39627	0.2802	112.51	5.28562	0.2811	127.55	0.07356	0.0022460
115.00	115.34	5.50216	0.2614	115.00	5.35724	0.2607	127.60	0.10884	0.0033680
117.50	117.91	5.60905	0.2440	117.51	5.39928	0.2411	127.67	0.17464	0.0054460
120.00	120.52	5.71732	0.2277	120.00	5.36719	0.2200	127.78	0.31594	0.0099070
122.50	123.26	5.83072	0.2118	122.51	5.09545	0.1922	128.02	0.70201	0.0219800
125.00	126.49	5.96403	0.1954	125.00	3.71261	0.1292	128.76	2.21922	0.0682500

Table 20: The nominal mass value of neutral boson h , m_h^{nom} and the mass, width and product of cross section and $\mu^+\mu^-$branching ratio for the neutral boson A, h and H. The values are obtained with PYTHIA(v.6.226).

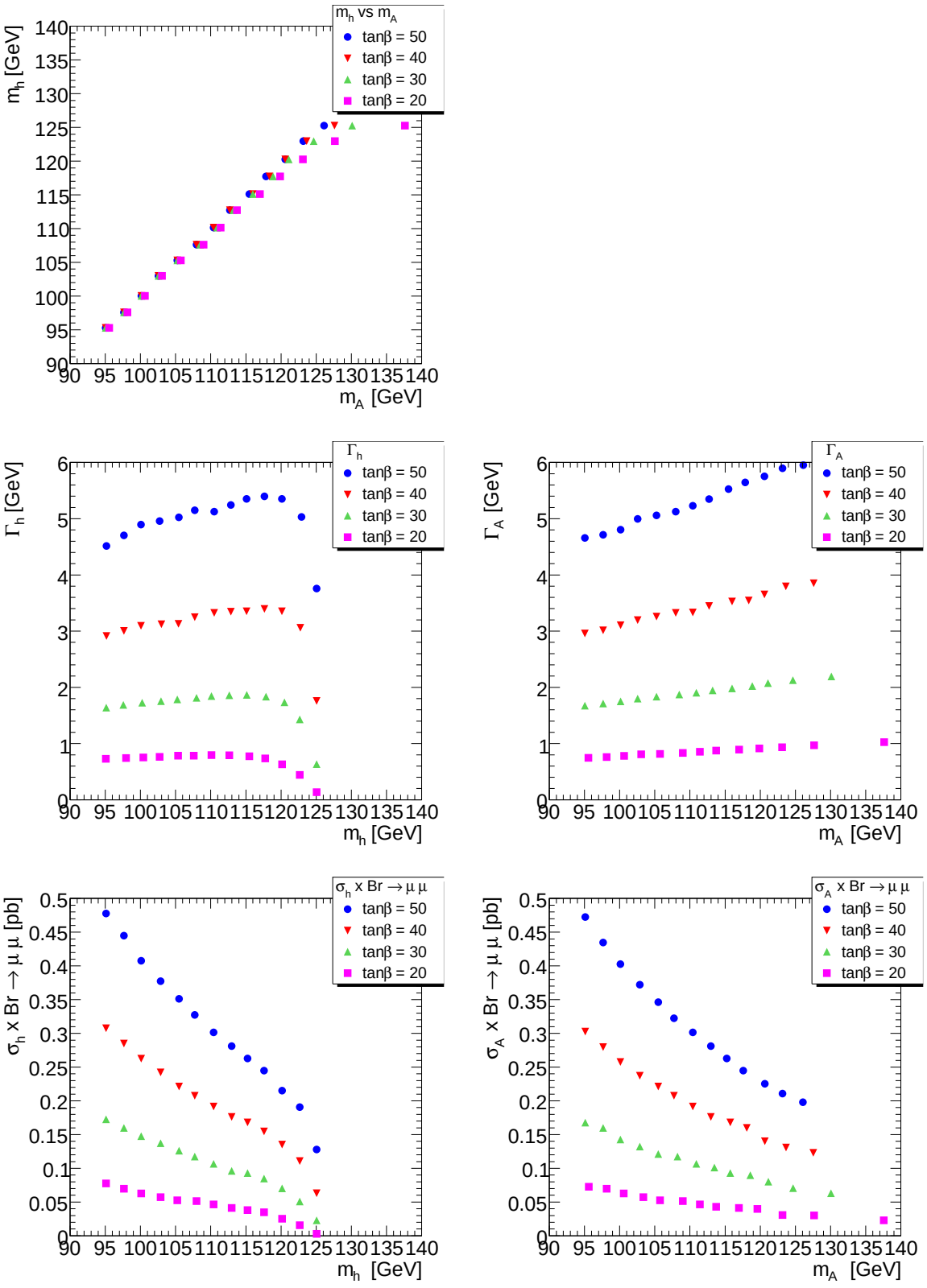

Figure 19: a) Mass of the neutral A boson, m_{A}, as a function of the mass of the neutral h boson, m_{h} (top left). b) The width in $\mu^+\mu^-$ of the neutral h boson, Γ_{h}, as a function of m_{h} (middle left). c) The width in $\mu^+\mu^-$ of the neutral A boson, Γ_{A}, as a function of m_{A} (middle right). d) The production cross section of the neutral h boson times the muon pair branching ratio, $\sigma_{\mathrm{h}} \cdot \mathrm{Br} \to \mu\mu$, as a function of m_{h} (bottom left.) e) The production cross section of the neutral A boson times the muon pair branching ratio, $\sigma_{\mathrm{A}} \cdot \mathrm{Br} \to \mu\mu$, as a function of m_{A} (bottom right). The values at $\tan\beta = 50, 40, 30, 20$ are shown (Tab. 14, Tab. 16, Tab. 18, Tab. 20) [17,18].

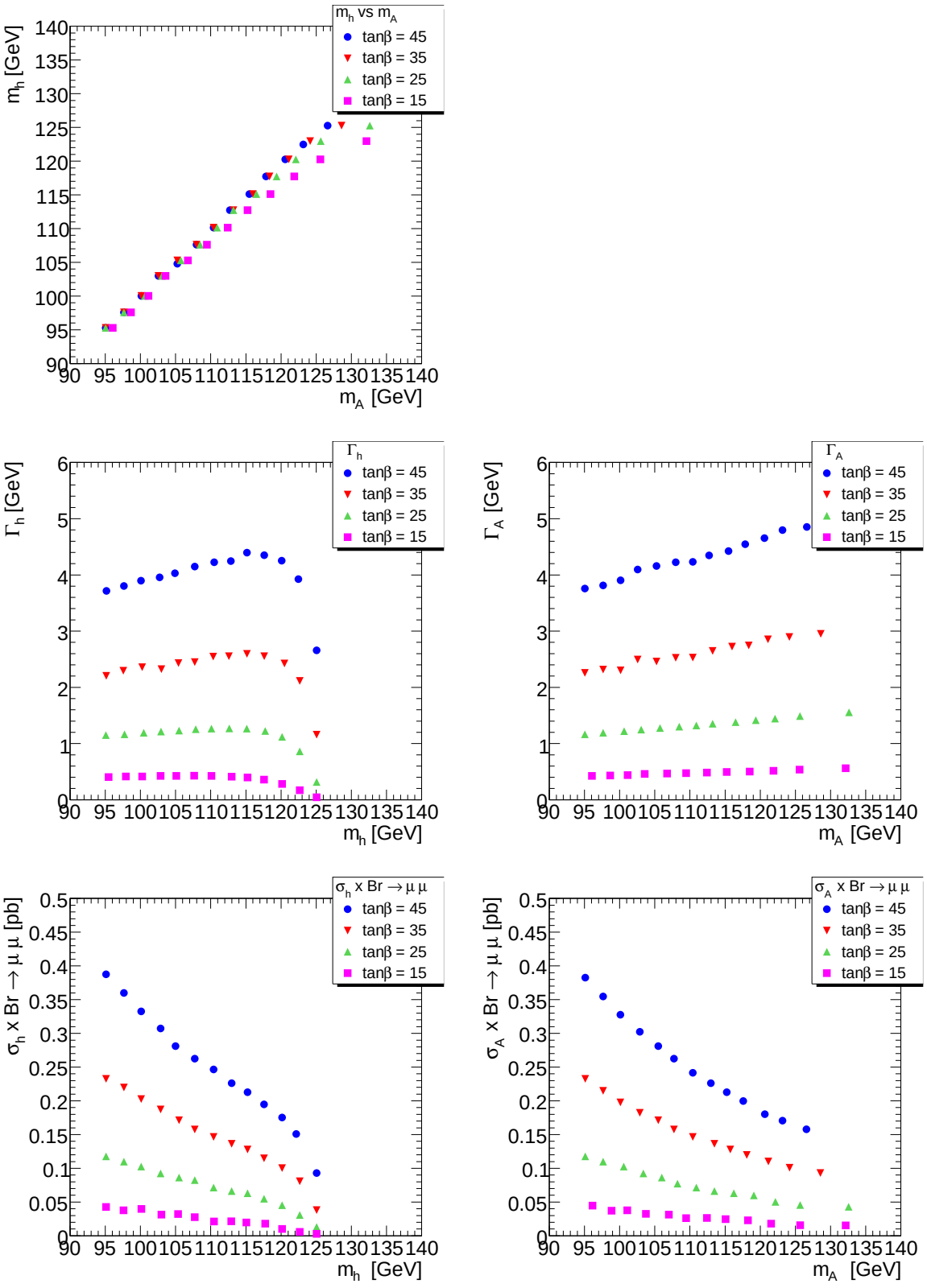

Figure 20: a) Mass of the neutral A boson, m_{A}, as a function of the mass of the neutral h boson, m_{h} (top left). b) The width in $\mu^+\mu^-$ of the neutral h boson, Γ_{h}, as a function of m_{h} (middle left). c) The width in $\mu^+\mu^-$ of the neutral A boson, Γ_{A}, as a function of m_{A} (middle right). d) The production cross section of the neutral h boson times the muon pair branching ratio, $\sigma_{\mathrm{h}} \cdot \mathrm{Br} \rightarrow \mu\mu$, as a function of m_{h} (bottom left) e) The production cross section of the neutral A boson times the muon pair branching ratio, $\sigma_{\mathrm{A}} \cdot \mathrm{Br} \rightarrow \mu\mu$, as a function of m_{A} (bottom right). The values at $\tan\beta = 45, 35, 25, 15$ are shown (Tab. 13, Tab. 15, Tab. 17, Tab. 19) [17,18].

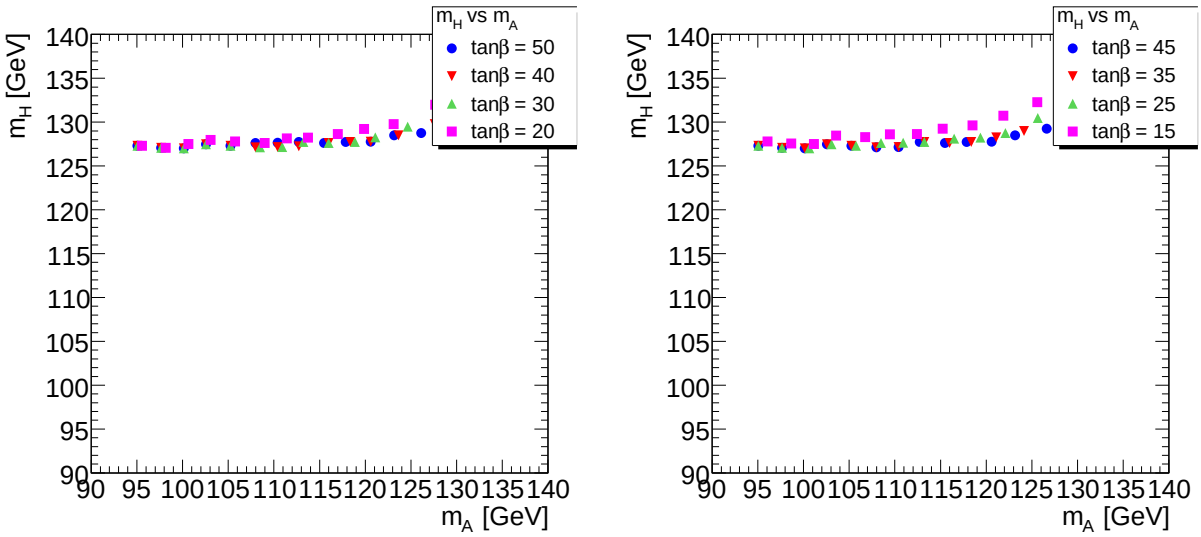

Figure 21: The mass, m_{H}, of the neutral Higgs boson H is shown as a function of the mass of the neutral A boson, m_{A}, for tanβ values = 50, 40, 30, 20 on the left (Tab. 14, Tab. 16, Tab. 18, Tab. 20) and for tanβ values = 45, 35, 25, 15 on the right (Tab. 13, Tab. 15, Tab. 17, Tab. 19) [17,18].

B Appendix: Center and width of mass window for h, A, H Higgs bosons selection

Table caption:
Tab. 21 (tanβ =15), Tab. 22 (tanβ =20), Tab. 23 (tanβ =25), Tab. 24 (tanβ =30), Tab. 25 (tanβ =35), Tab. 26 (tanβ =40), Tab. 27 (tanβ =45), Tab. 28 (tanβ =50):

The nominal mass value of the lightest neutral MSSM Higgs boson, $m_{\mathrm{h}}^{\mathrm{nom}}$, the corresponding value of the A Higgs boson mass, $m_{\mathrm{A}}^{\mathrm{corr}}$, corrected for the experimental effects (Sec. 8), and the selection window, ξ_{A}, calculated as a function of the A natural width and experimental resolution (Sec. 8), are reported in the first three columns. The corresponding quantities for the other two neutral bosons are listed in columns 4, 5 (h boson) and 6, 7 (H boson).

$\tan\beta = 15$

$\mathbf{m}_{\mathrm{h}}^{\mathrm{nom}}$ [10^3MeV]	$m_{\mathrm{A}}^{\mathrm{corr}}$ [MeV]	ξ_{A} [MeV]	$m_{\mathrm{h}}^{\mathrm{corr}}$ [MeV]	ξ_{h} [MeV]	$m_{\mathrm{H}}^{\mathrm{corr}}$ [MeV]	ξ_{H} [MeV]
95.00	95250	2504	94180	2476	126930	3322
97.50	97860	2572	96680	2541	127030	3324
100.00	100490	2641	99190	2606	127160	3327
102.50	103140	2710	101680	2671	127310	3331
105.00	105830	2780	104180	2736	127490	3336
107.50	108560	2851	106680	2801	127730	3342
110.00	111380	2924	109190	2866	128030	3350
112.50	114300	3000	111690	2931	128450	3361
115.00	117400	3081	114180	2995	129050	3377
117.50	120840	3171	116690	3059	129980	3401
120.00	125000	3279	119190	3123	131640	3446
122.50	131230	3441	121680	3186	135360	3544
125.00	150180	3935	124190	3250	151790	3976

Table 21: Table caption in forehead of Appendix B.

$\tan\beta = 20$

$\mathbf{m}_{\mathrm{h}}^{\mathrm{nom}}$ [10^3MeV]	$m_{\mathrm{A}}^{\mathrm{corr}}$ [MeV]	ξ_{A} [MeV]	$m_{\mathrm{h}}^{\mathrm{corr}}$ [MeV]	ξ_{h} [MeV]	$m_{\mathrm{H}}^{\mathrm{corr}}$ [MeV]	ξ_{H} [MeV]
95.00	94830	2507	94180	2489	126580	3312
97.50	97390	2574	96690	2555	126640	3314
100.00	99960	2641	99190	2620	126700	3316
102.50	102540	2709	101680	2685	126790	3318
105.00	105150	2777	104190	2750	126890	3320
107.50	107780	2846	106690	2816	127020	3324
110.00	110450	2916	109190	2880	127190	3328
112.50	113170	2987	111680	2944	127410	3334
115.00	116000	3061	114180	3008	127740	3343
117.50	119010	3140	116690	3071	128240	3356
120.00	122380	3227	119180	3132	129120	3381
122.50	126810	3343	121680	3191	131050	3436
125.00	136930	3608	124190	3250	138670	3646

Table 22: Table caption in forehead of Appendix B.

$\tan\,\beta = 25$

$\mathbf{m}_{\mathrm{h}}^{\mathrm{nom}}$ $[10^3\mathrm{MeV}]$	$m_{\mathrm{A}}^{\mathrm{corr}}$ [MeV]	ξ_{A} [MeV]	$m_{\mathrm{h}}^{\mathrm{corr}}$ [MeV]	ξ_{h} [MeV]	$m_{\mathrm{H}}^{\mathrm{corr}}$ [MeV]	ξ_{H} [MeV]
95.00	94640	2531	94190	2517	126450	3309
97.50	97170	2597	96680	2583	126480	3310
100.00	99720	2665	99190	2649	126530	3311
102.50	102270	2732	101690	2714	126580	3312
105.00	104830	2799	104180	2780	126640	3314
107.50	107410	2867	106680	2845	126730	3316
110.00	110020	2936	109190	2910	126830	3319
112.50	112660	3006	111690	2974	126970	3323
115.00	115360	3077	114180	3037	127180	3328
117.50	118180	3151	116690	3099	127490	3337
120.00	121220	3232	119190	3156	128030	3353
122.50	124890	3328	121690	3206	129200	3390
125.00	131780	3510	124180	3253	133600	3534

Table 23: Table caption in forehead of Appendix B.

$\tan\,\beta = 30$

$\mathbf{m}_{\mathrm{h}}^{\mathrm{nom}}$ $[10^3\mathrm{MeV}]$	$m_{\mathrm{A}}^{\mathrm{corr}}$ [MeV]	ξ_{A} [MeV]	$m_{\mathrm{h}}^{\mathrm{corr}}$ [MeV]	ξ_{h} [MeV]	$m_{\mathrm{H}}^{\mathrm{corr}}$ [MeV]	ξ_{H} [MeV]
95.00	94530	2579	94180	2567	126410	3308
97.50	97060	2647	96690	2634	126430	3308
100.00	99580	2714	99180	2700	126460	3309
102.50	102120	2782	101690	2767	126500	3310
105.00	104660	2850	104180	2833	126540	3311
107.50	107220	2919	106690	2899	126600	3313
110.00	109790	2987	109190	2965	126670	3315
112.50	112380	3057	111680	3029	126770	3318
115.00	115020	3127	114190	3092	126910	3321
117.50	117730	3200	116680	3152	127120	3327
120.00	120590	3276	119180	32058	127480	3339
122.50	123880	3364	121690	3243	128270	3368
125.00	129180	3506	124190	3261	131070	3492

Table 24: Table caption in forehead of Appendix B.

$\tan\beta = 35$

$\mathbf{m}_{\mathrm{h}}^{\mathrm{nom}}$ $[10^3\mathrm{MeV}]$	$m_{\mathrm{A}}^{\mathrm{corr}}$ [MeV]	ξ_{A} [MeV]	$m_{\mathrm{h}}^{\mathrm{corr}}$ [MeV]	ξ_{h} [MeV]	$m_{\mathrm{H}}^{\mathrm{corr}}$ [MeV]	ξ_{H} [MeV]
95.00	94470	2660	94190	2647	126420	3308
97.50	96980	2728	96680	2716	126440	3309
100.00	99500	2798	99180	2784	126460	3309
102.50	102030	2867	101690	2852	126490	3310
105.00	104560	2936	104190	2920	126520	3311
107.50	107100	3006	106690	2987	126560	3312
110.00	109650	3076	109190	3054	126610	3313
112.50	112220	3146	111690	3119	126680	3315
115.00	114810	3217	114180	3182	126780	3318
117.50	117460	3290	116680	3241	126930	3322
120.00	120220	3365	119180	3290	127190	3331
122.50	123270	3448	121680	3313	127740	3356
125.00	127680	3569	124190	3284	129650	3480

Table 25: Table caption in forehead of Appendix B.

$\tan\beta = 40$

$\mathbf{m}_{\mathrm{h}}^{\mathrm{nom}}$ $[10^3\mathrm{MeV}]$	$m_{\mathrm{A}}^{\mathrm{corr}}$ [MeV]	ξ_{A} [MeV]	$m_{\mathrm{h}}^{\mathrm{corr}}$ [MeV]	ξ_{h} [MeV]	$m_{\mathrm{H}}^{\mathrm{corr}}$ [MeV]	ξ_{H} [MeV]
95.00	94420	2780	94180	2766	126460	3309
97.50	96930	2851	96680	2837	126480	3310
100.00	99450	2922	99190	2907	126490	3310
102.50	101970	2994	101690	2978	126510	3311
105.00	104490	3065	104190	3048	126540	3311
107.50	107020	3137	106690	3117	126570	3312
110.00	109560	3209	109190	3186	126610	3313
112.50	112110	3281	111690	3253	126660	3315
115.00	114680	3354	114190	3317	126730	3317
117.50	117290	3428	116680	3376	126850	3320
120.00	119980	3504	119180	3422	127040	3327
122.50	122880	3586	121680	3430	127440	3349
125.00	126730	3695	124180	3337	128790	3479

Table 26: Table caption in forehead of Appendix B.

$\tan\beta = 45$

$\mathbf{m}_{\mathrm{h}}^{\mathrm{nom}}$ $[10^3\mathrm{MeV}]$	$m_{\mathrm{A}}^{\mathrm{corr}}$ [MeV]	ξ_{A} [MeV]	$m_{\mathrm{h}}^{\mathrm{corr}}$ [MeV]	ξ_{h} [MeV]	$m_{\mathrm{H}}^{\mathrm{corr}}$ [MeV]	ξ_{H} [MeV]
95.00	94390	2946	94180	2930	126530	3311
97.50	96900	3021	96680	3004	126540	3311
100.00	99410	3096	99180	3078	126550	3312
102.50	101920	3170	101680	31523	126570	3312
105.00	104430	3245	104170	3225	126590	3313
107.50	106960	3320	106680	3298	126610	3313
110.00	109490	3395	109180	3369	126640	3314
112.50	112030	3470	111680	3439	126680	3315
115.00	114580	3546	114180	3506	126740	3317
117.50	117170	3622	116680	3566	126830	3320
120.00	119810	3700	119180	3610	126970	3325
122.50	122610	3783	121670	3606	127270	3344
125.00	126110	3887	124180	3438	128270	3480

Table 27: Table caption in forehead of Appendix B.

$\tan\beta = 50$

$\mathbf{m}_{\mathrm{h}}^{\mathrm{nom}}$ $[10^3\mathrm{MeV}]$	$m_{\mathrm{A}}^{\mathrm{corr}}$ [MeV]	ξ_{A} [MeV]	$m_{\mathrm{h}}^{\mathrm{corr}}$ [MeV]	ξ_{h} [MeV]	$m_{\mathrm{H}}^{\mathrm{corr}}$ [MeV]	ξ_{H} [MeV]
95.00	94370	3165	94180	3145	126610	3313
97.50	96880	3244	96690	3224	126620	3313
100.00	99390	3323	99190	3303	126630	3314
102.50	101900	3402	101690	3381	126640	3314
105.00	104410	3481	104190	3458	126660	3314
107.50	106930	3560	106690	3535	126680	3315
110.00	109450	3639	109190	3610	126700	3316
112.50	111980	3719	111690	3684	126730	3316
115.00	114520	3798	114180	3754	126780	3318
117.50	117090	3879	116690	3817	126850	3320
120.00	119700	3961	119180	3861	126960	3325
122.50	122440	4047	121690	3848	127200	3342
125.00	125670	4148	124180	3611	127940	3477

Table 28: Table caption in forehead of Appendix B.

C Appendix: Distributions of variables used in the selection

The distributions are normalized at $\int \mathcal{L}\,\mathrm{d}t$ 300 fb^{-1}, used in the selection procedure (Tab. 7) are plotted before the concerned cut is applied, for the following signal and background processes (color code in brackets) at the reference point, $\tan\beta = 45$ and $m_{\mathrm{A}} = 110.31$ GeV ($m_{\mathrm{h}} = 110$ GeV , $m_{\mathrm{H}} = 127.46$ GeV), (Sec. 8.1):

$\mathrm{b\bar{b}A} \to \mathrm{b\bar{b}}\mu^+\mu^-$ (light blue);
$\mathrm{b\bar{b}h} \to \mathrm{b\bar{b}}\mu^+\mu^-$ (dark blue);
$\mathrm{b\bar{b}H} \to \mathrm{b\bar{b}}\mu^+\mu^-$ (purple);
$\mathrm{b\bar{b}Z} \to \mathrm{b\bar{b}}\mu^+\mu^-$ (yellow);
$\mathrm{t\bar{t}} \to \mathrm{b\bar{b}}\mu^+\mu^-\nu\bar{\nu}$ (gray);
$\mathrm{ZZ} \to \mathrm{b\bar{b}}\mu^+\mu^-$ (green).

Background events may contribute to the corresponding distribution with more than one entry.

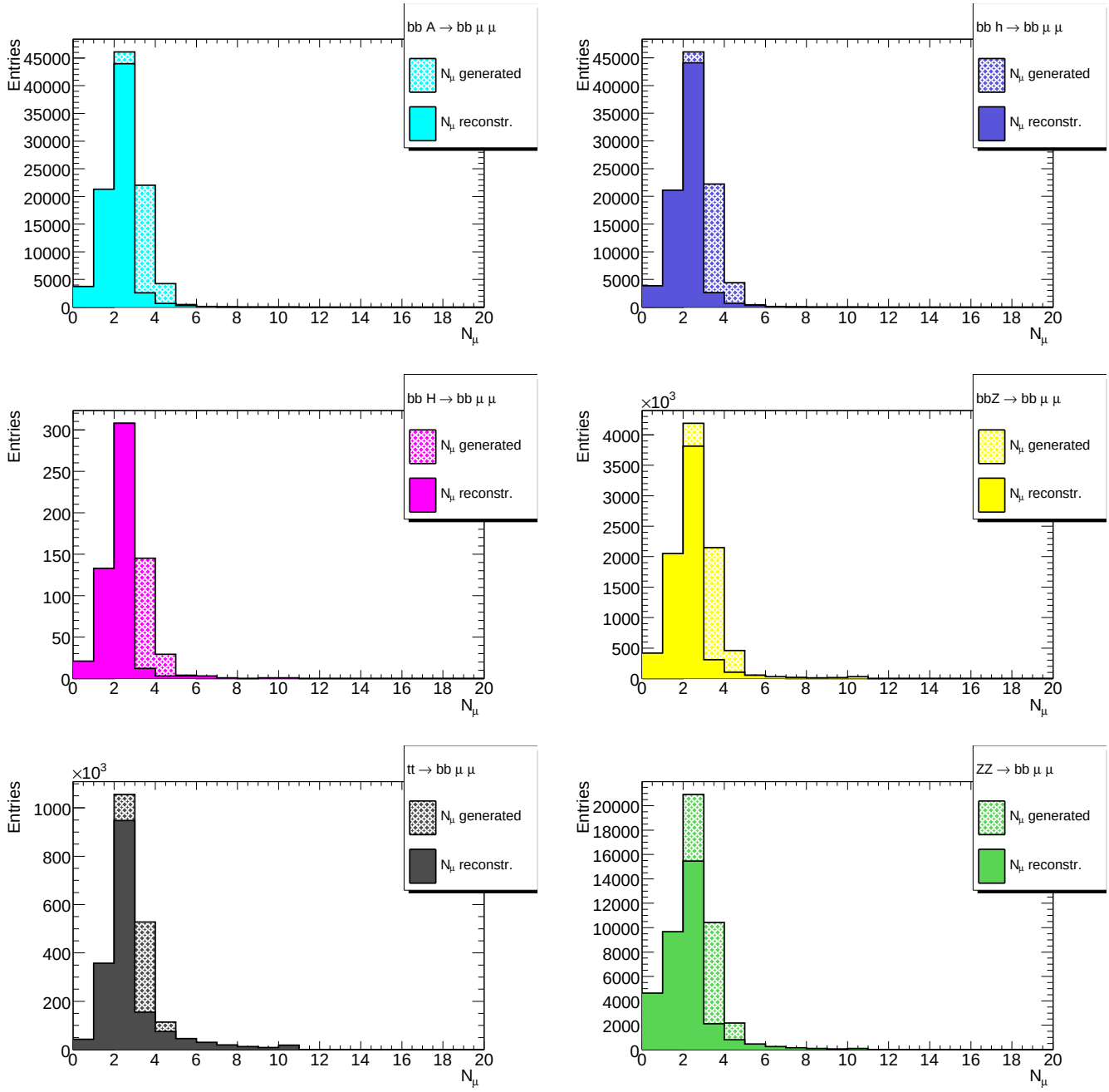

Figure 22: **Without cuts.** Distributions of the number of muons, N_μ, generated (hatched) and reconstructed (full color) for the following processes at the reference point, $\tan\beta = 45$ and $m_A = 110.31$ GeV (see forehead Appendix C):
a) $b\bar{b}A \rightarrow b\bar{b}\mu^+\mu^-$ events (top left, light blue); b) $b\bar{b}h \rightarrow b\bar{b}\mu^+\mu^-$ events (top right, dark blue); c) $b\bar{b}H \rightarrow b\bar{b}\mu^+\mu^-$ events (middle left, purple); e) $b\bar{b}Z \rightarrow b\bar{b}\mu^+\mu^-$ events (middle right, yellow); f) $t\bar{t} \rightarrow b\bar{b}\mu^+\mu^-\nu\bar{\nu}$ events (bottom right, gray); g) $ZZ \rightarrow b\bar{b}\mu^+\mu^-$ events (bottom right, green).

The distributions are plotted without any cut.

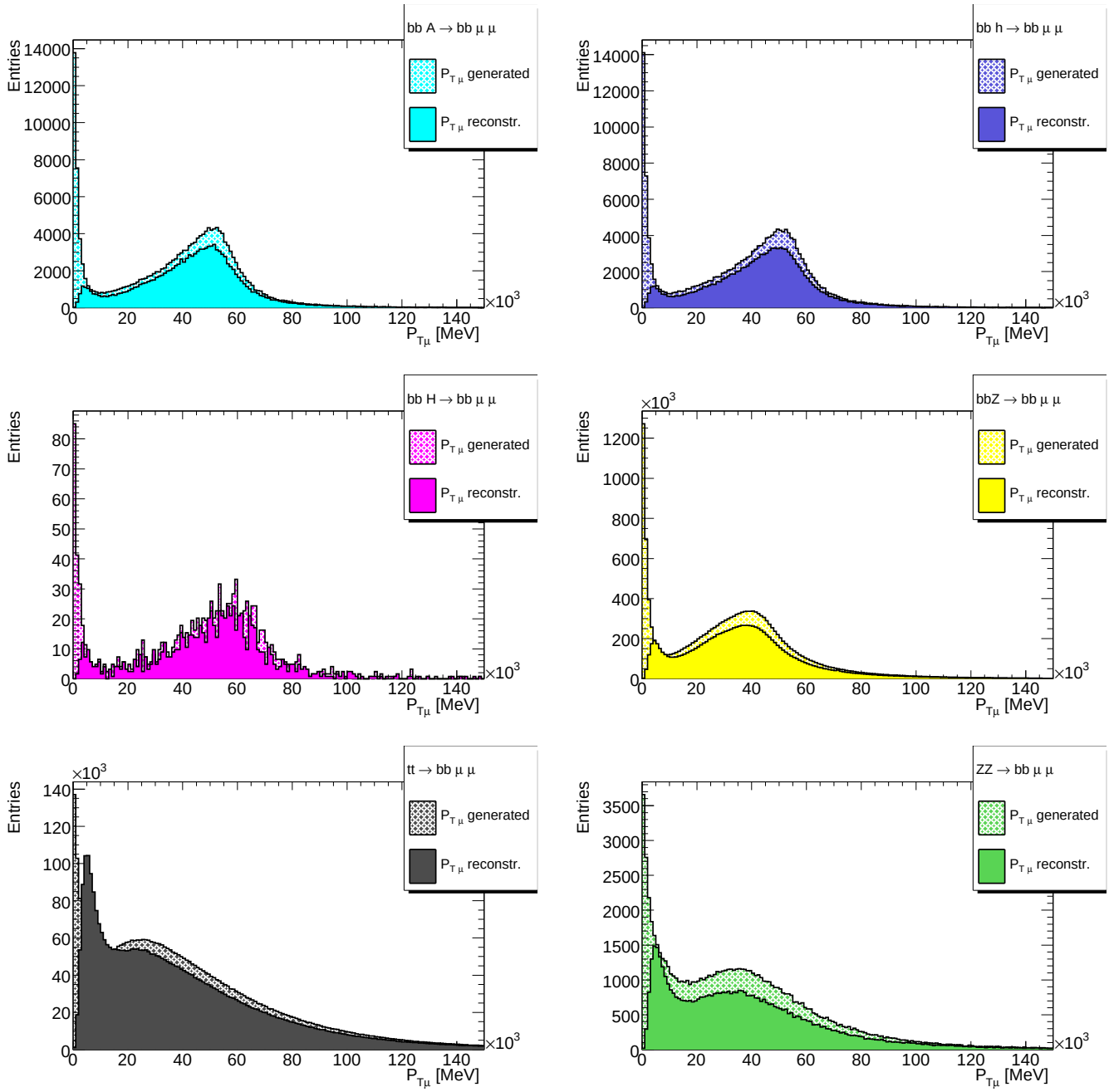

Figure 23:
Without cuts. Distributions of the muon transverse momentum, $P_{T\mu}$, generated (hatched) and reconstructed (full color) for the following processes at the reference point $\tan\beta = 45$ and $m_A = 110.31$ GeV (see forehead Appendix C):
a) $b\bar{b}A \rightarrow b\bar{b}\mu^+\mu^-$ events (top left, light blue); b) $b\bar{b}h \rightarrow b\bar{b}\mu^+\mu^-$ events (top right, dark blue); c) $b\bar{b}H \rightarrow b\bar{b}\mu^+\mu^-$ events (middle left, purple); e) $b\bar{b}Z \rightarrow b\bar{b}\mu^+\mu^-$ events (middle right, yellow); f) $t\bar{t} \rightarrow b\bar{b}\mu^+\mu^-\nu\bar{\nu}$ events (bottom right, gray); g) $ZZ \rightarrow b\bar{b}\mu^+\mu^-$ events (bottom right, green).

The distributions are plotted without any cut.

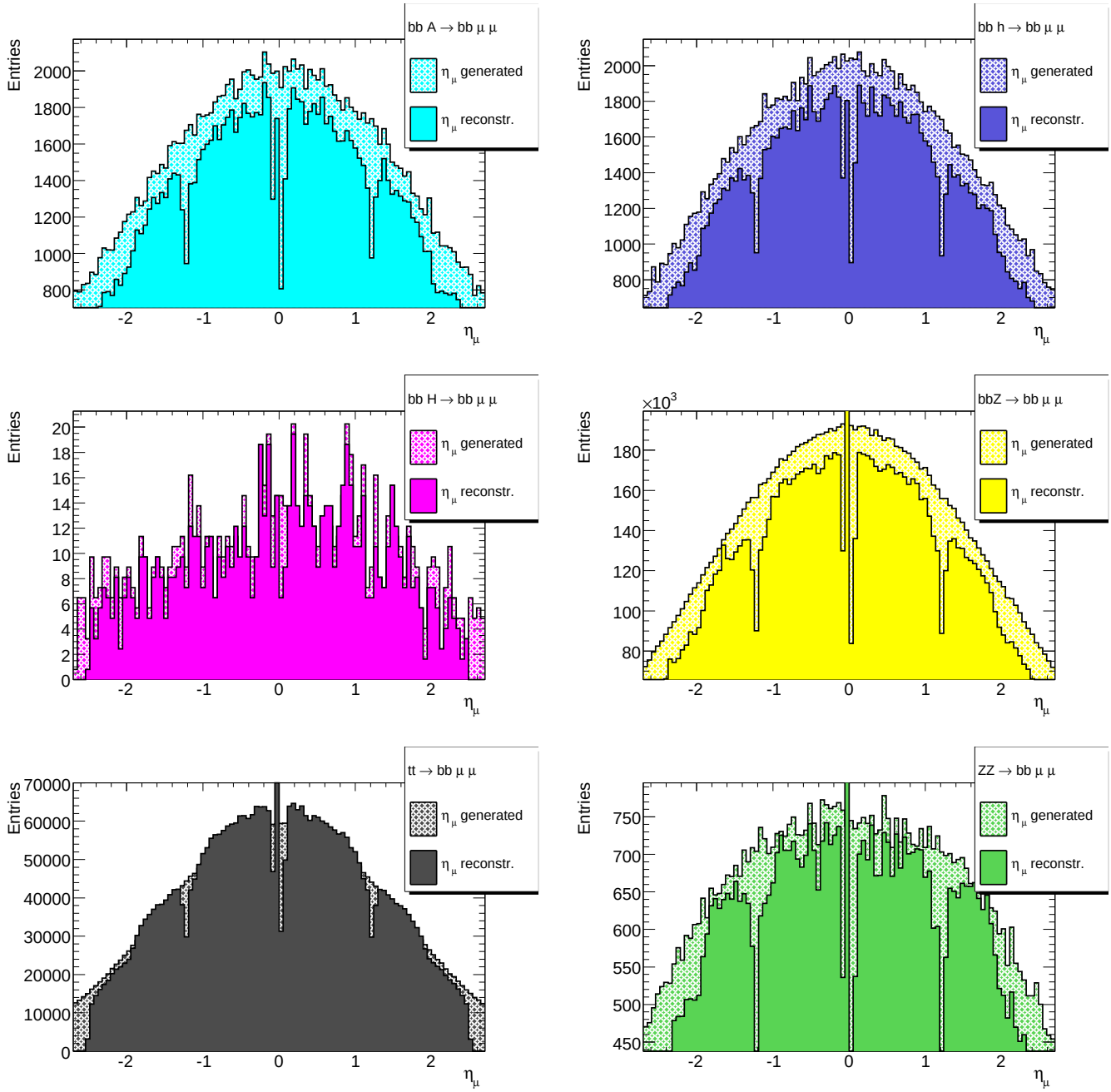

Figure 24: **Without cuts.** Distributions of the muon pseudorapidity, η_μ, generated (hatched) and reconstructed (full color) for the following processes at the reference point $\tan\beta = 45$ and $m_A = 110.31$ GeV (see forehead Appendix C):
a) $b\bar{b}A \rightarrow b\bar{b}\mu^+\mu^-$ events (top left, light blue); b) $b\bar{b}h \rightarrow b\bar{b}\mu^+\mu^-$ events (top right, dark blue); c) $b\bar{b}H \rightarrow b\bar{b}\mu^+\mu^-$ events (middle left, purple); e) $b\bar{b}Z \rightarrow b\bar{b}\mu^+\mu^-$ events (middle right, yellow); f) $t\bar{t} \rightarrow b\bar{b}\mu^+\mu^-\nu\bar{\nu}$ events (bottom right, gray); g) $ZZ \rightarrow b\bar{b}\mu^+\mu^-$ events (bottom right, green).

The distributions are plotted without any cut.

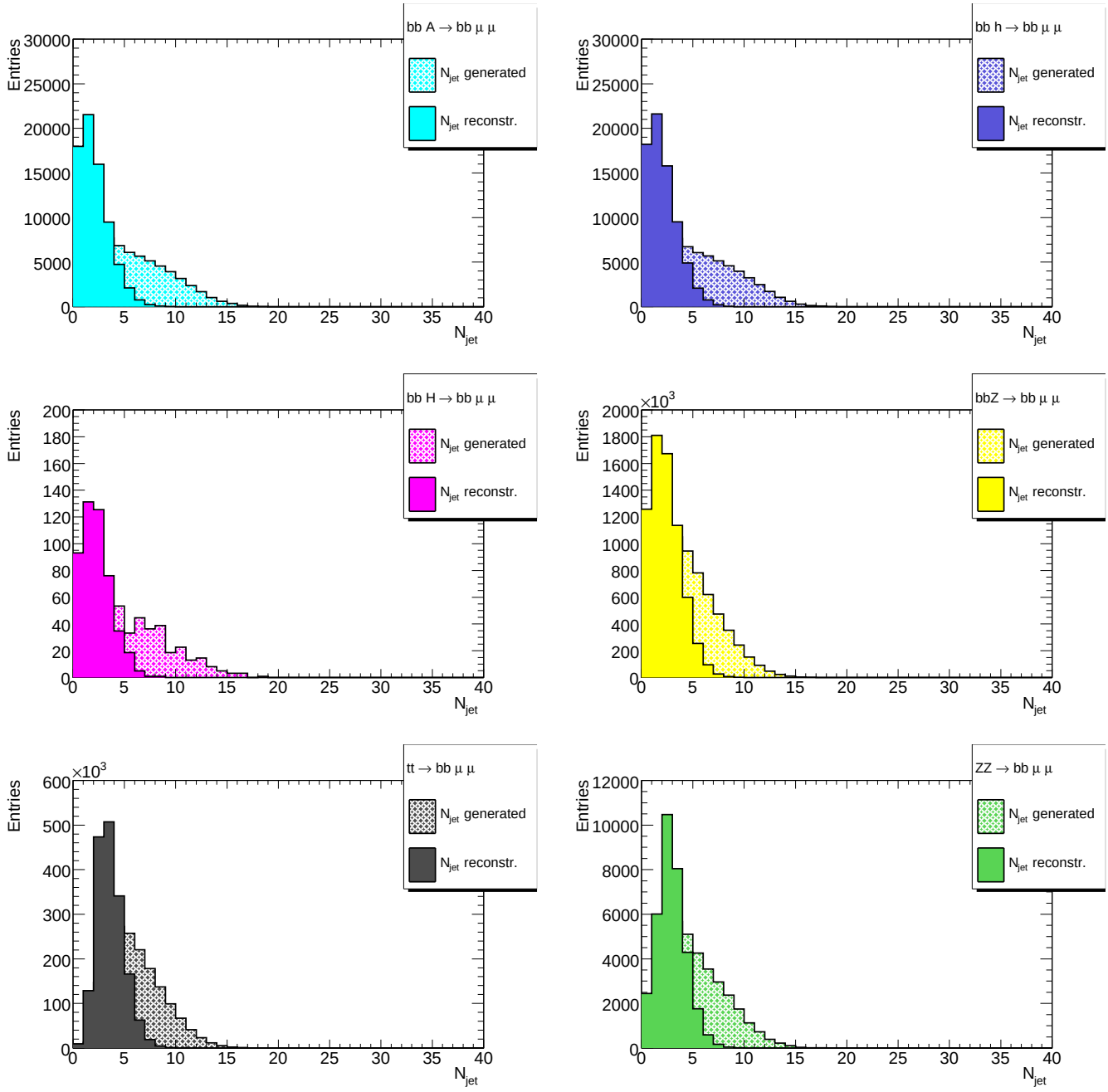

Figure 25: **Without cuts.** Distributions of the number of jets, N_{jet}, generated (hatched) and reconstructed (full color) for the following processes at reference point, $\tan\beta = 45$ and $m_{\text{A}} = 110.31$ GeV (see forehead Appendix C):
a) $\text{b}\bar{\text{b}}\text{A} \rightarrow \text{b}\bar{\text{b}}\mu^+\mu^-$ events (top left, light blue); b) $\text{b}\bar{\text{b}}\text{h} \rightarrow \text{b}\bar{\text{b}}\mu^+\mu^-$ events (top right, dark blue); c) $\text{b}\bar{\text{b}}\text{H} \rightarrow \text{b}\bar{\text{b}}\mu^+\mu^-$ events (middle left, purple); e) $\text{b}\bar{\text{b}}\text{Z} \rightarrow \text{b}\bar{\text{b}}\mu^+\mu^-$ events (middle right, yellow); f) $\text{t}\bar{\text{t}} \rightarrow \text{b}\bar{\text{b}}\mu^+\mu^-\nu\bar{\nu}$ events (bottom right, gray); g) $\text{ZZ} \rightarrow \text{b}\bar{\text{b}}\mu^+\mu^-$ events (bottom right, green).

The distributions are plotted without any cut.

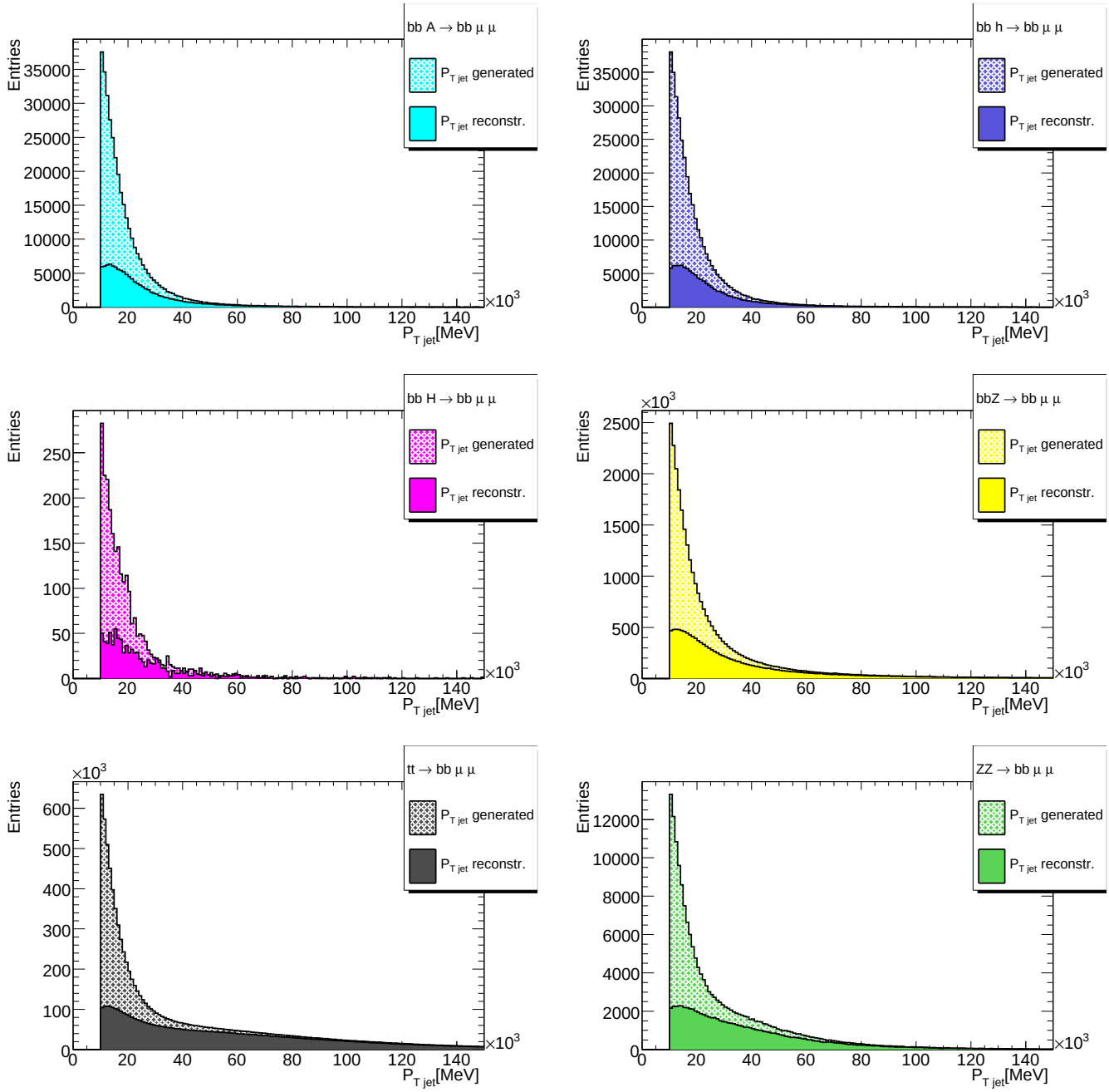

Figure 26: **Without cuts.** Distributions of the transverse momentum of jets, P_{Tjet}, generated (hatched) and reconstructed (full color) for the following processes at the reference point, $\tan\beta = 45$ and $m_{\mathrm{A}} = 110.31$ GeV (see forehead Appendix C):
a) $\mathrm{b\bar{b}A} \rightarrow \mathrm{b\bar{b}}\mu^+\mu^-$ events (top left, light blue); b) $\mathrm{b\bar{b}h} \rightarrow \mathrm{b\bar{b}}\mu^+\mu^-$ events (top right, dark blue); c) $\mathrm{b\bar{b}H} \rightarrow \mathrm{b\bar{b}}\mu^+\mu^-$ events (middle left, purple); e) $\mathrm{b\bar{b}Z} \rightarrow \mathrm{b\bar{b}}\mu^+\mu^-$ events (middle right, yellow); f) $\mathrm{t\bar{t}} \rightarrow \mathrm{b\bar{b}}\mu^+\mu^-\nu\bar{\nu}$ events (bottom right, gray); g) $\mathrm{ZZ} \rightarrow \mathrm{b\bar{b}}\mu^+\mu^-$ events (bottom right, green).

The distributions are plotted without any cut.

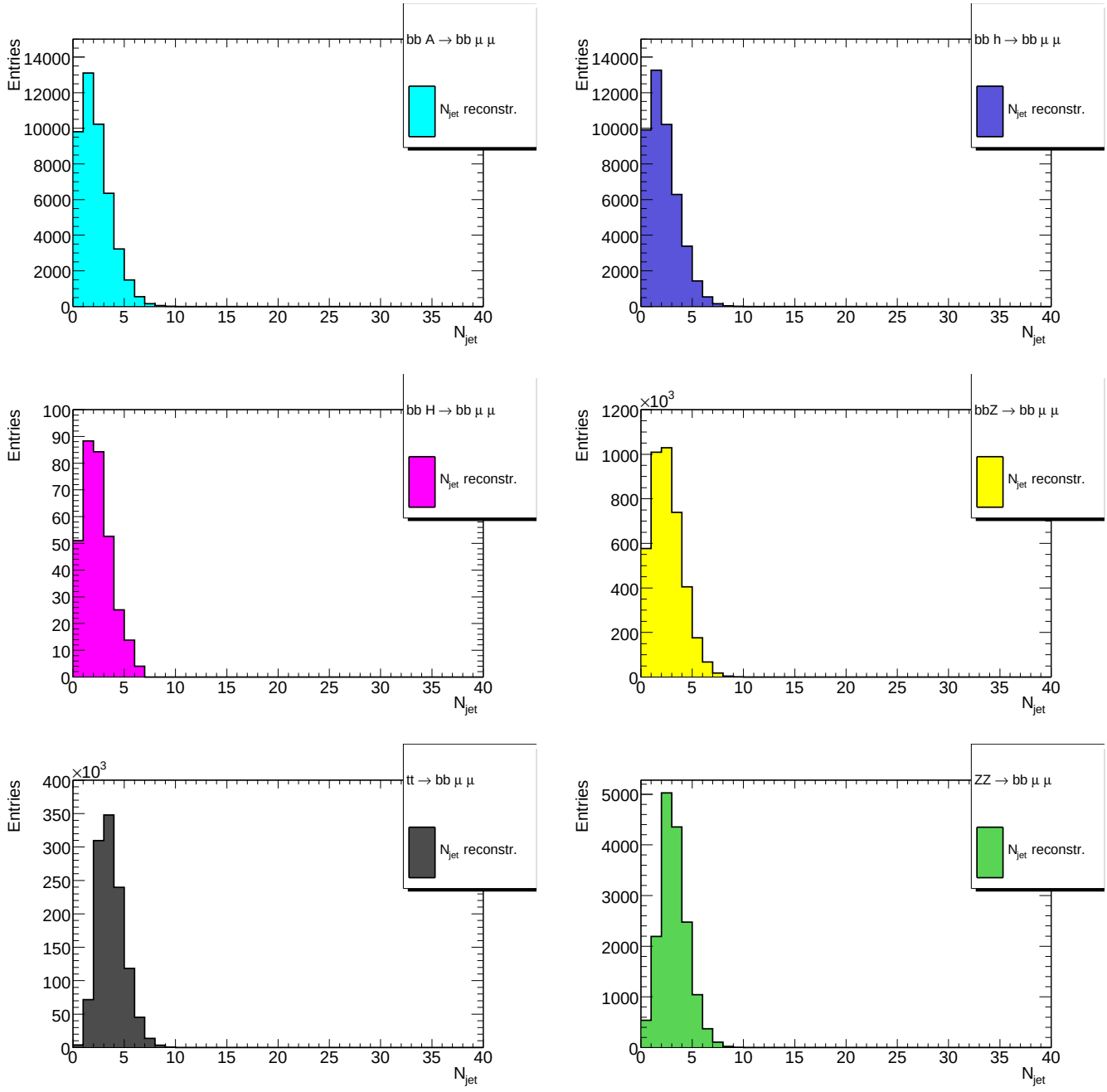

Figure 27: **After cut 1.** Distributions of the reconstructed number of jets, N_{jet}, are plotted after cuts 1 (Tab. 7) for the following processes at the reference point, $\tan\beta = 45$ and $m_{\text{A}} = 110.31$ GeV (see forehead Appendix C): a) $b\bar{b}A \to b\bar{b}\mu^+\mu^-$ events (top left, light blue); b) $b\bar{b}h \to b\bar{b}\mu^+\mu^-$ events (top right, dark blue); c) $b\bar{b}H \to b\bar{b}\mu^+\mu^-$ events (middle left, purple); e) $b\bar{b}Z \to b\bar{b}\mu^+\mu^-$ events (middle right, yellow); f) $t\bar{t} \to b\bar{b}\mu^+\mu^-\nu\bar{\nu}$ events (bottom right, gray); g) $ZZ \to b\bar{b}\mu^+\mu^-$ events (bottom right, green).

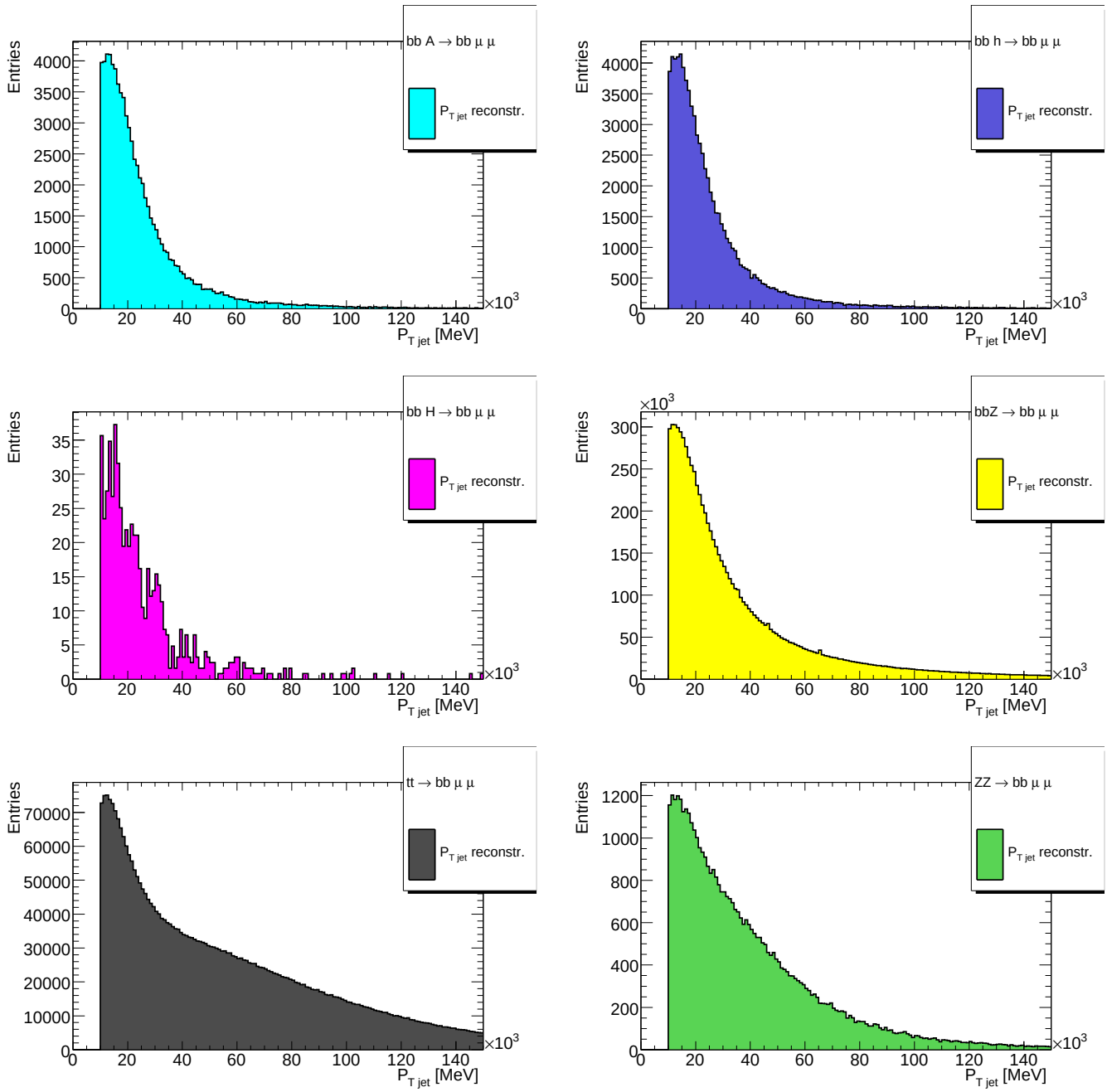

Figure 28: **After cut 1.** Distributions of the reconstructed transverse momentum of jets, P_{Tjet}, are plotted after cuts 1 (Tab. 7), for the following processes at the reference point, $\tan\beta = 45$ and $m_{\mathrm{A}} = 110.31$ GeV (see forehead Appendix C):
a) $b\bar{b}A \to b\bar{b}\mu^+\mu^-$ events (top left, light blue); b) $b\bar{b}h \to b\bar{b}\mu^+\mu^-$ events (top right, dark blue); c) $b\bar{b}H \to b\bar{b}\mu^+\mu^-$ events (middle left, purple); e) $b\bar{b}Z \to b\bar{b}\mu^+\mu^-$ events (middle right, yellow); f) $t\bar{t} \to b\bar{b}\mu^+\mu^-\nu\bar{\nu}$ events (bottom right, gray); g) $ZZ \to b\bar{b}\mu^+\mu^-$ events (bottom right, green).

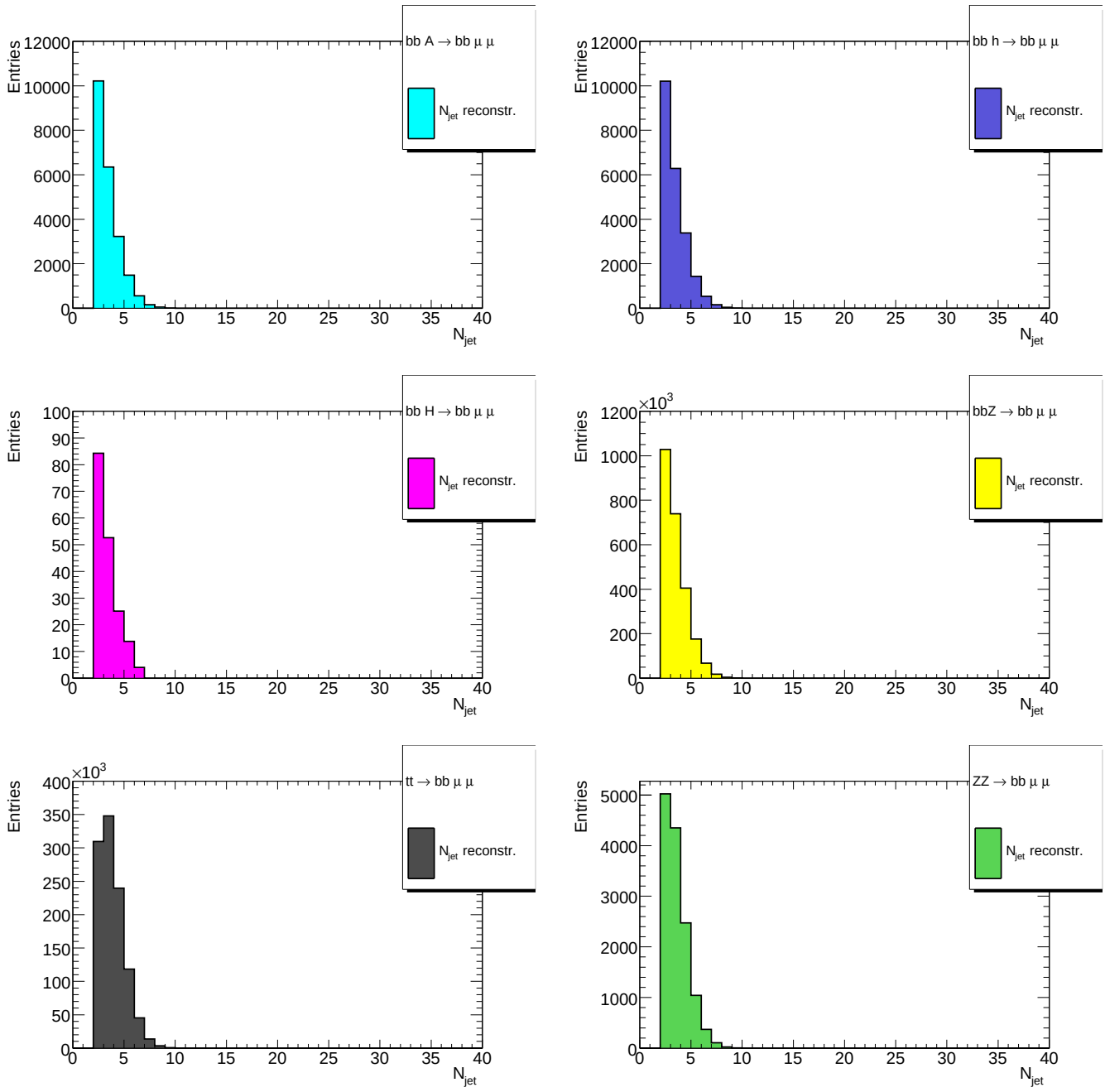

Figure 29: **After cut 2.** Distributions of the reconstructed number of jets, N_{jet}, are plotted after cuts 1 and 2 (Tab. 7) for the following processes at the reference point, $\tan\beta = 45$ and $m_{\text{A}} = 110.31$ GeV (see forehead Appendix C):
a) $b\bar{b}A \to b\bar{b}\mu^+\mu^-$ events (top left, light blue); b) $b\bar{b}h \to b\bar{b}\mu^+\mu^-$ events (top right, dark blue); c) $b\bar{b}H \to b\bar{b}\mu^+\mu^-$ events (middle left, purple); e) $b\bar{b}Z \to b\bar{b}\mu^+\mu^-$ events (middle right, yellow); f) $t\bar{t} \to b\bar{b}\mu^+\mu^-\nu\bar{\nu}$ events (bottom right, gray); g) $ZZ \to b\bar{b}\mu^+\mu^-$ events (bottom right, green).

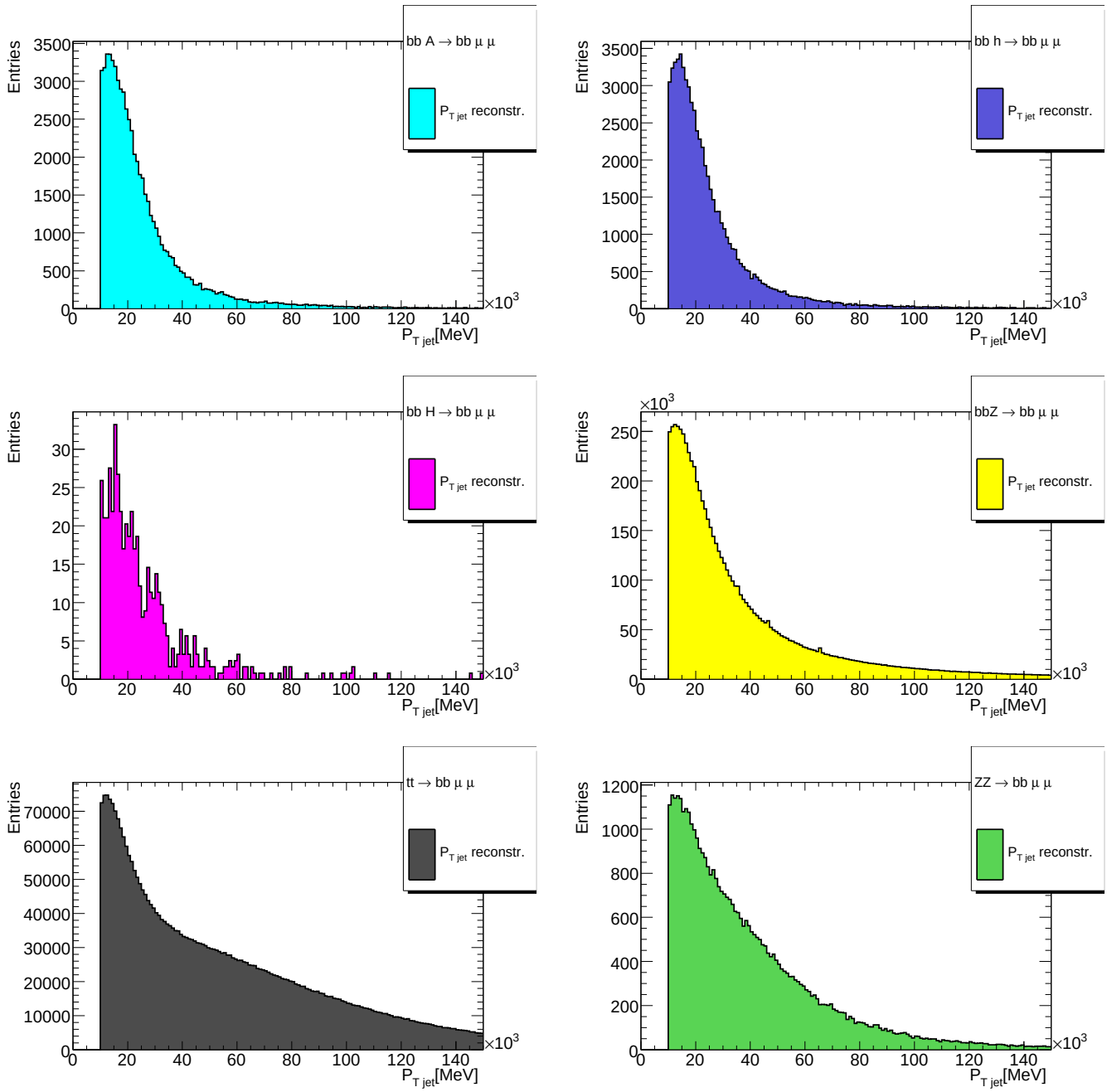

Figure 30: **After cut 2.** Distributions of the reconstructed transverse momentum of jets, P_{Tjet}, are plotted after cuts 1 and 2 (Tab. 7) for the following processes at the reference point, $\tan\beta = 45$ and $m_{\mathrm{A}} = 110.31$ GeV (see forehead Appendix C):
a) $b\bar{b}A \to b\bar{b}\mu^+\mu^-$ events (top left, light blue); b) $b\bar{b}h \to b\bar{b}\mu^+\mu^-$ events (top right, dark blue); c) $b\bar{b}H \to b\bar{b}\mu^+\mu^-$ events (middle left, purple); e) $b\bar{b}Z \to b\bar{b}\mu^+\mu^-$ events (middle right, yellow); f) $t\bar{t} \to b\bar{b}\mu^+\mu^-\nu\bar{\nu}$ events (bottom right, gray); g) $ZZ \to b\bar{b}\mu^+\mu^-$ events (bottom right, green).

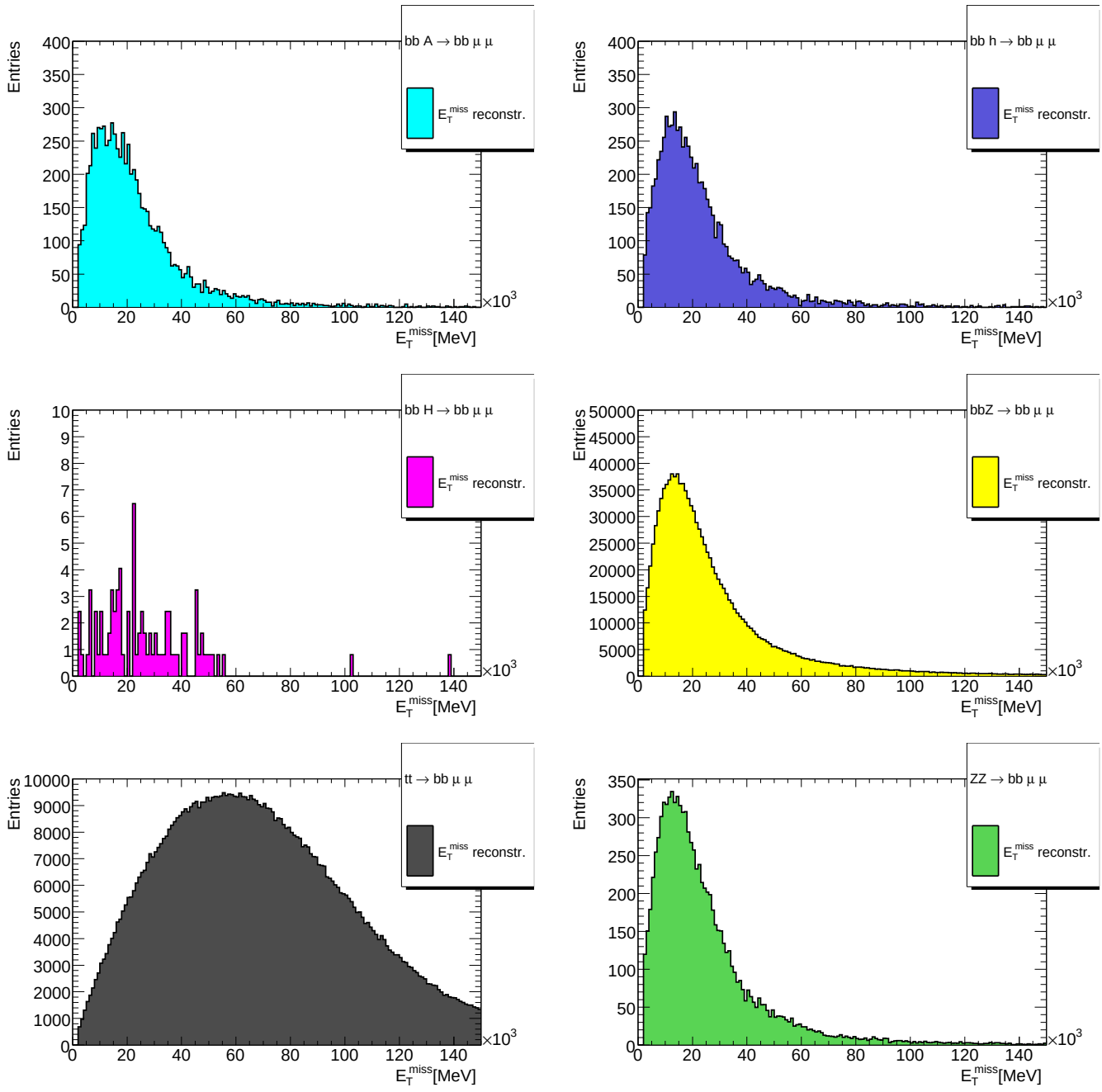

Figure 31: **After cut 3.** Distributions of the reconstructed missing transverse energy in the event, E_T^{miss}, are plotted after cuts 1,2 and 3 (Tab. 7) for the following processes at the reference point, $\tan\beta = 45$ and $m_{\text{A}} = 110.31$ GeV (see forehead Appendix C):
a) $b\bar{b}A \to b\bar{b}\mu^+\mu^-$ events (top left, light blue); b) $b\bar{b}h \to b\bar{b}\mu^+\mu^-$ events (top right, dark blue); c) $b\bar{b}H \to b\bar{b}\mu^+\mu^-$ events (middle left, purple); e) $b\bar{b}Z \to b\bar{b}\mu^+\mu^-$ events (middle right, yellow); f) $t\bar{t} \to b\bar{b}\mu^+\mu^-\nu\bar{\nu}$ events (bottom right, gray); g) $ZZ \to b\bar{b}\mu^+\mu^-$ events (bottom right, green).

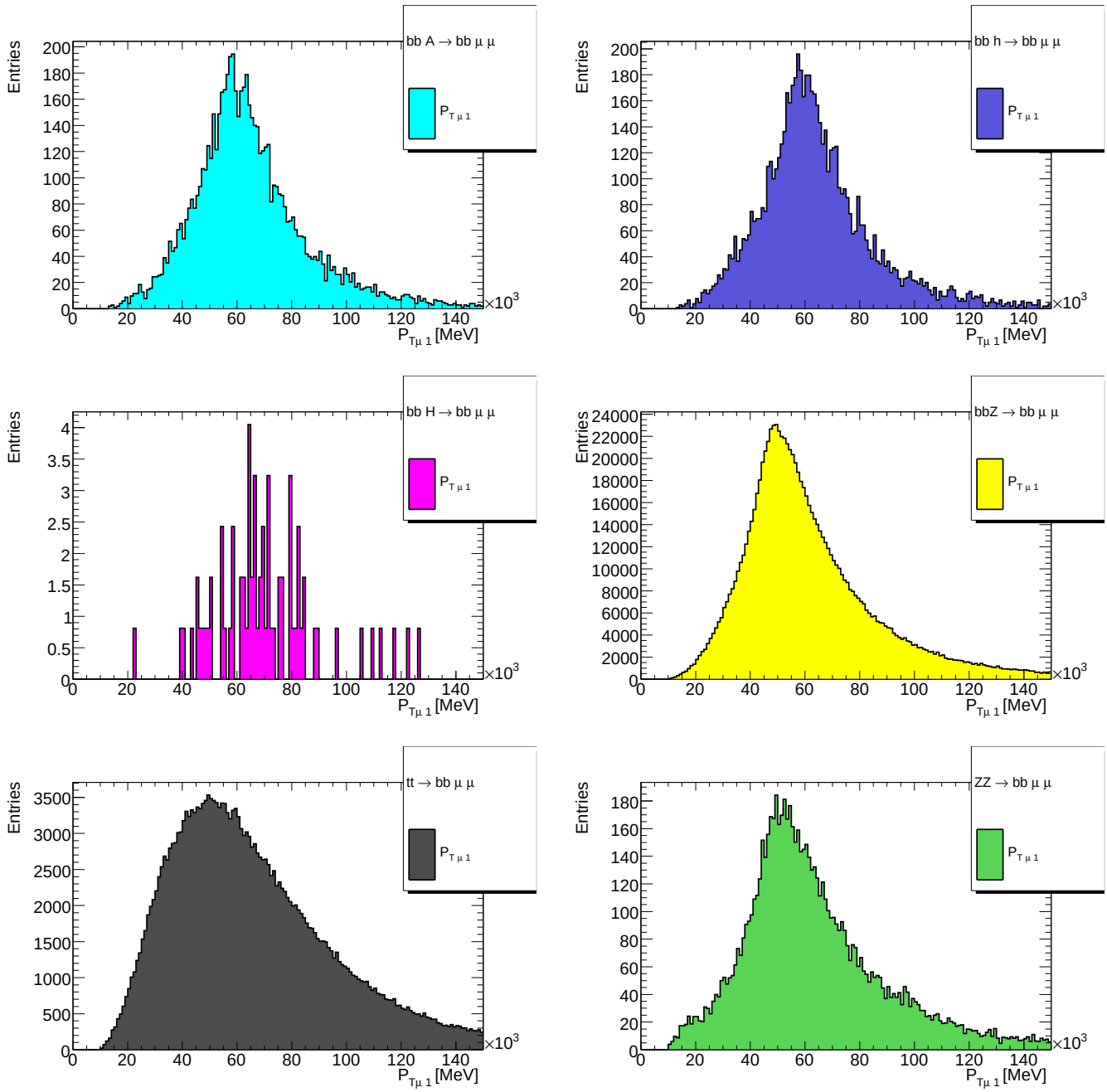

Figure 32: **After cut 4.** Distributions of the first most large muon reconstructed transverse momentum, $P_{\mathrm{T}\mu 1}$ are plotted after cuts 1,2,3 and 4 (Tab. 7) for the following processes at the reference point, $\tan\beta = 45$ and m_{A} 110.31 GeV (see forehead Appendix C):
a) $b\bar{b}A \rightarrow b\bar{b}\mu^+\mu^-$ events (top left, light blue); b) $b\bar{b}h \rightarrow b\bar{b}\mu^+\mu^-$ events (top right, dark blue); c) $b\bar{b}H \rightarrow b\bar{b}\mu^+\mu^-$ events (middle left, purple); e) $b\bar{b}Z \rightarrow b\bar{b}\mu^+\mu^-$ events (middle right, yellow); f) $t\bar{t} \rightarrow b\bar{b}\mu^+\mu^-\nu\bar{\nu}$ events (bottom right, gray); g) $ZZ \rightarrow b\bar{b}\mu^+\mu^-$ events (bottom right, green).

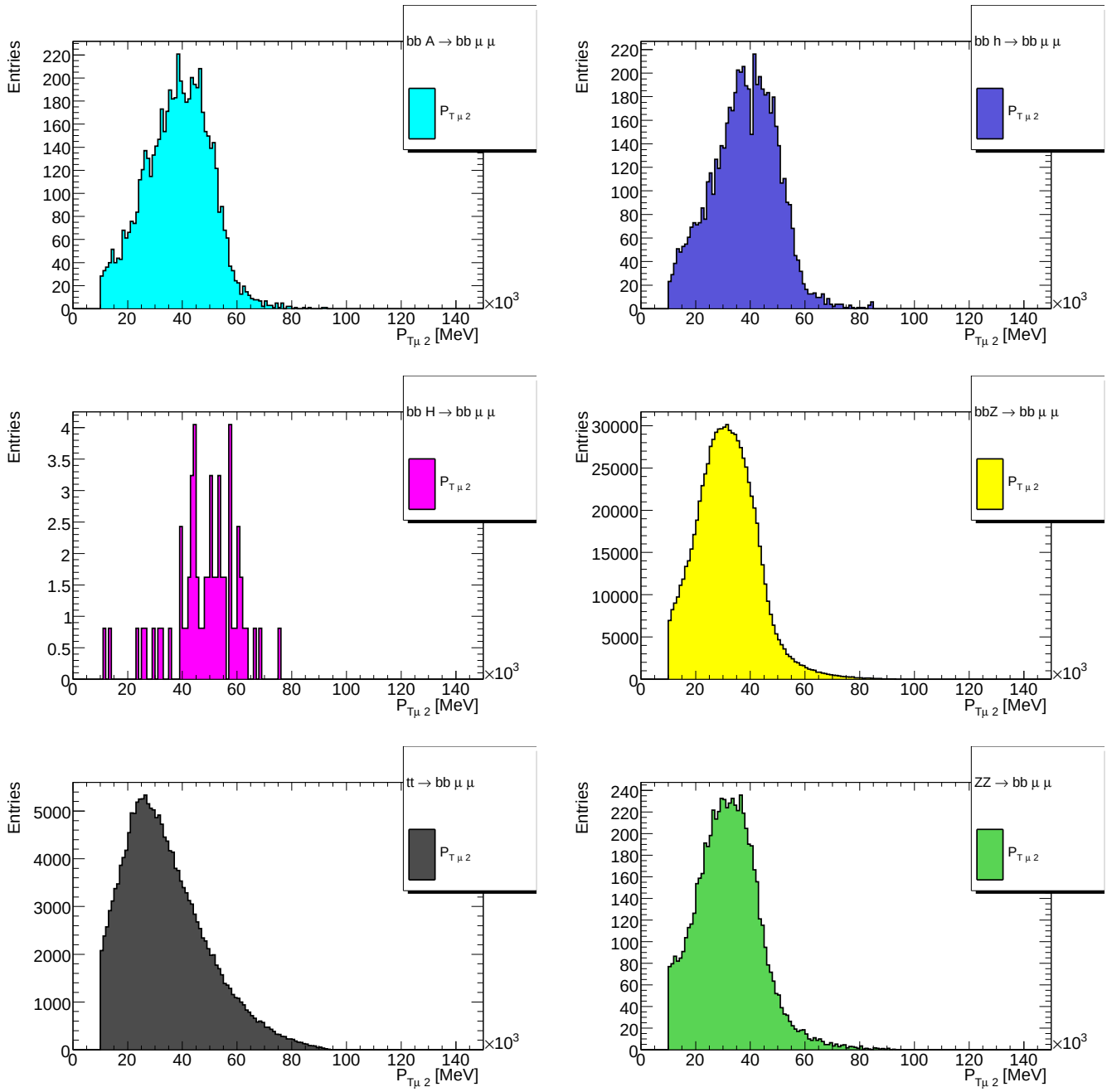

Figure 33: **After cut 5.** Distributions of the second most large muon reconstructed transverse momentum, $P_{\mathrm{T}\mu 2}$, are plotted after cuts 1– 5 (Tab. 7) for the following processes at the reference point, $\tan\beta = 45$ and $m_{\mathrm{A}} = 110.31$ GeV (see forehead Appendix C):
a) $b\bar{b}A \to b\bar{b}\mu^+\mu^-$ events (top left, light blue); b) $b\bar{b}h \to b\bar{b}\mu^+\mu^-$ events (top right, dark blue); c) $b\bar{b}H \to b\bar{b}\mu^+\mu^-$ events (middle left, purple); e) $b\bar{b}Z \to b\bar{b}\mu^+\mu^-$ events (middle right, yellow); f) $t\bar{t} \to b\bar{b}\mu^+\mu^-\nu\bar{\nu}$ events (bottom right, gray); g) $ZZ \to b\bar{b}\mu^+\mu^-$ events (bottom right, green). (Tab. 7).

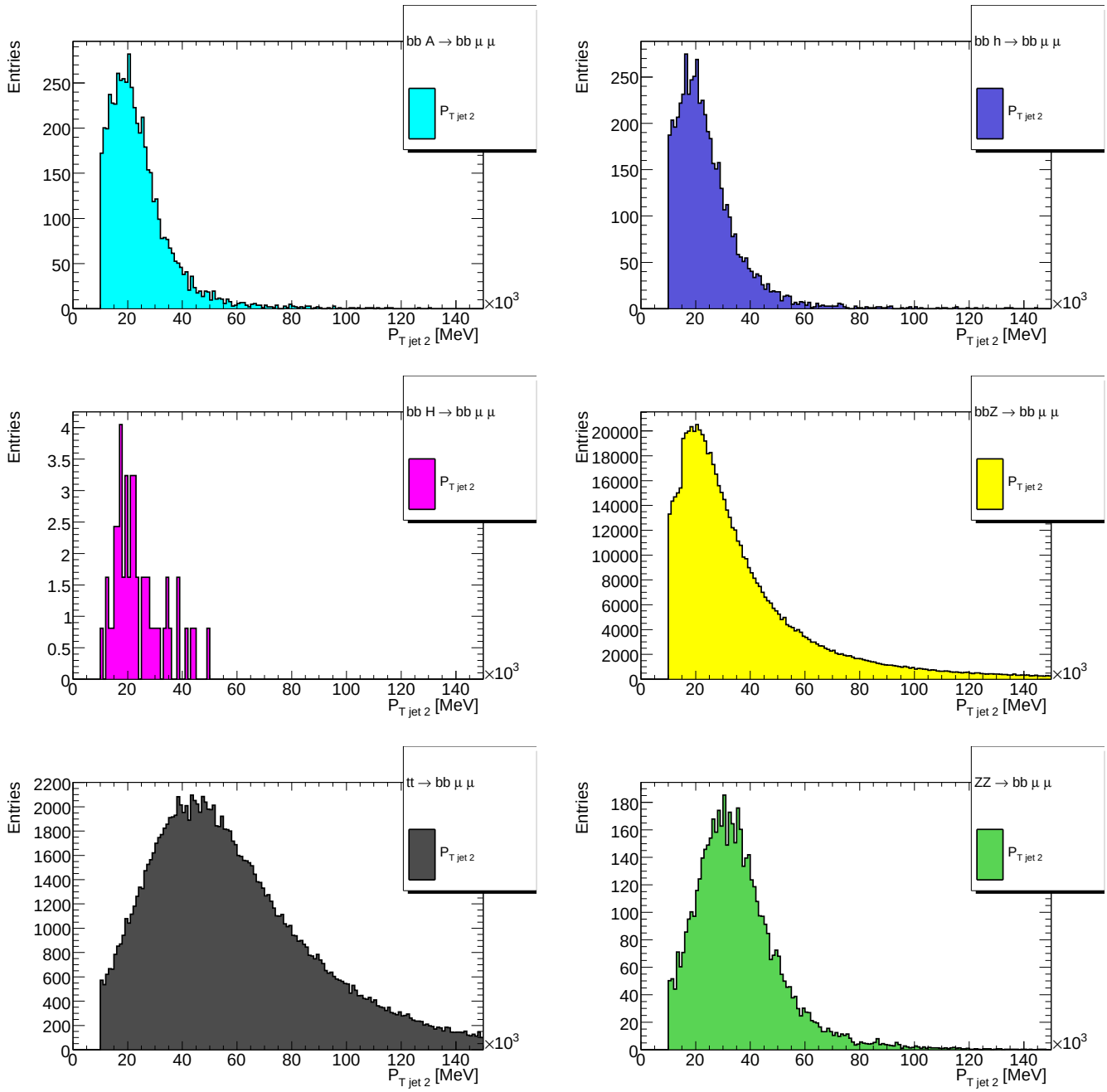

Figure 34: **After cut 6.** Distributions of the second most large jet reconstructed transverse momentum, P_{Tjet2}, are plotted after cuts 1– 6 (Tab. 7) for the following processes at the reference point, $\tan\beta = 45$ and $m_{\mathrm{A}} = 110.31$ GeV (see forehead Appendix C):
a) $b\bar{b}A \rightarrow b\bar{b}\mu^+\mu^-$ events (top left, light blue); b) $b\bar{b}h \rightarrow b\bar{b}\mu^+\mu^-$ events (top right, dark blue); c) $b\bar{b}H \rightarrow b\bar{b}\mu^+\mu^-$ events (middle left, purple); e) $b\bar{b}Z \rightarrow b\bar{b}\mu^+\mu^-$ events (middle right, yellow); f) $t\bar{t} \rightarrow b\bar{b}\mu^+\mu^-\nu\bar{\nu}$ events (bottom right, gray); g) $ZZ \rightarrow b\bar{b}\mu^+\mu^-$ events (bottom right, green).

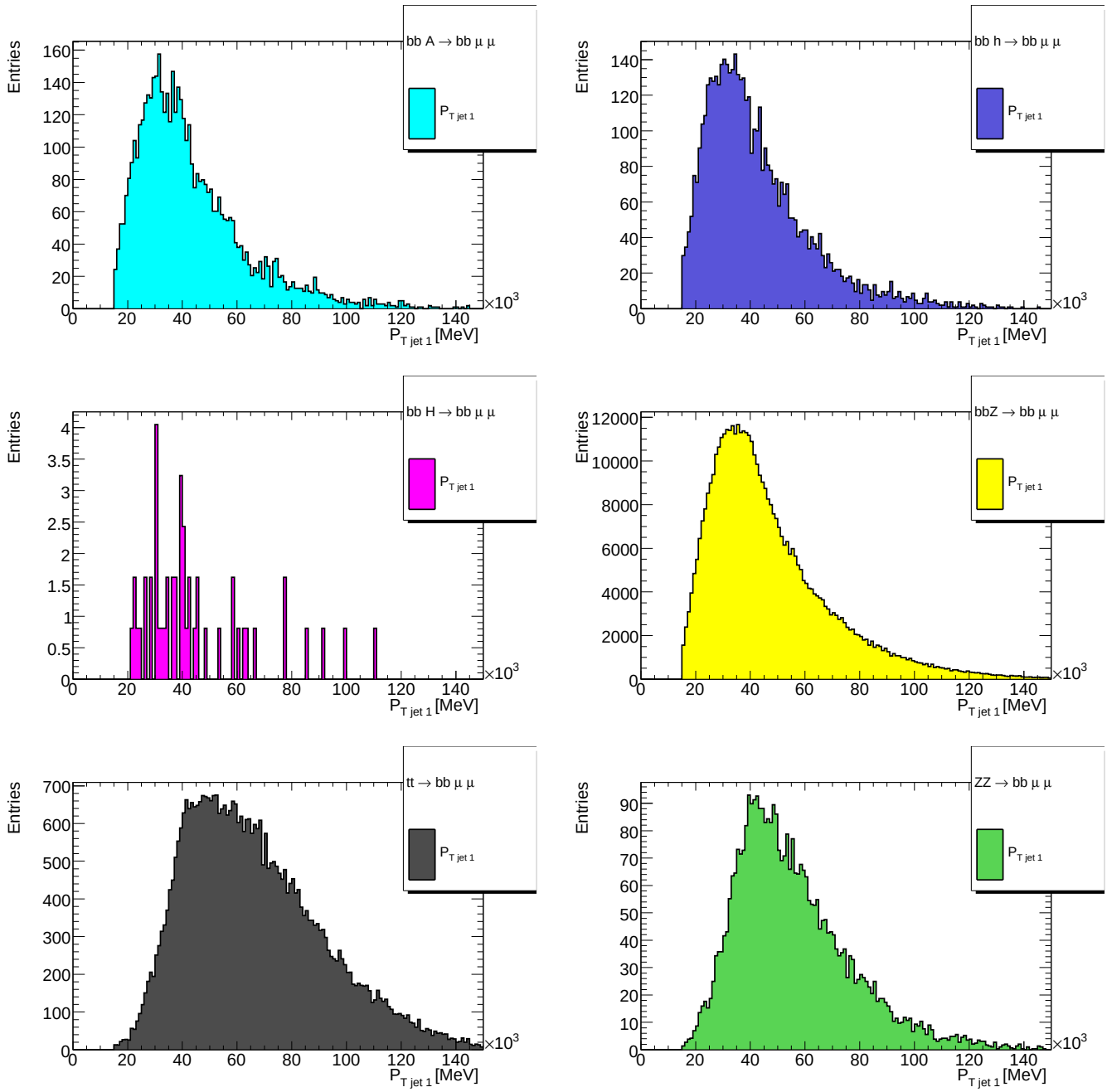

Figure 35: **After cut 7.** Distributions of the first most large jet reconstructed transverse momentum, P_{Tjet1}, are plotted after cuts 1– 7 (Tab. 7) for the following processes at reference point, $\tan\beta = 45$ and $m_{\mathrm{A}} = 110.31$ GeV (see forehead Appendix C):
a) $b\bar{b}A \to b\bar{b}\mu^+\mu^-$ events (top left, light blue); b) $b\bar{b}h \to b\bar{b}\mu^+\mu^-$ events (top right, dark blue); c) $b\bar{b}H \to b\bar{b}\mu^+\mu^-$ events (middle left, purple); e) $b\bar{b}Z \to b\bar{b}\mu^+\mu^-$ events (middle right, yellow); f) $t\bar{t} \to b\bar{b}\mu^+\mu^-\nu\bar{\nu}$ events (bottom right, gray); g) $ZZ \to b\bar{b}\mu^+\mu^-$ events (bottom right, green).

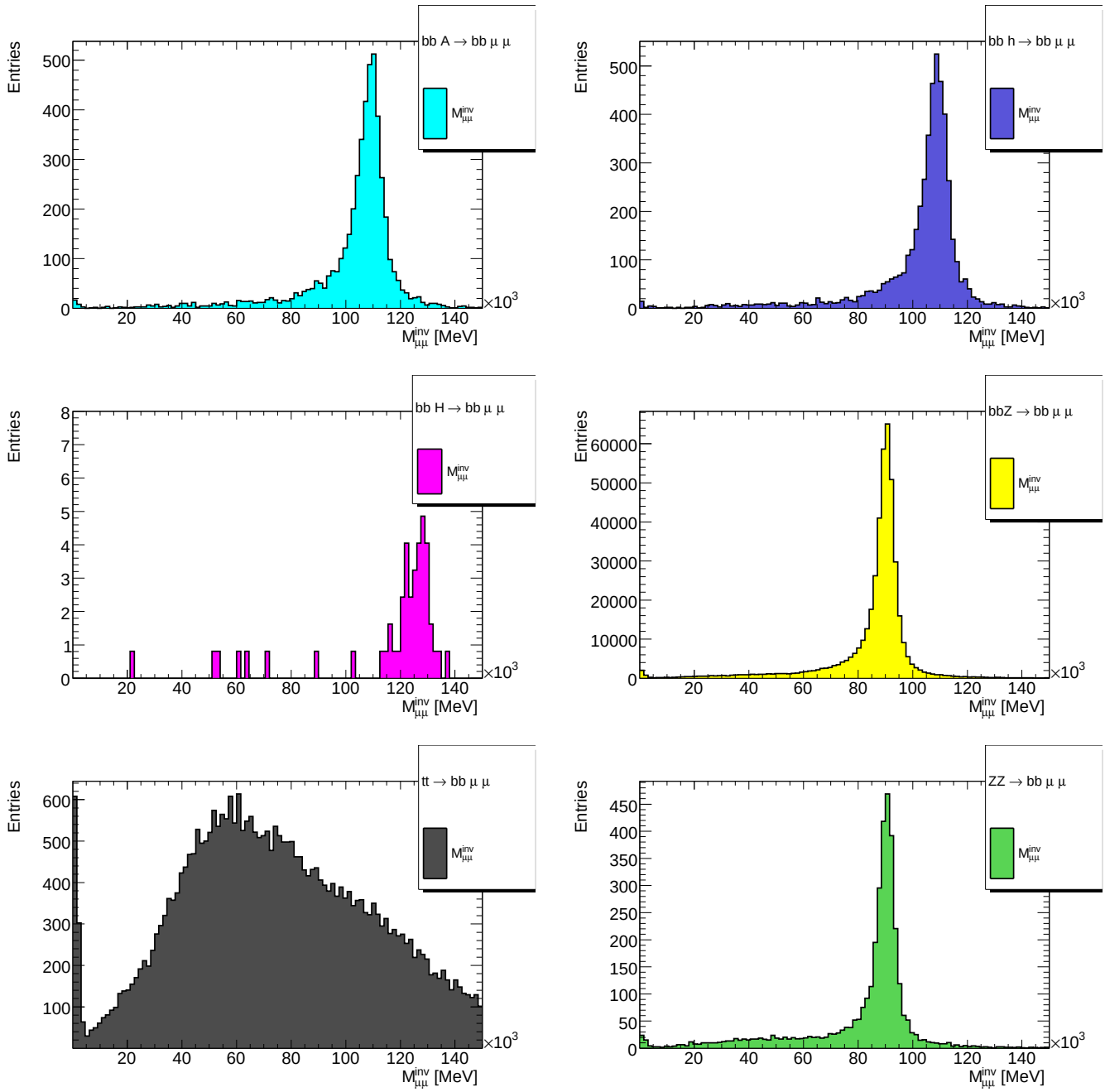

Figure 36: **After cut 8.** Distributions of the reconstructed $\mu^+\mu^-$ invariant mass, $M^{\rm inv}_{\mu\mu}$ are plotted after cuts 1– 8 (Tab. 7) for the following processes at the reference point, tanβ = 45 and $m_{\rm A}$ = 110.31 GeV (see forehead Appendix C):
a) $b\bar{b}A \to b\bar{b}\mu^+\mu^-$ events (top left, light blue); b) $b\bar{b}h \to b\bar{b}\mu^+\mu^-$ events (top right, dark blue); c) $b\bar{b}H \to b\bar{b}\mu^+\mu^-$ events (middle left, purple); e) $b\bar{b}Z \to b\bar{b}\mu^+\mu^-$ events (middle right, yellow); f) $t\bar{t} \to b\bar{b}\mu^+\mu^-\nu\bar{\nu}$ events (bottom right, gray); g) $ZZ \to b\bar{b}\mu^+\mu^-$ events (bottom right, green).

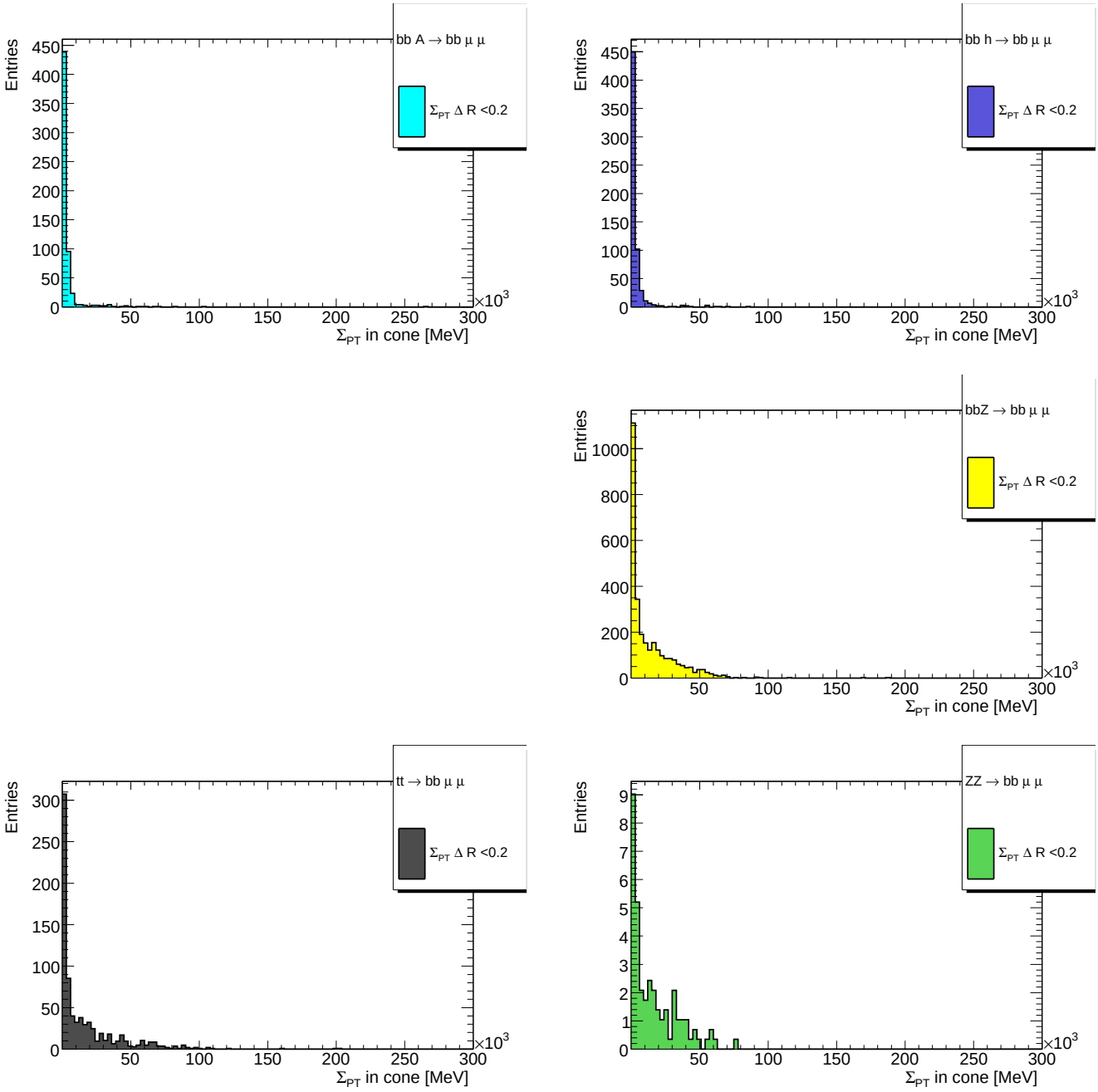

Figure 37: **After cut 9.** Distributions of the sum of the momenta (absolute value) of the reconstructed tracks, $\Sigma|P_{\mathrm{Ttracks}}|$, in a cone $\Delta\mathrm{R} < 0.2$ around the μ direction, are plotted after cuts 1– 9 (Tab. 7) for the following processes at the reference point, $\tan\beta = 45$ and $m_{\mathrm{A}} = 110.31$ GeV (see forehead Appendix C):
a) $b\bar{b}A \to b\bar{b}\mu^+\mu^-$ events (top left, light blue); b) $b\bar{b}h \to b\bar{b}\mu^+\mu^-$ events (top right, dark blue); e) $b\bar{b}Z \to b\bar{b}\mu^+\mu^-$ events (middle right, yellow); f) $t\bar{t} \to b\bar{b}\mu^+\mu^-\nu\bar{\nu}$ events (bottom right, gray); g) $ZZ \to b\bar{b}\mu^+\mu^-$ events (bottom right, green).

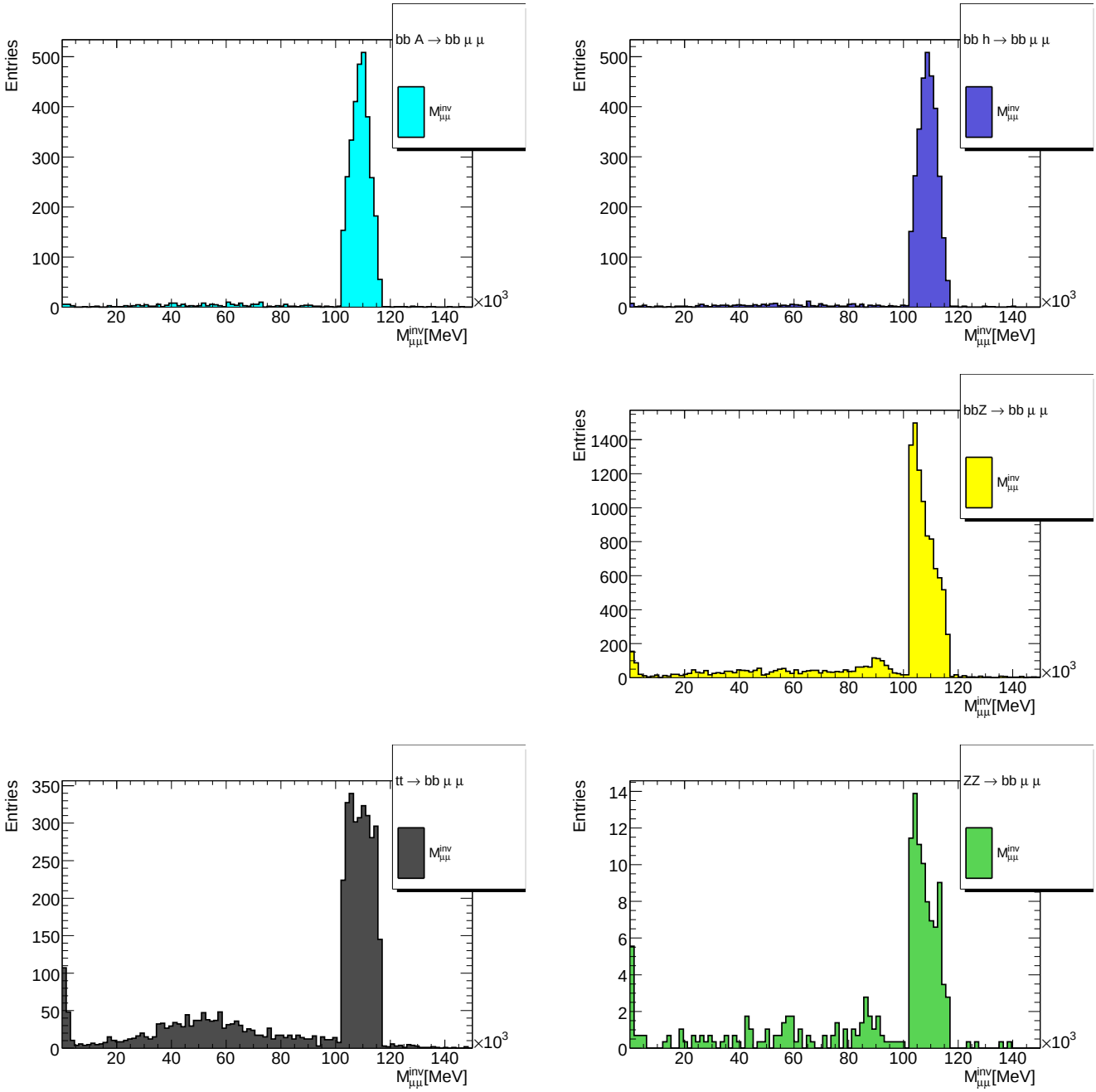

Figure 38: **After cut 10.** Distributions of the reconstructed $\mu^+\mu^-$ invariant mass, $M^{\text{inv}}_{\mu\mu}$, are plotted after cuts 1–10 (Tab. 7) for the following processes at the reference point, $\tan\beta = 45$ and $m_{\text{A}} = 110.31$ GeV (see forehead Appendix C):
a) $b\bar{b}A \to b\bar{b}\mu^+\mu^-$ events (top left, light blue); b) $b\bar{b}h \to b\bar{b}\mu^+\mu^-$ events (top right, dark blue); d) $b\bar{b}Z \to b\bar{b}\mu^+\mu^-$ events (middle right, yellow); e) $t\bar{t} \to b\bar{b}\mu^+\mu^-\nu\bar{\nu}$ events (bottom right, gray); f) $ZZ \to b\bar{b}\mu^+\mu^-$ events (bottom right, green).

D Appendix: Sample of h /A signal and background events. Analysis results

Table caption for Tables entitled: Events sample of h/A boson search:

Tab. 29 (tanβ =15), Tab. 31 (tanβ =20), Tab. 33 (tanβ =25), Tab. 35 (tanβ =30), Tab. 37 (tanβ =35), Tab. 39 (tanβ =40), Tab. 41 (tanβ =45), Tab. 43 (tanβ =50).
Column 1 gives the nominal mass value of the lightest neutral MSSM Higgs boson, $m_{\rm h}^{\rm nom}$. Columns 2 to 5 give the corresponding value of the A Higgs boson mass, $m_{\rm A}$, the number of events expected at $\int \mathcal{L}\,{\rm d}t \approx 300$ fb^{-1}, $\rm N_A^{exp300}$, the number of Monte Carlo generated events, $\rm N_A^{MC}$ and their weight in the analysis, $\rm w_A$. Columns 6 to 9 give the same quantities $m_{\rm h}$, $\rm N_h^{exp300}$, $\rm N_h^{MC}$ and $\rm w_h$ for the h boson.

Table captions for Tables entitled: Selection and Significance oft h/A boson search:

Tab. 30 (tanβ =15), Tab. 32 (tanβ =20), Tab. 34 (tanβ =25), Tab. 36 (tanβ =30), 38 (tanβ =35), Tab. 40 (tanβ =40), Tab. 42 (tanβ =45), Tab. 44 (tanβ =50).
Columns 1 of each table gives the the nominal mass value of the neutral lightest MSSM Higgs boson, $m_{\rm h}^{\rm nom}$. Columns 2 and 3 give the number of signal events selected as A , $\rm N_A^{sel}$, and h, $\rm N_h^{sel}$.
Columns 4 to 6 give the number of events selected in the background samples of Z , $\rm N_{zbb}^{sel}$, of $\rm t\bar{t}$, $\rm N_{tt}^{sel}$, and of ZZ, $\rm N_{zz}^{sel}$.
Columns 7 to 9 show the significance $\frac{S}{\sqrt{B}}$ of the h/A boson search, $S_{\rm h,\,A}^{300}$, $S_{\rm h,\,A}^{30}$and $S_{\rm h,\,A}^{10}$, for $\int \mathcal{L}\,{\rm d}t \approx 300$, 30 and 10 fb^{-1}, respectively.

tan β = 15 - Events sample of h/A boson search

$\mathbf{m}_{\mathrm{h}}^{\mathrm{nom}}$ [GeV]	m_{A} [GeV]	$\mathrm{N}_{\mathrm{A}}^{\mathrm{exp300}}$	$\mathrm{N}_{\mathrm{A}}^{\mathrm{MC}}$	w_{A}	m_{h} [GeV]	$\mathrm{N}_{\mathrm{h}}^{\mathrm{exp300}}$	$\mathrm{N}_{\mathrm{h}}^{\mathrm{MC}}$	w_{h}
95.00	96.07	12393	15283	0.81	95.00	12684	15398	0.82
97.50	98.68	11424	11998	0.95	97.50	11655	11570	1.00
100.00	101.31	10554	10797	0.98	100.01	10725	10776	1.00
102.50	103.96	9747	10196	0.96	102.50	9843	10200	0.96
105.00	106.65	9009	9162	0.98	105.00	9033	9197	0.98
107.50	109.38	8340	8400	0.99	107.50	8241	8799	0.94
110.00	112.20	7707	7790	0.99	110.01	7473	7999	0.93
112.50	115.12	7107	10398	0.68	112.51	6663	6163	1.08
115.00	118.22	6534	8192	0.80	115.00	5817	6399	0.91
117.50	121.66	5973	8212	0.73	117.51	4817	5000	0.96
120.00	125.82	5361	9600	0.56	120.01	3546	4000	0.89
122.50	132.05	4584	8000	0.57	122.50	1948	2398	0.81
125.00	151.00	2954	8996	0.33	125.01	405	800	0.51

Table 29: Table caption in forehead of Appendix D.

tan β = 15 - Selection and Significance for h/A boson search

$\mathbf{m}_{\mathrm{h}}^{\mathrm{nom}}$ [GeV]	$\mathrm{N}_{\mathrm{A}}^{\mathrm{sel}}$	$\mathrm{N}_{\mathrm{h}}^{\mathrm{sel}}$	$\mathrm{N}_{\mathrm{zbb}}^{\mathrm{sel}}$	$\mathrm{N}_{\mathrm{tt}}^{\mathrm{sel}}$	$\mathrm{N}_{\mathrm{zz}}^{\mathrm{sel}}$	$S_{\mathrm{h,\ A}}^{300}$	$S_{\mathrm{h,\ A}}^{30}$	$S_{\mathrm{h,\ A}}^{10}$
95.00	690	682	100131	2686	4355	2.44	0.77	0.45
97.50	550	549	54476	2743	2426	3.16	1.00	0.58
100.00	512	493	23442	2786	1064	4.37	1.38	0.80
102.50	489	435	7982	2484	412	6.43	2.03	1.17
105.00	468	444	6978	2858	348	6.82	2.16	1.25
107.50	394	442	4888	2907	267	7.07	2.236	1.29
110.00	401	393	2890	3666	208	7.82	2.47	1.43
112.50	580	283	2903	2939	173	7.46	2.36	1.36
115.00	435	324	2421	2986	145	7.22	2.28	1.32
117.50	428	253	2061	3027	131	6.55	2.07	1.20
120.00	515	190	1815	3138	109	5.54	1.75	1.01
122.50	384	119	1648	3465	96	3.86	1.22	0.70
125.00	280	44	1262	3241	87	1.51	0.48	0.28

Table 30: Table caption in forehead of Appendix D.

tan β = 20 - Events sample of h/A boson search

$\mathbf{m}_{\mathrm{h}}^{\mathrm{nom}}$ [GeV]	m_{A} [GeV]	$\mathrm{N}_{\mathrm{A}}^{\mathrm{exp300}}$	$\mathrm{N}_{\mathrm{A}}^{\mathrm{MC}}$	w_{A}	m_{h} [GeV]	$\mathrm{N}_{\mathrm{h}}^{\mathrm{exp300}}$	$\mathrm{N}_{\mathrm{h}}^{\mathrm{MC}}$	w_{h}
95.00	95.65	22314	24796	0.90	95.00	22761	24595	0.93
97.50	98.21	20640	24594	0.84	97.51	20985	23397	0.90
100.00	100.78	19059	23996	0.79	100.01	19341	23088	0.84
102.50	103.36	17679	19876	0.89	102.50	17844	22798	0.78
105.00	105.97	16356	17500	0.93	105.01	16428	24397	0.67
107.50	108.60	15174	16593	0.91	107.51	15114	24596	0.61
110.00	111.27	14061	15498	0.90	110.01	13872	15976	0.87
112.50	113.99	13038	15000	0.87	112.50	12621	24399	0.52
115.00	116.82	12057	12900	0.93	115.00	11289	23799	0.47
117.50	119.83	11136	12701	0.88	117.51	9813	23798	0.41
120.00	123.20	10191	11315	0.90	120.00	7860	11998	0.66
122.50	127.63	9093	10997	0.83	122.50	5022	10797	0.47
125.00	137.75	7107	8795	0.81	137.75	1356	9000	0.15

Table 31: Table caption in forehead of Appendix D.

tan β = 20 - Selection and Significance for h/A search

$\mathbf{m}_{\mathrm{h}}^{\mathrm{nom}}$ [GeV]	$\mathrm{N}_{\mathrm{A}}^{\mathrm{sel}}$	$\mathrm{N}_{\mathrm{h}}^{\mathrm{sel}}$	$\mathrm{N}_{\mathrm{zbb}}^{\mathrm{sel}}$	$\mathrm{N}_{\mathrm{tt}}^{\mathrm{sel}}$	$\mathrm{N}_{\mathrm{zz}}^{\mathrm{sel}}$	$S_{\mathrm{h,\ A}}^{300}$	$S_{\mathrm{h,\ A}}^{30}$	$S_{\mathrm{h,\ A}}^{10}$
95.00	1142	1108	99433	2501	4312	4.48	1.42	0.82
97.50	1116	1020	54482	2646	2424	5.43	1.72	0.99
100.00	1130	1082	23419	2677	1066	7.96	2.51	1.45
102.50	936	1050	11451	2663	529	10.18	3.22	1.86
105.00	789	1116	6845	2719	337	11.46	3.62	2.09
107.50	799	1188	4767	2755	256	13.03	4.12	2.38
110.00	782	769	3571	2746	202	13.73	4.34	2.51
112.50	734	1242	2803	2727	166	13.93	4.41	2.54
115.00	665	1085	2038	2569	122	13.88	4.39	2.53
117.50	608	1094	1692	2524	111	12.78	4.04	2.33
120.00	603	598	1660	2788	104	11.95	3.78	2.18
122.50	586	571	1504	2920	83	9.76	3.08	1.78
125.00	379	455	1491	3606	93	4.63	1.47	0.85

Table 32: Table caption in forehead of Appendix D.

tan β = 25 - Events sample of h/A boson search

$\mathbf{m}_{\mathrm{h}}^{\mathrm{nom}}$ [GeV]	m_{A} [GeV]	$\mathrm{N}_{\mathrm{A}}^{\mathrm{exp300}}$	$\mathrm{N}_{\mathrm{A}}^{\mathrm{MC}}$	w_{A}	m_{h} [GeV]	$\mathrm{N}_{\mathrm{h}}^{\mathrm{exp300}}$	$\mathrm{N}_{\mathrm{h}}^{\mathrm{MC}}$	w_{h}
95.00	95.46	35160	36916	0.95	95.01	35730	37671	0.95
97.50	97.99	32490	34957	0.93	97.50	32970	34192	0.96
100.00	100.54	30030	31429	0.96	100.01	30480	31122	0.98
102.50	103.09	27834	29394	0.95	102.51	28161	29306	0.96
105.00	105.65	25815	26993	0.96	105.00	26007	26350	0.99
107.50	108.23	23940	24600	0.97	107.50	24036	24199	0.99
110.00	110.84	22263	24534	0.91	110.01	22146	24400	0.91
112.50	113.48	20694	21798	0.95	112.51	20310	21799	0.93
115.00	116.18	19212	19331	0.99	115.00	18450	18889	0.98
117.50	119.00	17796	17799	1.00	117.51	16407	17396	0.94
120.00	122.04	16431	16797	0.98	120.01	13827	13558	1.02
122.50	125.71	14958	12996	1.15	122.51	9789	9999	0.98
125.00	132.60	12561	11799	1.06	125.00	3270	3266	1.00

Table 33: Table caption in forehead of Appendix D.

tan β = 25 - Selection and Significance for h/A search

$\mathbf{m}_{\mathrm{h}}^{\mathrm{nom}}$ [GeV]	$\mathrm{N}_{\mathrm{A}}^{\mathrm{sel}}$	$\mathrm{N}_{\mathrm{h}}^{\mathrm{sel}}$	$\mathrm{N}_{\mathrm{zbb}}^{\mathrm{sel}}$	$\mathrm{N}_{\mathrm{tt}}^{\mathrm{sel}}$	$\mathrm{N}_{\mathrm{zz}}^{\mathrm{sel}}$	$S_{\mathrm{h,\ A}}^{300}$	$S_{\mathrm{h,\ A}}^{30}$	$S_{\mathrm{h,\ A}}^{10}$
95.00	1592	1647	100916	2590	4391	6.67	2.11	1.22
97.50	1402	1425	55704	2623	2474	7.77	2.46	1.42
100.00	1397	1426	23855	2646	1078	11.95	3.78	2.18
102.50	1371	1388	11541	2626	534	16.15	5.11	2.95
105.00	1203	1202	6883	2674	335	17.98	5.68	3.28
107.50	1174	1103	4764	2712	254	20.00	6.32	3.65
110.00	1181	1200	3544	2683	200	21.66	6.85	3.96
112.50	1057	1044	2758	2653	162	21.72	6.87	3.96
115.00	895	930	2758	2652	163	19.76	6.25	3.61
117.50	844	864	1869	2653	123	20.69	6.54	3.78
120.00	785	613	1613	2612	103	18.21	5.76	3.32
122.50	631	470	1419	2686	79	15.98	5.05	2.92
125.00	562	183	1371	3078	84	10.27	3.25	1.88

Table 34: Table caption in forehead of Appendix D.

tan β = 30 - Events sample of h/A boson search

$\mathbf{m}_{\mathrm{h}}^{\mathrm{nom}}$ [GeV]	m_{A} [GeV]	$\mathrm{N}_{\mathrm{A}}^{\mathrm{exp300}}$	$\mathrm{N}_{\mathrm{A}}^{\mathrm{MC}}$	w_{A}	m_{h} [GeV]	$\mathrm{N}_{\mathrm{h}}^{\mathrm{exp300}}$	$\mathrm{N}_{\mathrm{h}}^{\mathrm{MC}}$	w_{h}
95.00	95.35	50820	53591	0.95	95.01	51600	52145	0.99
97.50	97.88	46890	48772	0.96	97.51	47640	44796	1.06
100.00	100.40	43440	44707	0.97	100.01	44070	43657	1.01
102.50	102.94	40290	44145	0.91	102.51	40740	43914	0.93
105.00	105.48	37380	39418	0.95	105.00	37710	39713	0.95
107.50	108.04	34680	39197	0.88	107.51	34950	39192	0.89
110.00	110.61	32310	32872	0.98	110.01	32250	32304	1.00
112.50	113.20	30030	32603	0.92	112.51	29769	31990	0.93
115.00	115.84	27951	29422	0.95	115.01	27279	29100	0.94
117.50	118.55	25983	29488	0.88	117.51	24627	29757	0.83
120.00	121.41	24090	23997	1.00	120.01	21381	23790	0.90
122.50	124.70	22122	23900	0.93	122.51	16278	24595	0.66
125.00	130.00	19359	20486	0.95	125.01	6561	20999	0.31

Table 35: Table caption in forehead of Appendix D.

tan β = 30 - Selection and Significance for h/A search

$\mathbf{m}_{\mathrm{h}}^{\mathrm{nom}}$ [GeV]	$\mathrm{N}_{\mathrm{A}}^{\mathrm{sel}}$	$\mathrm{N}_{\mathrm{h}}^{\mathrm{sel}}$	$\mathrm{N}_{\mathrm{zbb}}^{\mathrm{sel}}$	$\mathrm{N}_{\mathrm{tt}}^{\mathrm{sel}}$	$\mathrm{N}_{\mathrm{zz}}^{\mathrm{sel}}$	$S_{\mathrm{h,\,A}}^{300}$	$S_{\mathrm{h,\,A}}^{30}$	$S_{\mathrm{h,\,A}}^{10}$
95.00	2262	2137	102855	2613	4472	9.15	2.89	1.67
97.50	2070	1889	57367	2640	2545	11.44	3.62	2.09
100.00	2007	1885	24847	2659	1121	16.53	5.23	3.02
102.50	1930	1909	11876	2650	554	21.38	6.76	3.90
105.00	1802	1739	7030	2682	348	25.61	8.10	4.68
107.50	1692	1721	4850	2718	253	26.90	8.51	4.91
110.00	1475	1393	3310	2571	186	29.37	9.29	5.36
112.50	1541	1506	2794	2648	165	30.87	9.76	5.63
115.00	1355	1385	2251	2650	135	30.43	9.62	5.56
117.50	1363	1357	1884	2609	122	29.01	9.17	5.30
120.00	1177	1056	1598	2558	100	28.05	8.87	5.12
122.50	1136	1176	1365	2585	76	25.13	7.95	4.59
125.00	909	1040	1300	2813	75	16.13	5.10	2.95

Table 36: Table caption in forehead of Appendix D.

tan β = 35 - Events sample of h/A boson search

$\mathbf{m}_h^{nom}$ [GeV]	m_A [GeV]	N_A^{exp300}	N_A^{MC}	w_A	m_h [GeV]	N_h^{exp300}	N_h^{MC}	w_h
95.00	95.29	69360	72595	0.96	95.01	70230	73152	0.96
97.50	97.80	63960	66227	0.97	97.50	64890	67536	0.96
100.00	100.32	59250	62782	0.94	100.00	60000	60819	0.99
102.50	102.85	54960	57800	0.95	102.51	55560	57655	0.96
105.00	105.38	51000	52155	0.98	105.01	51450	51477	1.00
107.50	107.92	47370	48992	0.97	107.51	47700	49390	0.97
110.00	110.47	44070	46461	0.95	110.01	44190	46793	0.94
112.50	113.04	41070	42196	0.97	112.51	40860	42387	0.96
115.00	115.63	38220	39716	0.96	115.00	37650	38993	0.97
117.50	118.28	35610	37590	0.95	117.50	34320	37044	0.93
120.00	121.04	33090	34466	0.96	120.00	30390	34302	0.89
122.50	124.09	30600	31795	0.96	122.50	24414	31369	0.78
125.00	128.50	27348	28597	0.96	125.01	11589	28596	0.41

Table 37: Table caption in forehead of Appendix D.

tan β = 35 - Selection and Significance for h/A search

$\mathbf{m}_h^{nom}$ [GeV]	N_A^{sel}	N_h^{sel}	N_{zbb}^{sel}	N_{tt}^{sel}	N_{zz}^{sel}	$S_{h,\,A}^{300}$	$S_{h,\,A}^{30}$	$S_{h,\,A}^{10}$
95.00	2937	2892	105658	2677	4581	11.83	3.74	2.16
97.50	2760	2756	60764	2705	2689	14.78	4.67	2.70
100.00	2653	2583	26490	2731	1193	21.01	6.64	3.84
102.50	2492	2380	11431	2622	528	28.74	9.09	5.25
105.00	2271	2206	7225	2731	354	33.30	10.53	6.08
107.50	2130	2158	4999	2776	260	36.24	11.46	6.62
110.00	2061	1978	3687	2720	207	37.70	11.92	6.88
112.50	1848	1982	2876	2692	165	40.08	12.68	7.32
115.00	1717	1731	2313	2686	139	38.68	12.23	7.06
117.50	1633	1670	1910	2639	122	38.38	12.14	7.01
120.00	1623	1536	1620	2565	102	38.26	12.10	6.99
122.50	1447	1446	1363	2547	78	34.71	10.97	6.34
125.00	1236	1356	1252	2648	71	24.18	7.65	4.41

Table 38: Table caption in forehead of Appendix D.

tan β = 40 - Events sample of h/A boson search

$\mathbf{m}_{\mathrm{h}}^{\mathrm{nom}}$ [GeV]	m_{A} [GeV]	$\mathrm{N}_{\mathrm{A}}^{\mathrm{exp300}}$	$\mathrm{N}_{\mathrm{A}}^{\mathrm{MC}}$	w_{A}	m_{h} [GeV]	$\mathrm{N}_{\mathrm{h}}^{\mathrm{exp300}}$	$\mathrm{N}_{\mathrm{h}}^{\mathrm{MC}}$	w_{h}
95.00	95.24	90510	94579	0.96	95.01	91710	94983	0.97
97.50	97.75	83640	87349	0.96	97.50	84720	87225	0.97
100.00	100.27	77340	80987	0.95	100.01	78360	81385	0.96
102.50	102.79	71880	76384	0.94	102.51	72630	74672	0.97
105.00	105.31	66750	69330	0.96	105.01	67290	69656	0.97
107.50	107.84	61980	65390	0.95	107.51	62460	65352	0.96
110.00	110.38	57660	59904	0.96	110.01	57960	59963	0.97
112.50	112.93	53730	56094	0.96	112.51	53640	56498	0.95
115.00	115.50	50040	51242	0.98	115.01	49620	52190	0.95
117.50	118.11	46680	48393	0.96	117.50	45570	47914	0.95
120.00	120.80	43440	45123	0.96	120.00	40950	45793	0.89
122.50	123.70	40320	40793	0.99	122.50	34110	40993	0.83
125.00	127.55	36570	41386	0.88	125.01	18639	41268	0.45

Table 39: Table caption in forehead of Appendix D.

tan β = 40 - Selection and Significance for h/A search

$\mathbf{m}_{\mathrm{h}}^{\mathrm{nom}}$ [GeV]	$\mathrm{N}_{\mathrm{A}}^{\mathrm{sel}}$	$\mathrm{N}_{\mathrm{h}}^{\mathrm{sel}}$	$\mathrm{N}_{\mathrm{zbb}}^{\mathrm{sel}}$	$\mathrm{N}_{\mathrm{tt}}^{\mathrm{sel}}$	$\mathrm{N}_{\mathrm{zz}}^{\mathrm{sel}}$	$S_{\mathrm{h,\ A}}^{300}$	$S_{\mathrm{h,\ A}}^{30}$	$S_{\mathrm{h,\ A}}^{10}$
95.00	3776	3719	109930	2762	4763	14.96	4.73	2.73
97,50	3480	3542	65863	2787	2906	18.10	5.72	3.30
100,00	3373	3296	28972	2819	1297	25.46	8.05	4.65
102,50	3040	3087	13577	2825	630	33.30	10.53	6.08
105.00	2899	2919	7801	2853	392	40.72	12.88	7.43
107.50	2771	2854	5290	2860	279	45.65	14.43	8.33
110.00	2710	2626	3880	2801	221	49.60	15.69	9.06
112.50	2417	2366	3009	2784	172	48.28	15.27	8.81
115.00	2232	2267	2414	2770	144	49.49	15.65	9.03
117.50	2196	2074	1994	2721	125	49.79	15.74	9.09
120.00	1913	2003	1668	2630	105	46.97	14.85	8.57
122.50	1772	1745	1403	2579	81	43.68	13.81	7.98
125.00	1770	1886	1239	2589	69	34.02	10.76	6.21

Table 40: Table caption in forehead of Appendix D.

tan β = 45 - Events sample of h/A boson search

$\mathbf{m}_{\mathrm{h}}^{\mathrm{nom}}$ [GeV]	m_{A} [GeV]	$\mathrm{N}_{\mathrm{A}}^{\mathrm{exp300}}$	$\mathrm{N}_{\mathrm{A}}^{\mathrm{MC}}$	w_{A}	m_{h} [GeV]	$\mathrm{N}_{\mathrm{h}}^{\mathrm{exp300}}$	$\mathrm{N}_{\mathrm{h}}^{\mathrm{MC}}$	w_{h}
95.00	95.21	114060	113780	1.00	95.00	116040	115355	1.00
97.50	97.72	105660	109469	0.97	97.50	107100	104219	1.03
100.00	100.23	98070	101821	0.96	100.00	99060	100828	0.98
102.50	102.74	90870	94594	0.96	102.50	92040	94534	0.97
105.00	105.25	84330	88619	0.95	104.99	85230	88958	0.96
107.50	107.78	78390	81303	0.96	107.50	79140	80125	0.99
110.00	110.31	72900	74965	0.97	110.00	73500	76152	0.97
112.50	112.85	68130	71110	0.96	112.50	68160	70520	0.97
115.00	115.40	63540	62814	1.01	115.00	63180	64391	0.98
117.50	117.99	59160	61394	0.96	117.50	58200	60303	0.97
120.00	120.63	55170	56593	0.97	120.00	52740	57167	0.92
122.50	123.43	51330	51168	1.00	122.49	45210	52991	0.85
125.00	126.93	46920	48397	0.97	125.00	27651	48591	0.57

Table 41: Table caption in forehead of Appendix D.

tan β = 45 - Selection and Significance for h/A search

$\mathbf{m}_{\mathrm{h}}^{\mathrm{nom}}$ [GeV]	$\mathrm{N}_{\mathrm{A}}^{\mathrm{sel}}$	$\mathrm{N}_{\mathrm{h}}^{\mathrm{sel}}$	$\mathrm{N}_{\mathrm{zbb}}^{\mathrm{sel}}$	$\mathrm{N}_{\mathrm{tt}}^{\mathrm{sel}}$	$\mathrm{N}_{\mathrm{zz}}^{\mathrm{sel}}$	$S_{\mathrm{h,\ A}}^{300}$	$S_{\mathrm{h,\ A}}^{30}$	$S_{\mathrm{h,\ A}}^{10}$
95.00	4353	4432	115360	2920	4982	17.89	5.66	3.27
97.50	4479	4013	72977	2929	3212	21.46	6.79	3.92
100.00	4052	3973	33169	2973	1464	29.10	9.20	5.31
102.50	3782	3752	15251	2968	696	39.16	12.38	7.15
105.00	3609	3651	8583	2989	436	48.12	15.22	8.79
107.50	3272	3343	5710	3000	300	53.13	16.80	9.70
110.00	3110	3165	4260	2969	260	56.14	17.75	10.25
112.50	2986	2881	3196	2935	180	58.04	18.35	10.60
115.00	2558	2650	2546	2891	156	57.76	18.27	10.55
117.50	2546	2442	2119	2852	131	56.94	18.01	10.40
120.00	2396	2527	1748	2736	112	59.03	18.67	10.78
122.50	2105	2313	1461	2662	82	54.70	17.30	9.99
125.00	1925	2168	1247	2598	70	43.54	13.77	7.95

Table 42: Table caption in forehead of Appendix D.

tan β = 50 - Events sample of h/A boson search

$\mathbf{m}_{\mathrm{h}}^{\mathrm{nom}}$ [GeV]	m_{A} [GeV]	$\mathrm{N}_{\mathrm{A}}^{\mathrm{exp300}}$	$\mathrm{N}_{\mathrm{A}}^{\mathrm{MC}}$	w_{A}	m_{h} [GeV]	$\mathrm{N}_{\mathrm{h}}^{\mathrm{exp300}}$	$\mathrm{N}_{\mathrm{h}}^{\mathrm{MC}}$	w_{h}
95.00	95.19	141030	146387	0.96	95.00	143130	145173	0.99
97.50	97.70	130470	136789	0.96	97.51	132090	136584	0.97
100.00	100.21	120900	124074	0.97	100.01	122130	124981	0.98
102.50	102.72	112110	116547	0.96	102.51	113220	114908	0.99
105.00	105.23	104040	107951	0.96	105.01	105270	108443	0.97
107.50	107.75	96870	99906	0.97	107.51	97830	101129	0.97
110.00	110.27	90180	93785	0.96	110.01	90750	92787	0.98
112.50	112.80	84060	87111	0.96	112.51	84330	87851	0.96
115.00	115.34	78420	82181	0.95	115.00	78210	81327	0.96
117.50	117.91	73200	75609	0.97	117.51	72330	75390	0.96
120.00	120.52	68310	70590	0.97	120.00	66000	67745	0.97
122.50	123.26	63540	65191	0.97	122.51	57660	61741	0.93
125.00	126.49	58620	60993	0.96	125.00	38760	39990	0.97

Table 43: Table caption in forehead of Appendix D.

tan β = 50 - Selection and Significance for h/A search

$\mathbf{m}_{\mathrm{h}}^{\mathrm{nom}}$ [GeV]	$\mathrm{N}_{\mathrm{A}}^{\mathrm{sel}}$	$\mathrm{N}_{\mathrm{h}}^{\mathrm{sel}}$	$\mathrm{N}_{\mathrm{zbb}}^{\mathrm{sel}}$	$\mathrm{N}_{\mathrm{tt}}^{\mathrm{sel}}$	$\mathrm{N}_{\mathrm{zz}}^{\mathrm{sel}}$	$S_{\mathrm{h,\ A}}^{300}$	$S_{\mathrm{h,\ A}}^{30}$	$S_{\mathrm{h,\ A}}^{10}$
95.00	5573	5421	121723	3124	5268	21.15	6.69	3.86
97.50	5238	5278	82353	3152	3614	24.17	7.64	4.41
100.00	4815	4917	39368	3170	1726	32.56	10.30	5.94
102.50	4483	4474	17643	3174	801	43.71	13.82	7.98
105.00	4202	4265	9632	3192	488	53.85	17.03	9.83
107.50	4126	4061	6308	3170	336	62.34	19.71	11.38
110.00	3910	3808	4584	3138	250	66.80	21.13	12.20
112.50	3709	3517	3478	3150	190	68.69	21.72	12.54
115.00	3382	3426	2756	3056	165	70.08	22.16	12.80
117.50	3079	3214	2274	3026	137	69.45	21.96	12.68
120.00	2893	2760	1882	2903	120	67.10	21.22	12.25
122.50	2657	2629	1553	2825	85	65.55	20.73	11.97
125.00	2440	1761	1285	2658	70	56.16	17.76	10.25

Table 44: Table caption in forehead of Appendix D.

E Appendix: Sample of H signal and background events. Analysis results.

Table captions for Tables entitled: Events sample of H boson search:

Tab. 45 (tanβ =15), Tab. 47 (tanβ =20), Tab. 49 (tanβ =25), Tab. 51 (tanβ =30), Tab. 53 (tanβ =35), Tab. 55 (tanβ =40), Tab. 57 (tanβ =45), Tab. 59 (tanβ =50).
Columns 1 to 5 of each table give:
the nominal mass value of the lightest neutral MSSM Higgs boson, $m_{\rm h}^{\rm nom}$, the corresponding value of the H Higgs boson mass, $m_{\rm H}$, the number of events expected, $\rm N_H^{exp_{300}}$, for $\int \mathcal{L}\,{\rm d}t \approx$ 300 fb^{-1}, the number of Monte Carlo generated events, $\rm N_H^{MC}$, and their weight in the analysis, $\rm w_H$.

Table captions for Tables entitled: Selection and Significance of the H boson search:

Tab. 46 (tanβ =15), Tab. 48 (tanβ =20), Tab. 50 (tanβ =25), Tab. 52 (tanβ =30), Tab. 54 (tanβ =35), Tab. 56 (tanβ =40), Tab. 58 (tanβ =45), Tab. 60 (tanβ =50).
Columns 1 to 5 of each table give:
the nominal mass value of the neutral lightest MSSM Higgs boson, $m_{\rm h}^{\rm nom}$, the number of signal events selected in the H sample, $\rm N_H^{sel}$, the number of events selected in the background samples of Z , $\rm N_{zbb}^{sel}$, of $\rm t\bar{t}$, $\rm N_{tt}^{sel}$, and of ZZ, $\rm N_{zz}^{sel}$.
Columns 6 to 8 show:
the significance $\frac{S}{\sqrt{B}}$ of the H boson search, $S_{\rm H}^{300}$, $S_{\rm H}^{30}$ and $S_{\rm H}^{10}$ for $\int \mathcal{L}\,{\rm d}t \approx$ 300, 30 and 10 fb^{-1}, respectively.

$\tan\beta = 15$ - Events sample of H boson search

$\mathbf{m}_{\mathrm{h}}^{\mathrm{nom}}$ $[10^3\mathrm{MeV}]$	m_{H} [MeV]	$\mathrm{N}_{\mathrm{H}}^{\mathrm{exp300}}$	$\mathrm{N}_{\mathrm{H}}^{\mathrm{MC}}$	w_{H}
95.00	127750	112	800	0.14
97.50	127850	134	600	0.22
100.00	127980	172	200	0.86
102.50	128130	216	600	0.36
107.50	128550	361	400	0.90
110.00	128850	481	400	1.20
112.50	129270	659	600	1.10
115.00	129870	928	800	1.16
117.50	130800	1346	1200	1.12
120.00	132460	1989	799	2.49
122.50	136180	2790	3399	0.82
125.00	152610	2649	3398	0.78

Table 45: Table caption in forehead of Appendix E.

$\tan\beta = 15$ - Selection and Significance of H boson search

$\mathbf{m}_{\mathrm{h}}^{\mathrm{nom}}$ $[10^3\mathrm{MeV}]$	$\mathrm{N}_{\mathrm{H}}^{\mathrm{sel}}$	$\mathrm{N}_{\mathrm{sel}}^{\mathrm{zbb}}$	$\mathrm{N}_{\mathrm{sel}}^{\mathrm{tt}}$	$\mathrm{N}_{\mathrm{sel}}^{\mathrm{zz}}$	S_{H}^{300}	S_{H}^{30}	S_{H}^{10}
95.00*	4	818	1922	47	0.01	0.00	0.00
97.50*	26	818	1922	47	0.10	0.03	0.02
100.00*	8	818	1922	47	0.12	0.04	0.02
102.50*	25	818	1922	47	0.15	0.05	0.03
107.50*	18	818	1922	47	0.27	0.09	0.05
110.00*	15	818	1922	47	0.30	0.10	0.06
112.50*	34	818	1922	47	0.63	0.20	0.11
115.00*	27	818	1922	47	0.53	0.17	0.10
117.50*	56	818	1922	47	1.06	0.33	0.19
120.00	34	689	1804	39	1.51	0.48	0.28
122.50	149	547	1671	33	2.34	0.74	0.43
125.00	77	197	1064	28	1.59	0.50	0.29

Table 46: Table caption in forehead of Appendix E. For the masses marked with (*) the selection window, ξ_{H}, and the central value, $m_{\mathrm{H}}^{\mathrm{corr}}$, corresponding to m_{H}= 129870 MeV were used (m_{h}=115.00 GeV).

tan β = 20 - Events sample of H boson search

$\mathbf{m}_{\mathrm{h}}^{\mathrm{nom}}$ $[10^3\mathrm{MeV}]$	m_{H} [MeV]	$\mathrm{N}_{\mathrm{H}}^{\mathrm{exp300}}$	$\mathrm{N}_{\mathrm{H}}^{\mathrm{MC}}$	w_{H}
95.00	127400	112	800	0.14
97.50	127460	139	800	0.17
105.00	127710	284	200	1.42
110.00	128010	506	600	0.84
112.50	128230	705	1000	0.71
115.00	128560	1029	1800	0.57
117.50	129060	1577	1600	0.99
120.00	129940	2554	2800	0.91
122.50	131870	4284	5000	0.86
125.00	139490	5916	6600	0.90

Table 47: Table caption in forehead of Appendix E.

tan β = 20 - Selection and Significance of H boson search

$\mathbf{m}_{\mathrm{h}}^{\mathrm{nom}}$ $[10^3\mathrm{MeV}]$	$\mathrm{N}_{\mathrm{H}}^{\mathrm{sel}}$	$\mathrm{N}_{\mathrm{sel}}^{\mathrm{zbb}}$	$\mathrm{N}_{\mathrm{sel}}^{\mathrm{tt}}$	$\mathrm{N}_{\mathrm{sel}}^{\mathrm{zz}}$	S_{H}^{300}	S_{H}^{30}	S_{H}^{10}
95.00*	40	883	1962	48	0.09	0.03	0.02
97.50*	32	883	1962	48	0.09	0.03	0.02
105.00*	11	883	1962	48	0.26	0.08	0.05
110.00*	19	883	1962	48	0.26	0.08	0.05
112.50*	46	883	1962	48	0.53	0.17	0.10
115.00*	78	883	1962	48	0.73	0.23	0.13
117.50*	49	883	1962	48	0.79	0.25	0.14
120.00*	146	883	1962	48	2.19	0.69	0.40
122.50	237	713	1842	38	3.57	1.13	0.65
125.00	245	438	1559	35	4.49	1.41	0.82

Table 48: Table caption in forehead of Appendix E. For the masses marked with (*) the selection window, ξ_{H}, and the central value, $m_{\mathrm{H}}^{\mathrm{corr}}$, corresponding to m_{H}= 128560 MeV wereused (m_{h}=115.00 GeV).

$\tan\beta = 25$ - Events sample of H boson search

$\mathbf{m}_{\mathrm{h}}^{\mathrm{nom}}$ $[10^3\mathrm{MeV}]$	m_{H} [MeV]	$\mathrm{N}_{\mathrm{H}}^{\mathrm{exp300}}$	$\mathrm{N}_{\mathrm{H}}^{\mathrm{MC}}$	w_{H}
95.00	127270	111	600	0.19
97.50	127300	138	600	0.23
100.00	127350	173	600	0.29
102.50	127400	220	800	0.28
105.00	127460	284	600	0.47
107.50	127550	376	800	0.47
110.00	127650	513	800	0.64
112.50	127790	721	2000	0.36
115.00	128000	1068	2000	0.53
117.50	128310	1681	1600	1.05
120.00	128850	2878	4000	0.72
122.50	130020	5385	4999	1.08
125.00	134420	9516	9000	1.06

Table 49: Table caption in forehead of Appendix E.

$\tan\beta = 25$ - Selection and Significance of H boson search

$\mathbf{m}_{\mathrm{h}}^{\mathrm{nom}}$ $[10^3\mathrm{MeV}]$	$\mathrm{N}_{\mathrm{H}}^{\mathrm{sel}}$	$\mathrm{N}_{\mathrm{sel}}^{\mathrm{zbb}}$	$\mathrm{N}_{\mathrm{sel}}^{\mathrm{tt}}$	$\mathrm{N}_{\mathrm{sel}}^{\mathrm{zz}}$	S_{H}^{300}	S_{H}^{30}	S_{H}^{10}
95.00*	29	919	2022	52	0.09	0.03	0.02
97.50*	25	919	2022	52	0.09	0.03	0.02
100.00*	26	919	2022	52	0.12	0.04	0.02
102.50*	33	919	2022	52	0.15	0.05	0.03
105.00*	28	919	2022	52	0.21	0.07	0.04
107.50*	43	919	2022	52	0.33	0.10	0.06
110.00*	43	919	2022	52	0.45	0.14	0.08
112.50*	99	919	2022	52	0.58	0.18	0.11
115.00*	99	919	2022	52	0.85	0.27	0.16
117.50*	80	919	2022	52	1.36	0.43	0.25
120.00*	179	919	2022	52	2.08	0.66	0.38
122.50	198	810	1926	45	3.60	1.14	0.66
125.00	385	608	1757	38	7.51	2.37	1.37

Table 50: Table captions in forehead of Appendix E. For the masses marked with (*) the selection window, ξ_{H}, and the central value, $m_{\mathrm{H}}^{\mathrm{corr}}$, corresponding to m_{H}= 127550 MeV were used (m_{h}=107.50 GeV).

$\tan\beta = 30$ - Events sample of H boson search

$\mathbf{m_h^{nom}}$ $[10^3\mathrm{MeV}]$	m_H [MeV]	$N_H^{exp_{300}}$	N_H^{MC}	w_H
95.00	127230	109	800	0.14
97.50	127250	136	600	0.23
100.00	127280	171	600	0.29
102.50	127320	217	600	0.36
105.00	127360	282	800	0.35
107.50	127420	374	800	0.47
110.00	127490	511	600	0.85
112.50	127590	723	1799	0.40
115.00	127730	1078	1599	0.67
117.50	127940	1723	1799	0.96
120.00	128300	3033	3399	0.89
122.50	129090	6123	6360	0.96
125.00	131890	13026	12152	1.07

Table 51: Table caption in forehead of Appendix E.

$\tan\beta = 30$ - Selection and Significance of H boson search

$\mathbf{m_h^{nom}}$ $[10^3\mathrm{MeV}]$	N_H^{sel}	N_{sel}^{zbb}	N_{sel}^{tt}	N_{sel}^{zz}	S_H^{300}	S_H^{30}	S_H^{10}
95.00*	44	916	2014	51	0.10	0.03	0.02
97.50*	22	916	2014	51	0.08	0.03	0.02
100.00*	29	916	2014	51	0.13	0.04	0.02
102.50*	33	916	2014	51	0.19	0.06	0.04
105.00*	32	916	2014	51	0.18	0.06	0.03
107.50*	33	916	2014	51	0.25	0.08	0.05
110.00*	18	916	2014	51	0.25	0.08	0.05
112.50*	83	916	2014	51	0.54	0.17	0.10
115.00*	60	916	2014	51	0.65	0.21	0.12
117.50*	83	916	2014	51	1.29	0.41	0.23
120.00	156	896	1974	49	2.28	0.72	0.42
122.50	315	872	1951	49	5.00	1.58	0.91
125.00	504	727	1870	39	9.42	2.98	1.72

Table 52: Table captions in forehead of Appendix E. For the masses marked with (*) the selection window, ξ_H, and the central value, m_H^{corr}, corresponding to m_H= 127590 MeV were used (m_h=112.50 GeV).

$\tan\beta = 35$ - Events sample of H boson search

$\mathbf{m}_{\mathrm{h}}^{\mathrm{nom}}$ $[10^3\mathrm{MeV}]$	m_{H} [MeV]	$\mathrm{N}_{\mathrm{H}}^{\mathrm{exp}_{300}}$	$\mathrm{N}_{\mathrm{H}}^{\mathrm{MC}}$	w_{H}
95.00	127240	108	800	0.14
97.50	127260	134	800	0.17
100.00	127280	168	200	0.84
102.50	127310	214	496	0.43
105.00	127340	278	799	0.35
107.50	127380	369	599	0.62
110.00	127430	505	600	0.84
112.50	127500	717	400	1.79
115.00	127600	1073	1400	0.77
117.50	127750	1727	993	1.74
120.00	128010	3102	1600	1.94
122.50	128560	6528	7799	0.84
125.00	130470	16068	17731	0.91

Table 53: Table caption in forehead of Appendix E.

$\tan\beta = 35$ - Selection and Significance of H boson search

$\mathbf{m}_{\mathrm{h}}^{\mathrm{nom}}$ $[10^3\mathrm{MeV}]$	$\mathrm{N}_{\mathrm{H}}^{\mathrm{sel}}$	$\mathrm{N}_{\mathrm{sel}}^{\mathrm{zbb}}$	$\mathrm{N}_{\mathrm{sel}}^{\mathrm{tt}}$	$\mathrm{N}_{\mathrm{sel}}^{\mathrm{zz}}$	S_{H}^{300}	S_{H}^{30}	S_{H}^{10}
95.00*	39	921	2030	52	0.08	0.03	0.01
97.50*	42	921	2030	52	0.11	0.04	0.02
100.00*	11	921	2030	52	0.15	0.05	0.03
102.50*	32	921	2030	52	0.22	0.07	0.04
105.00*	37	921	2030	52	0.21	0.07	0.04
107.50*	35	921	2030	52	0.35	0.11	0.06
110.00*	23	921	2030	52	0.31	0.10	0.06
112.50*	14	921	2030	52	0.40	0.13	0.07
115.00*	64	921	2030	52	0.79	0.25	0.14
117.50*	53	921	2030	52	1.49	0.47	0.27
120.00	78	905	1983	50	2.46	0.78	0.45
122.50	349	886	1968	48	4.79	1.52	0.87
125.00	736	801	1956	43	11.23	3.55	2.05

Table 54: Table captions in forehead of Appendix E. For the masses marked with (*) the selection window, ξ_{H}, and the central value, $m_{\mathrm{H}}^{\mathrm{corr}}$, corresponding to m_{H}= 127500 MeV were used (m_{h}=112.50 GeV).

$\tan\beta = 40$ - Events sample of H boson search

$\mathbf{m}_{\mathrm{h}}^{\mathrm{nom}}$ $[10^3\mathrm{MeV}]$	m_{H} [MeV]	$\mathrm{N}_{\mathrm{H}}^{\mathrm{exp}_{300}}$	$\mathrm{N}_{\mathrm{H}}^{\mathrm{MC}}$	w_{H}
95.00	127280	105	800	0.13
97.50	127300	131	800	0.16
100.00	127310	165	800	0.21
102.50	127330	210	599	0.35
105.00	127360	273	600	0.46
107.50	127390	363	800	0.45
110.00	127430	497	600	0.83
112.50	127480	707	1800	0.39
115.00	127550	1060	2000	0.53
117.50	127670	1711	2000	0.86
120.00	127860	3093	3800	0.81
122.50	128260	6696	7997	0.84
125.00	129610	18345	19590	0.94

Table 55: Table caption in forehead of Appendix E.

$\tan\beta = 40$ - Selection and Significance of H boson search

$\mathbf{m}_{\mathrm{h}}^{\mathrm{nom}}$ $[10^3\mathrm{MeV}]$	$\mathrm{N}_{\mathrm{H}}^{\mathrm{sel}}$	$\mathrm{N}_{\mathrm{sel}}^{\mathrm{zbb}}$	$\mathrm{N}_{\mathrm{sel}}^{\mathrm{tt}}$	$\mathrm{N}_{\mathrm{sel}}^{\mathrm{zz}}$	S_{H}^{300}	S_{H}^{30}	S_{H}^{10}
95.00*	32	921	2029	52	0.07	0.02	0.01
97.50*	40	921	2029	52	0.11	0.03	0.02
100.00*	38	921	2029	52	0.13	0.04	0.02
102.50*	27	921	2029	52	0.15	0.05	0.03
105.00*	32	921	2029	52	0.23	0.07	0.04
107.50*	30	921	2029	52	0.22	0.07	0.04
110.00*	26	921	2029	52	0.35	0.11	0.06
112.50*	88	921	2029	52	0.56	0.18	0.10
115.00*	106	921	2029	52	0.91	0.29	0.17
117.50*	90	921	2029	52	1.24	0.39	0.23
120.00	178	911	1993	50	2.35	0.74	0.43
122.50	369	901	1976	49	5.04	1.59	0.92
125.00	826	857	1994	47	12.74	4.03	2.33

Table 56: Table captions in forehead of Appendix E. For the masses marked with (*) the selection window, ξ_{H}, and the central value, $m_{\mathrm{H}}^{\mathrm{corr}}$, corresponding to m_{H}= 127480 MeV were used (m_{h}=112.50 GeV).

$\tan\beta = 45$ - Events sample of H boson search

$\mathbf{m}_{\mathrm{h}}^{\mathrm{nom}}$ $[10^3\mathrm{MeV}]$	m_{H} [MeV]	$\mathrm{N}_{\mathrm{H}}^{\mathrm{exp}_{300}}$	$\mathrm{N}_{\mathrm{H}}^{\mathrm{MC}}$	w_{H}
95.00	127350	104	800	0.13
97.50	127360	128	703	0.18
100.00	127370	161	800	0.20
102.50	127390	205	800	0.26
105.00	127410	266	800	0.33
107.50	127430	355	599	0.59
110.00	127460	486	600	0.81
112.50	127500	692	1799	0.38
115.00	127560	1036	2000	0.52
117.50	127650	1679	1800	0.93
120.00	127790	3045	3799	0.80
122.50	128090	6678	8000	0.83
125.00	129090	19854	21796	0.91

Table 57: Table caption in forehead of Appendix E.

$\tan\beta = 45$ - Selection and Significance of H boson search

$\mathbf{m}_{\mathrm{h}}^{\mathrm{nom}}$ $[10^3\mathrm{MeV}]$	$\mathrm{N}_{\mathrm{H}}^{\mathrm{sel}}$	$\mathrm{N}_{\mathrm{sel}}^{\mathrm{zbb}}$	$\mathrm{N}_{\mathrm{sel}}^{\mathrm{tt}}$	$\mathrm{N}_{\mathrm{sel}}^{\mathrm{zz}}$	S_{H}^{300}	S_{H}^{30}	S_{H}^{10}
95.00*	36	921	2031	52	0.07	0.02	0.01
97.50*	25	921	2031	52	0.07	0.02	0.01
100.00*	32	921	2031	52	0.10	0.03	0.02
102.50*	32	921	2031	52	0.13	0.04	0.02
105.00*	28	921	2031	52	0.15	0.05	0.03
107.50*	34	921	2031	52	0.32	0.10	0.06
110.00*	32	921	2031	52	0.41	0.13	0.08
112.50*	85	921	2031	52	0.53	0.17	0.10
115.00*	111	921	2031	52	0.93	0.29	0.17
117.50*	77	921	2031	52	1.16	0.37	0.21
120.00	162	911	1998	48	2.11	0.67	0.38
122.50	374	907	1982	50	5.08	1.61	0.93
125.00	908	897	2013	51	13.45	4.25	2.45

Table 58: Table captions in forehead of Appendix E. For the masses marked with (*) the selection window, ξ_{H}, and the central value, $m_{\mathrm{H}}^{\mathrm{corr}}$, corresponding to m_{H}= 127500 MeV were used (m_{h}=112.50 GeV).

$\tan\beta = 50$ - Events sample of H boson search

$\mathbf{m}_{\mathrm{h}}^{\mathrm{nom}}$ $[10^3\mathrm{MeV}]$	m_{H} [MeV]	$\mathrm{N}_{\mathrm{H}}^{\mathrm{exp}_{300}}$	$\mathrm{N}_{\mathrm{H}}^{\mathrm{MC}}$	w_{H}
95.00	127430	101	799	0.13
97.50	127440	125	800	0.16
100.00	127450	158	800	0.20
102.50	127460	200	800	0.25
105.00	127480	260	800	0.33
107.50	127500	346	800	0.43
110.00	127520	474	800	0.59
112.50	127550	673	2000	0.34
115.00	127600	1010	2000	0.51
117.50	127670	1633	2000	0.82
120.00	127780	2972	3399	0.87
122.50	128020	6594	7572	0.87
125.00	128760	20475	19729	1.04

Table 59: Table caption in forehead of Appendix E.

$\tan\beta = 50$ - Selection and Significance of H boson search

$\mathbf{m}_{\mathrm{h}}^{\mathrm{nom}}$ $[10^3\mathrm{MeV}]$	$\mathrm{N}_{\mathrm{H}}^{\mathrm{sel}}$	$\mathrm{N}_{\mathrm{sel}}^{\mathrm{zbb}}$	$\mathrm{N}_{\mathrm{sel}}^{\mathrm{tt}}$	$\mathrm{N}_{\mathrm{sel}}^{\mathrm{zz}}$	S_{H}^{300}	S_{H}^{30}	S_{H}^{10}
95.00*	34	916	2015	51	0.07	0.02	0.01
97.50*	32	916	2015	51	0.08	0.03	0.01
100.00*	50	916	2015	51	0.16	0.05	0.03
102.50*	31	916	2015	51	0.13	0.04	0.02
105.00*	34	916	2015	51	0.18	0.06	0.03
107.50*	37	916	2015	51	0.26	0.08	0.05
110.00*	32	916	2015	51	0.31	0.10	0.06
112.50*	80	916	2015	51	0.43	0.14	0.08
115.00*	89	916	2015	51	0.73	0.23	0.13
117.50*	85	916	2015	51	1.12	0.35	0.20
120.00*	143	916	2015	51	2.02	0.64	0.37
122.50	353	907	1992	50	5.00	1.58	0.91
125.00	818	905	2025	50	13.75	4.35	2.51

Table 60: Table captions in forehead of Appendix E. For the masses marked with (*) the selection window, ξ_{H}, and the central value, $m_{\mathrm{H}}^{\mathrm{corr}}$, corresponding to m_{H}= 127600 MeV were used (m_{h}=115.00 GeV).

F Appendix: Sample of h/A/H signal and background events. Analysis results

Table captions for Tables entitled: Selection and Significance of h/A/H boson search:

Tab. 61 (tanβ =15), Tab. 62 (tanβ =20), Tab. 63 (tanβ =25), Tab. 64 (tanβ =30), Tab. 65 (tanβ =35), Tab. 66 (tanβ =40), Tab. 67 (tanβ =45), Tab. 68 (tanβ =50).
Columns 1 to 5 of tables give:
the nominal mass value of the neutral lightest MSSM Higgs boson, $m_{\rm h}^{\rm nom}$, the corresponding value of the H Higgs boson mass, $m_{\rm H}$, the number of events selected in the background samples of Z, $\rm N_{zbb}^{sel}$, of $\rm t\bar{t}$, $\rm N_{tt}^{sel}$, of ZZ, $\rm N_{zz}^{sel}$, in a window not overlapping those used in Appendix. D.
Columns 6 to 9 show:
the significance, $\frac{S}{\sqrt{B}}$, of the search of h/A/H bosons, $S^{300}_{\rm h,\ A,\ H}$, $S^{30}_{\rm h,\ A,\ H}$ and $S^{10}_{\rm h,\ A,\ H}$ at $\int \mathcal{L}\,{\rm d}t \approx$ 300 fb^{-1}, 30 fb^{-1} , 10 fb^{-1}, and the search of h/A bosons,$S^{300}_{\rm h,\ A}$ for $\int \mathcal{L}\,{\rm d}t \approx 300$ fb^{-1}.

tan β = 15 - Selection and Significance for h/A/H boson search

$\mathbf{m}_{\mathrm{h}}^{\mathrm{nom}}$ $[10^3\mathrm{MeV}]$	m_{H} [MeV]	$\mathrm{N}_{\mathrm{sel}}^{\mathrm{zbb}}$	$\mathrm{N}_{\mathrm{sel}}^{\mathrm{tt}}$	$\mathrm{N}_{\mathrm{sel}}^{\mathrm{zz}}$	$S_{\mathrm{h,\ A,\ H}}^{300}$	$S_{\mathrm{h,\ A,\ H}}^{30}$	$S_{\mathrm{h,\ A,\ H}}^{10}$	$S_{\mathrm{h,\ A}}^{300}$
122.50	136180	110	429	9	5.09	1.64	0.93	3.86
125.00	152610	14	94	5	2.27	0.73	0.19	1.51

Table 61: Table caption in forehead of Appendix F.

tan β = 20 - Selection and Significance for h/A/H boson search

$\mathbf{m}_{\mathrm{h}}^{\mathrm{nom}}$ $[10^3\mathrm{MeV}]$	m_{H} [MeV]	$\mathrm{N}_{\mathrm{sel}}^{\mathrm{zbb}}$	$\mathrm{N}_{\mathrm{sel}}^{\mathrm{tt}}$	$\mathrm{N}_{\mathrm{sel}}^{\mathrm{zz}}$	$S_{\mathrm{h,\ A,\ H}}^{300}$	$S_{\mathrm{h,\ A,\ H}}^{30}$	$S_{\mathrm{h,\ A,\ H}}^{10}$	$S_{\mathrm{h,\ A}}^{300}$
122.50	131870	149	525	12	11.69	3.77	2.14	9.76
125.00	139490	30	168	5	7.25	2.34	0.76	4.63

Table 62: Table caption in forehead of Appendix F.

tan β = 25 - Selection and Significance for h/A/H boson search

$\mathbf{m}_{\mathrm{h}}^{\mathrm{nom}}$ $[10^3\mathrm{MeV}]$	m_{H} [MeV]	$\mathrm{N}_{\mathrm{sel}}^{\mathrm{zbb}}$	$\mathrm{N}_{\mathrm{sel}}^{\mathrm{tt}}$	$\mathrm{N}_{\mathrm{sel}}^{\mathrm{zz}}$	$S_{\mathrm{h,\ A,\ H}}^{300}$	$S_{\mathrm{h,\ A,\ H}}^{30}$	$S_{\mathrm{h,\ A,\ H}}^{10}$	$S_{\mathrm{h,\ A}}^{300}$
122.50	130020	188	539	12	17.51	5.65	3.2	15.98
125.00	134420	45	195	4	15.20	4.9	2.78	10.27

Table 63: Table caption in forehead of Appendix F.

tan β = 30 - Selection and Significance for h/A/H boson search

$\mathbf{m}_{\mathrm{h}}^{\mathrm{nom}}$ $[10^3\mathrm{MeV}]$	m_{H} [MeV]	$\mathrm{N}_{\mathrm{sel}}^{\mathrm{zbb}}$	$\mathrm{N}_{\mathrm{sel}}^{\mathrm{tt}}$	$\mathrm{N}_{\mathrm{sel}}^{\mathrm{zz}}$	$S_{\mathrm{h,\ A,\ H}}^{300}$	$S_{\mathrm{h,\ A,\ H}}^{30}$	$S_{\mathrm{h,\ A,\ H}}^{10}$	$S_{\mathrm{h,\ A}}^{300}$
122.50	129090	217	526	11	27.01	8.71	4.94	25.13
125.00	131890	48	219	5	22.88	7.36	4.18	16.13

Table 64: Table caption in forehead of Appendix F.

tan β = 35 - Selection and Significance for h/A/H boson search

$\mathbf{m}_{\mathrm{h}}^{\mathrm{nom}}$ $[10^3\mathrm{MeV}]$	m_{H} [MeV]	$\mathrm{N}_{\mathrm{sel}}^{\mathrm{zbb}}$	$\mathrm{N}_{\mathrm{sel}}^{\mathrm{tt}}$	$\mathrm{N}_{\mathrm{sel}}^{\mathrm{zz}}$	$S_{\mathrm{h,\ A,\ H}}^{300}$	$S_{\mathrm{h,\ A,\ H}}^{30}$	$S_{\mathrm{h,\ A,\ H}}^{10}$	$S_{\mathrm{h,\ A}}^{300}$
122.50	128560	224	536	9	35.29	11.38	6.45	34.71
125.00	130470	62	224	6	32.66	10.54	5.09	24.18

Table 65: Table caption in forehead of Appendix F.

tan β = 40 - Selection and Significance for h/A/H boson search

$\mathbf{m}_{\mathrm{h}}^{\mathrm{nom}}$ $[10^3\mathrm{MeV}]$	m_{H} [MeV]	$\mathrm{N}_{\mathrm{sel}}^{\mathrm{zbb}}$	$\mathrm{N}_{\mathrm{sel}}^{\mathrm{tt}}$	$\mathrm{N}_{\mathrm{sel}}^{\mathrm{zz}}$	$S_{\mathrm{h,\ A,\ H}}^{300}$	$S_{\mathrm{h,\ A,\ H}}^{30}$	$S_{\mathrm{h,\ A,\ H}}^{10}$	$S_{\mathrm{h,\ A}}^{300}$
122.50	128260	218	504	9	43.95	14.18	8.03	43.68
125.00	129610	56	197	4	43.56	14.05	7.96	34.02

Table 66: Table caption in forehead of Appendix F.

tan β = 45 - Selection and Significance for h/A/H boson search

$\mathbf{m}_{\mathrm{h}}^{\mathrm{nom}}$ $[10^3\mathrm{MeV}]$	m_{H} [MeV]	$\mathrm{N}_{\mathrm{sel}}^{\mathrm{zbb}}$	$\mathrm{N}_{\mathrm{sel}}^{\mathrm{tt}}$	$\mathrm{N}_{\mathrm{sel}}^{\mathrm{zz}}$	$S_{\mathrm{h,\ A,\ H}}^{300}$	$S_{\mathrm{h,\ A,\ H}}^{30}$	$S_{\mathrm{h,\ A,\ H}}^{10}$	$S_{\mathrm{h,\ A}}^{300}$
120.00	127790	349	867	14	54.16	17.47	9.90	59.03
122.50	128090	205	465	8	54.61	17.62	9.98	54.70
125.00	129090	51	162	5	53.90	17.38	9.85	43.53

Table 67: Table caption in forehead of Appendix F.

tan β = 50 - Selection and Significance for h/A/H boson search

$\mathbf{m}_{\mathrm{h}}^{\mathrm{nom}}$ [10^3MeV]	m_{H} [MeV]	$\mathrm{N}_{\mathrm{sel}}^{\mathrm{zbb}}$	$\mathrm{N}_{\mathrm{sel}}^{\mathrm{tt}}$	$\mathrm{N}_{\mathrm{sel}}^{\mathrm{zz}}$	$S_{\mathrm{h,\ A,\ H}}^{300}$	$S_{\mathrm{h,\ A,\ H}}^{30}$	$S_{\mathrm{h,\ A,\ H}}^{10}$	$S_{\mathrm{h,\ A}}^{300}$
120.00	127780	793	173	142	60.72	19.59	11.10	67.10
122.50	128020	179	400	8	65.27	21.10	11.93	65.55
125.00	128760	35	117	3	66.70	21.52	12.19	56.16

Table 68: Table caption in forehead of Appendix F.

References

[1] S. Gentile, H. Bilokon, V. Chiarella, G. Nicoletti, Data based method for Z $\rightarrow \mu^+\mu^-$ background subtraction in ATLAS detector at LHC, 2006, Università La Sapienza, Sez. I.N.F.N., Roma, Laboratori Nazionali di Frascati, I.N.F.N, Frascati Italy, ATL-PHYS-PUB-2006-019.

[2] S. Gentile, M. Paniccia, P. Violini, Search for supersymmetric neutral Higgs h in the decay $\rightarrow \mu^+\mu^-$ in ATLAS detector at LHC, 2003, Università La Sapienza, Sez. I.N.F.N., Roma, Italy, ATL-PHYS-2003-015.

[3] H.-P. Nilles, Phys. Rep. **110** (1984) 1.

[4] H. E. Haber and G. L. Kane, Phys. Rep. **117** (1985) 75.

[5] R. Barbieri, Riv. Nuovo Cim. **11** (1988) n. 4.

[6] R. Barate *et al.*, Phys. Lett. **B565** (2003) 61.

[7] S. Schael *et al.*, Eur. Phys. J. **C47** (2006) 547.

[8] Search for charged Higgs bosons: Preliminary combined results using LEP data collected at energies up to 209 GeV, 2001, hep-ex/0107031.

[9] Stephen P. Martin, A supersymmetry primer, 1997, hep-ph/9709356.

[10] W.-M. Yao *et al.*, J. Phys. **G33** (2006) 1.

[11] J. F. Gunion *et al.*, "The Higgs Hunter's Guide", (Addison-Wesley, Redwood City, 1990).

[12] ATLAS Coll., ATLAS detector and Physics Performance:
Technical Design Report, Volume 2,
report CERN/LHCC/99-15 (1999).

[13] CMS Coll., CMS detector and Physics Performance:
Physics Technical Design Report, Volume 1,
report CERN/LHCC/2006-001 (2006).

[14] M. Schumacher, Investigation of the discovery potential for Higgs bosons of the minimal supersymmetric extension of the standard model (MSSM) with ATLAS, 2004, hep-ph/0410112.

[15] E. Richter-Was *et al.*, Int. J. Mod. Phys. **A13** (1998) 1371.

[16] K. S. Cranmer, B. Mellado, W. Quayle and Sau Lan Wu, ECONF **C030908** (2003) MODT004.

[17] B. P. Kersevan and E. Richter-Was, The Monte Carlo event generator AcerMC version 2.0 with interfaces to PYTHIA 6.2 and HERWIG 6.5, 2004, hep-ph/0405247.

[18] T. Sjostrand, L.Lonnblad and S. Mrenna, PYTHIA 6.226: Physics and manual, 2004, hep-ph/0405247.

[19] S. Agostinelli *et al.*, Nucl. Instrum. Methods Phys. Res. A **506** (2003) 250.

[20] J. Alison *et al.*, IEEE Transactions on Nuclear Science **53** (2006) 270.

[21] S. Mrenna, 2005, Private Communication.

[22] E. Pomarico, Studio del Processo di decadimento del bosone Z nel canale $\mu^+\mu^-$, 2005, Università La Sapienza, Roma.

[23] S. Corréard, V. Kostioukhine, J. Levêque, A. Rozanov, J.-B. de Vivie, b-tagging with DC1 data, 2003, ATL-COM-PHYS-2003-049.

[24] M. L. Mangano, M. Moretti, F. Piccinini, R. Pittau and A. D. Polosa, JHEP **07** (2003) 001.